UNIVERSITY OF TARTU
Faculty of Physics and Chemistry
Institute of Physical Chemistry

Kristjan Laes

Adsorption kinetics of tetrabutylammonium cations on Bi($01\bar{1}$) plane

Master's Thesis in physical and electrochemistry

Advisers: Ph.D, senior researcher chem. Mart Väärtnõu
prof. Enn Lust

Tartu 2004

CONTENTS

1 Introduction 3
2 Literature Overview 5
2.1 Thermodynamic conceptions of adsorption and basic equations for the calculation of the adsorption parameters of organic compounds at metal electrodes 5
2.2 Adsorption kinetics of organic compounds 8
2.3 Adsorption of organic compounds at the electrode | base electrolyte interface 14
2.4 Influence of the crystallographic structure of electrode surface on the adsorption of organic molecules 15
2.5 Adsorption of tetraalkylammonium cations on Bi, Hg and Au electrodes. 17
3 Experimental 20
4 Results and discussion 20
4.1 Cyclic voltammograms (CVs) 20
4.2 Complex plane (Z", Z') – plots 21
4.3 Fitting of impedance data 25
5 Conclusion 32
6 Kokkuvõte 33
7 References 34
8 Legends of figures 38

1 INTRODUCTION

This work is a part of project devoted to the study of the influence of the chemical composition of an adsorbate and of the crystallographic structure of bismuth surface on the adsorption kinetics of neutral organic molecules at the metal | solution interface [1, 2].

Adsorption behaviour of various organic compounds has been investigated by electrochemists for a long time [1-30] as the organic surface-active substances are involved in the conversion and storage process of energy and in electrosynthesis; used as corrosion inhibitors, regulators of metal deposition, and as catalysts in various electrochemical reactions. In spite of great theoretical and experimental interest, there is still no general concept to describe the electrosorption behaviour of various organic substances at solid and liquid electrodes as there are lot of possibilities of the orientation of the adsorbate molecules and of the partial charge transfer between adsorbate and adsorbent due to the great number of substance classes with different polar groups and molecular lengths, as well as due to the different structure of hydrocarbon chains [1, 2, 5, 30-33]. Therefore, the distance of the outer Helmholtz plane and the local field strength may be noticeably changed by the presence of strongly oriented dipoles [3, 8-14, 30-32]. Thus, the orientation of adsorbate dipoles at the electrode surface is a very important parameter to gain an insight into the mechanism of adsorption and is mainly derived from the adsorption studies based on the determination of the surface limiting capacitance, surface excess and limiting adsorption potential shift. Recently it has been pointed out that a more quantitative analysis using the molecular models gives rise to a certain degree of ambiguity and should be interpreted with a great caution.

In a series of recent publications [1 - 5, 25, 30 - 32] it has been demonstrated the systematic influence of structure of the electrode surface on the value of the free energy of adsorption of organic compounds, $\Delta G_{\mathrm{A}}^{0}$, at the Bi single crystal plane – electrolyte solution interface. It was found that the difference between the adsorption energies of organic compounds on the chemically different metals decreases if the molar weight of the adsorbate decreases [30 -33]. This tendency is valid for the bismuth single crystal plane electrodes with decreasing the adsorption activity of organic compound at the air–solution, as well as at the metal–electrolyte interfaces [1, 23, 25, 30 - 33].

Many organic compounds, having very strong adsorbate-adsorbate intermolecular interaction, are able to create up the two - dimensionally associated surface layers. Two–dimensional phase transition on the surface or in the adlayers have received an increased

attention in recent years as they are related to the various important aspects in the surface, interfacial and materials sciences, and nanotechnology, such as ordered adsorption, island nucleation and growth surface reconstruction and molecular electronics. Kinetic phenomena like catalytic activity and chirality of the surface, selective recognition of molecular functions, or oscillation of the chemical reactions are directly related to the phase formation processes at the interface.

The main aim of this work was to establish some systematic trends of the influence of the geometrical structure of hydrocarbon chain and of the chemical nature of functional groups of adsorbates on the various interfacial parameters, mainly on the attractive interaction constant a, limiting differential capacitance C^1, effective dipole moment μ_{eff} of the adsorbate molecule in the adsorptive state, formal charge transfer coefficient γ, limiting Gibbs adsorption $\Gamma_{\max}$, and on the number of water molecules n replaced by one adsorbate molecule.

2 LITERATURE OVERVIEW

2.1 Thermodynamic conceptions of adsorption and basic equations for the calculation of the adsorption parameters of organic compounds at metal electrodes

The thermodynamic method for the finding of the adsorption parameters of organic compound on metal electrode is based on the fundamental electrocapillary equation and at constant pressure and temperature it can be written in the form [8, 9, 23, 30-33]

$$d\gamma = -\sigma dE - \sum \Gamma_i d\mu_i = -\sigma dE - RT \sum \Gamma_i d \ln a_i \qquad (2.1.1)$$

where γ and σ are the interfacial tension and surface charge density respectively; Γ_i, a_i and μ_i are Gibbs adsorption, activity and chemical potential of the component *i*, respectively, *T* is the absolute temperature and *R* is the gas constant. If a_i = const., then $d\ln a_i = 0$, and under these circumstances the so-called Lippmann equation has been received

$$-\sigma = \left(\frac{\partial \gamma}{\partial E} \right)_{a_i} \qquad (2.1.2.)$$

According to the Lippmann equation the differential capacitance is obtained as

$$C = \frac{d\sigma}{dE} \qquad (2.1.3.)$$

and after substitution of Eq. (2.1.3) into the Eq. (2.1.2) we can get the relationship for the differential capacitance

$$C = \frac{d\sigma}{dE} = -\left(\frac{\partial^2 \gamma}{\partial E^2} \right)_{a_i} \qquad (2.1.4.)$$

For solid electrodes, to a first approximation the interfacial tension γ should be replaced by the reversible surface work γ' term [23, 30 - 33].

According to the Eq. (2.1.1) the Gibbs adsorption of neutral organic compound on the electrode surface at constant potential, temperature and pressure is defined by

$$\Gamma_{org} = -\frac{1}{RT} \left(\frac{\partial \gamma'}{\partial \ln a_{org}} \right)_{E,T,p} \qquad (2.1.5)$$

where a_{org} is the activity of organic compound in the solution [23].

Non - thermodynamic methods for the calculation of the adsorption parameters of organic compounds at the metal electrodes are based on various electrical double layer (EDL) models and physical conceptions [22 - 33].

The first quantitative theory for adsorption of organic compounds at liquid electrodes has been developed by A. N. Frumkin at 1925 [26] and nowadays the various modern models base on this model. In this conception the behaviour of organic compound at metal electrode is discussed as the two parallel capacitor equivalent circuit, where one of the capacitor characterize the adsorbed water monolayer on the electrode surface and the other characterize capacitor are determined by the adsorbed organic compound monolayer parameters. The surface charge for such a system is defined as

$$\sigma = \sigma_0(1- \theta) + \sigma'\theta \qquad (2.1.6)$$

where σ_0 is the surface charge for the base electrolyte in the surface inactive solution (where $c_{org} = 0$), σ' is the surface charge density for the solution where the surface coverage $\theta = 1$. Using Eqs. (2.1.3) and (2.1.6) it is possible to obtain that

$$\sigma = C_0E\ (1 - \theta) + C'\ (E_{\sigma=0} - E_N)\ \theta \qquad (2.1.7)$$

where C_0 is the differential capacitance, when $\theta = 0$, C' is the differential capacitance, when $\theta = 1$, $E_{\sigma=0}$ is the zero charge potential and E_N is equal to the change in the surface charge potential value due to the displacement of a monolayer of water molecules by a monolayer of organic adsorbate. After differentiation of Eq. (2.1.7) with respect to E, we shall receive [22 - 33]

$$C = C_0(1-\theta) + C'\theta + (\sigma'-\sigma_0)\frac{d\theta}{dE} \qquad (2.1.8),$$

At the maximal adsorption potential (E_{max}) the derivative $d\theta/dE = 0$ and under these circumstances we can receive

$$C = C_0\ (1-\theta) + C'\theta \qquad (2.1.9).$$

The experimental surface coverage values at $E=E_{max}$ can be estimated using the Frumkin's model of the two parallel condensers [26]

$$\theta=(C_0-C)/(C_0-C') \qquad (2.1.10)$$

Thereafter, to a first approximation, usually the applicability of the Frumkin adsorption isotherm [23, 26, 30 - 33]

$$Bc_{org} = \frac{\theta}{1-\theta}\exp(-2a\theta) \qquad (2.1.11)$$

has been assumed where B and a are the adsorption equilibrium constant and molecular interaction parameter at E_{max}, respectively,.

The surface pressure of the adsorbate film π, can be calculated by using the backintegration method based on Eq. (2.1.4) as follows

$$\pi(E) = \gamma'_{c=0} - \gamma'_c = \int_{E_0}^{E} \sigma_c dE - \int_{E_0}^{E} \sigma_{c=0} dE \qquad (2.1.12)$$

where subscripts c and c=0 indicate the presence or absence of the adsorbate in the bulk of the base electrolyte, respectively [1 – 5, 23, 26].

The values of Γ and Γ_{max} can be calculated according to the Eq. (2.1.13)

$$\Gamma = \frac{1}{RT}\left(\frac{\partial \pi}{\partial \ln c}\right)_{E,T,p} \qquad (2.1.13)$$

Usually the values of Γ_{max} can be calculated from the slope of the linear part of the π, log c_{org} dependences (constructed at E=const). Using the obtained Γ_{max} and surface charge density values, we can calculate the Gibbs adsorption values according to the relation

$$\Gamma = \frac{\sigma_\Gamma - \sigma_{\Gamma=0}}{\sigma_{\Gamma_{max}} - \sigma_{\Gamma=0}} \Gamma_{max} \qquad (2.1.14)$$

The values of $(\sigma_{\Gamma_{max}} - \sigma_{\Gamma=0})$ can be obtained by the extrapolation of the linear section of the $\sigma(E)$ -curves.

The orientation of the adsorbate molecule, which is reflected in the molecular area S_A and can be correlated by Γ_{max} (if Γ_{max} corresponds to θ_{max} = 1) as

$$S_A = \theta_{max}/\Gamma_{max} N_A \approx 1/\Gamma_{max} N_A \qquad (2.1.15)$$

where Γ_{max} is the maximum Gibbs excess for organic compound at the electrode surface; N_A is Avogadro's number. The experimental values of S_A can be compared with the projections of Courtauld models for vertical and flat orientations [30].

The standard Gibbs energy of adsorption ΔG_{ads}^{0} at E_{max} is obtained as [1 – 5, 8, 9, 23, 26]

$$\Delta G^{\circ}_{ads} = -RT \ln (55.5\, B_m) \qquad (2.1.16).$$

Usually the experimental data to calculate the adsorption parameters of organic compounds adsorption at the metal electrodes have been obtained by the electrochemical impedance or by the chronoculonometric measurements method.

2.2 Adsorption kinetics of organic compounds

Frumkin and Melik-Gaikazyan first observed the frequency-dependence of the impedance of an Hg electrode adsorbing neutral organic molecules [3, 8, 9, 23]. For the case of adsorption kinetics controlled entirely by the rate of diffusion, they deduced the following expressions for the frequency-related admittance of the electrode [1 –5, 8, 9, 23, 27]

$$C_p = C_{true} + \frac{\Delta C\left[\left(\frac{\partial \Gamma}{\partial c}\right)_E \left(\frac{\omega}{2D}\right)^{1/2} + 1\right]}{\left[\left(\frac{\partial \Gamma}{\partial c}\right)_E \left(\frac{\omega}{2D}\right)^{1/2} + 1\right]^2 + 1} \tag{2.2.1}$$

$$\frac{1}{\omega R_p} = \frac{\Delta C\left[\left(\frac{\partial \Gamma}{\partial c}\right)_E \left(\frac{\omega}{2D}\right)^{1/2}\right]}{\left[\left(\frac{\partial \Gamma}{\partial c}\right)_E \left(\frac{\omega}{2D}\right)^{1/2} + 1\right]^2 + 1} \tag{2.2.2}$$

where Γ is surface concentration; μ is chemical potential; and ω is angular frequency equal to $2\pi f$; C_p is a parallel interfacial capacitance; $C_{true}=(\partial q/\partial E)_{\Gamma,\mu}$ is an interfacial capacitance as ac frequency $f \to \infty$, $C_0 = (\partial q/\partial E)_{\Gamma,\mu} + (\partial q/\partial \Gamma)_E (\partial \Gamma/\partial E)_\mu$ is a differential capacitance as $f \to 0$; and $\Delta C = C_0 - C_{true} = (\partial q/\partial \Gamma)_E (\partial \Gamma/\partial E)_\mu$ is an adsorption capacitance, caused by the dependence of Γ (or surface coverage θ) on E [8, 9,12 – 14, 23, 27].

As shown by Armstrong et al. [12], if the diffusion controlled relaxation time ($\tau_D=1/2\pi f_D$) is defined as

$$\tau_D = (\partial \Gamma/\partial c)^2{}_E / D \tag{2.2.3}$$

and a Cole–Cole distribution [10] of relaxation times about τ_D is assumed (with the particular value α=0.5 in their Eq. (2.2.13) [10], which for the case of relaxation of dielectric polarization leads to the frequency dependence of the real ε' and imaginary ε'' parts of the complex dielectric constant ε*) then Eqs. (2.2.1) and (2.2.2) can be rewritten as

$$C_p = C_{true} + \frac{\left(\Delta C\left[1 + (0.5\omega\tau_D)^{1/2}\right]\right)}{1 + (2\omega\tau_D)^{1/2} + \omega\tau_D)} \tag{2.2.4}$$

$$1/\omega R_p = \frac{\Delta C(0.5\omega\tau_D)^{1/2}}{1+(2\omega\tau_D)^{1/2}+\omega\tau_D} \tag{2.2.5}$$

Eqs. (2.2.4) and (2.2.5) require that $1/\omega R_p$ versus C_p (so called Cole-Cole plots) should take the form of a quarter-circle, intersecting the C_p-axis at the values C_{true} and (C_{true} +ΔC) [10-12].

For the case of adsorption kinetics controlled entirely by the rate of a heterogeneous charge transfer process, Frumkin and Melik-Gaikazyan [8, 9] deduced the following equations for the frequency-related admittance of the electrode:

$$C_p = C_{true} + \frac{\Delta C(\partial\nu/\partial\Gamma)^2_{E,c}}{\omega^2+(\partial\nu/\partial\Gamma)^2_{E,c}} \tag{2.2.6}$$

$$1/\omega R_p = \frac{\Delta C(\partial\nu/\partial\Gamma)_{E,c}\,\omega}{\omega^2+(\partial\nu/\partial\Gamma)^2_{E,c}} \tag{2.2.7}$$

where ν in mol cm^{-2} s^{-1} is the net rate of adsorption due to the departure from equilibrium conditions.

If

$$\tau_K = \left(\frac{\partial\Gamma}{\partial\nu}\right)_{E,c} \tag{2.2.8}$$

is defined as the relaxation time of the heterogeneous charge transfer (adsorption) process (τ_K=1/2πf_K), then Eqs. (2.2.6) and (2.2.7) become

$$C_p = C_{true} + \frac{\Delta C}{1+\omega^2\tau_K^2} \tag{2.2.9}$$

$$1/\omega R_p = \frac{\Delta C\,\omega\tau_K}{1+\omega^2\tau_K^2} \tag{2.2.10}$$

Thus, according to [12, 27], the $1/\omega R_p$ versus C_p plot should take the form of a semi-circle with a centre C_p=ΔC/2+C_{true}; $1/\omega R_p$=0. Eqs. (2.2.9) and (2.2.10) have the same form as the Debye–Pellet equations for the relaxation in a dielectric with a single relaxation time [10,12]. It should be noted that on the basis of the Frumkin adsorption isotherm, the following equations for the diffusion relaxation time

$$\tau_D = \frac{\Gamma_m^2\theta^2(1-\theta)^2}{c^2D\left[1-2a\theta(1-\theta)^2\right]} \tag{2.2.11}$$

and for the adsorption relaxation time

$$\tau_K = \frac{\Gamma_m \theta(1-\theta)}{\nu_0[1-2a\theta(1-\theta)]} \tag{2.2.12}$$

have been derived by Retter and Jehring [14] with the Frumkin interaction coefficient a, adsorption exchange rate ν_0 and Γ_{max}, characterizing the influence of the maximal Gibbs adsorption and the surface coverage θ on the corresponding relaxation times.

The situation of mixed diffusion and heterogeneous charge transfer control was studied in the most general case by Lorenz and Möckel [22, 29]. The frequency-related admittance has been expressed by the relations

$$C_p = C_{true} + \frac{\Delta C\left[1+(0.5\omega\tau_D)^{1/2}\right]}{\left[(0.5\omega\tau_D)^{1/2}+\omega\tau_K\right]^2+\left[(0.5\omega\tau_D)^{1/2}+1\right]^2} \tag{2.2.13}$$

$$1/\omega R_p = \frac{\Delta C\left[(0.5\omega\tau_D)^{1/2}+\omega\tau_K\right]}{\left[(0.5\omega\tau_D)^{1/2}+\omega\tau_K\right]^2+\left[(0.5\omega\tau_D)^{1/2}+1\right]^2} \tag{2.2.14}$$

If τ_K and τ_D are of the same order, the $1/\omega R_p$ versus C_p plot gives a gradual transition from a quarter-circle (at low ω when there is effectively complete diffusion control) to a semi-circle (at high frequencies when the control is effectively heterogeneous)[34].

According to the Lorenz model the impedance values in parallel to C_{true} can be calculated as [22, 29]

$$Z_1' = (0.5\tau_D)^{1/2}\omega^{-1/2}\Delta C^{-1} + \tau_K \Delta C^{-1} \tag{2.2.15}$$

$$Z_1'' = (0.5\tau_D)^{1/2}\omega^{-1/2}\Delta C^{-1} + (\omega\Delta C)^{-1} \tag{2.2.16}$$

If the diffusion is the limiting stage of an adsorption process, then the equilibrium values of differential capacitance at $\omega \to 0$ can be obtained by the linear extrapolation of the ΔC, $\omega^{1/2}$-dependence to $\omega^{1/2}=0$, as well as being calculated by Eq. (2.2.17)

$$\Delta C(\omega=0) = \Delta C^2(\omega) R_p^2(\omega)\omega^2 + \{(\Delta C(\omega) R_p(\omega)\omega - 1) R_p(\omega)\omega\}^{-1} \tag{2.2.17}$$

where $\Delta C(\omega)$ and $R_p(\omega)$ are the values of the differential (additional) capacitance and parallel resistance at ω=const [1, 28]. Thus, by extrapolating the $R_S(\omega)$-values to $\omega \to \infty$, the solution resistance $R_S(\omega)=R_{el}$ was determined. Since the amount of organic compound added is small and does not affect the solution resistance, one can assume R_{el} to be equal to the ohmic component R_S of the impedance in the pure base electrolyte solution [8, 9].

If, at a given frequency, the adsorption process is characterized by the additional capacitance $\Delta C(\omega)$ and by the parallel resistance $R_p(\omega)$, which are assumed to be parallel in the equivalent circuit, then for a slow diffusion step

$$\cot\delta = R_p(\omega)\Delta C(\omega) = 1 + \sqrt{2D}/(\partial\Gamma/\partial c)_E/\sqrt{\omega} = 1 + M/\sqrt{\omega} \qquad (2.2.18)$$

where M is the slope of the cot δ vs $\omega^{-1/2}$ plots.

At very low frequencies noticeable deviations have been observed, explained according to Lorenz [22, 29] and Damaskin et al. [11,23, 27] by the two-dimensional association of the adsorbed molecules in the interfacial region. In this case the value of cot δ can be calculated as

$$\cot\delta = \frac{k_1\left(k_2 + k_1\frac{\sqrt{\omega}}{M}\right) + \left(\frac{\omega}{\omega_0}\right)^2\left(k_3 + \frac{\sqrt{\omega}}{M}\right)}{\left[k_1^2 + \left(\frac{\omega}{\omega_0}\right)^2\right]\left(\frac{\omega}{\omega_0} + \frac{\sqrt{\omega}}{M}\right) + \frac{\omega}{\omega_0}\left(k_1k_3 - k_2\right)} \qquad (2.2.19)$$

where ω_0 is the exchange rate of the two-dimensional association, and k_1, k_2 and k_3 are certain constants characterizing the process of two-dimensional association [11,23, 27].

Usually, the components of the adsorption impedance were calculated from the impedance data of the cell used for the measurements (series circuit), i.e. from $C_S(\omega)$ and $R_S(\omega)$ following the procedure described in Refs. [23, 27, 28].

Experimental impedance data can be analysed using the equivalent circuits illustrated in Fig. 5, where R_{el} is the electrolyte resistance, C_{dl} and C_{ad} are the double layer and adsorption capacitances, respectvely; CPE is the constant phase element; Z_W is Warburg-like diffusion impedance and R_{ad} is the adsorption or partial charge transfer resistance [1-5,9,11-21, 33 - 41]. C_n and R_n are the capacitance and resistance of the "needle" adsorption-desorption peak formation [20]. The value of C_{dl} characterises the capacitance of the metal | electrolyte interface at ac $f \to \infty$; and C_{ad} is caused by the dependence of the electrode surface coverage θ on the electrode potential E.

Studying the difference between five equivalent circuits presented in Fig. 5, there are two accurate ways to obtain an indication of how well the modelling function reproduces the experimental data set: (1) observing the parameter values and their relative error estimates (in %); (2) the chi-square function (χ^2) and the weighted sum of the squares (Δ^2) also give a good indication about the quality of the fit [2-5,17-19, 36 -39]. It should be noted that the value of χ^2 function should decrease by tenfold if a new circuit element is introduced into the

equivalent circuit system, and the simplest equivalent circuit should be taken as a more reliable model of the interface if the values of χ^2 function are comparable [16-19, 36 -39].

In the case of classical Frumkin-Melik-Gaikazyan equivalent cirquit [8 , 9] (Fig.5b) the specific impedance and capacitance functions have the following forms

$$Z(\omega) = R_{\mathrm{el}} + \cfrac{1}{\mathrm{j}\omega C_{\mathrm{dl}} + \cfrac{1}{\cfrac{\sigma_{\mathrm{ad}}}{\sqrt{\mathrm{j}\omega}} + \cfrac{1}{\mathrm{j}\omega C_{\mathrm{ad}}}}} \qquad (2.2.20)$$

and

$$C(\omega) = \frac{1}{\mathrm{j}\omega[Z(\omega) - R_{\mathrm{el}}]} = C_{\mathrm{dl}} + \frac{C_{\mathrm{ad}}}{1 + \sigma_{\mathrm{ad}} C_{\mathrm{ad}} \sqrt{\mathrm{j}\omega}} \qquad (2.2.21)$$

where $\sigma_{\mathrm{ad}}(\mathrm{j}\omega)^{-1/2}$ represents the diffusion (Warburg-like) impedance Z_{W} with its coefficient σ_{ad}.

For the better fit of the complex plane plots in the region of maximal adsorption (where a compact adsorption layer occurs at the some parts of the electrode surface), additionally the ZView for Windows (Version 2.2) fitting program can be used [19], where the generalised finite Warburg element (GFW) for a short circuit terminus model is expressed as

$$Z_{\mathrm{GFW}} = \frac{R_{\mathrm{D}} \tanh\left[(\mathrm{j}T\omega)^{\alpha_{\mathrm{cat}}}\right]}{(\mathrm{j}T\omega)^{\alpha_{\mathrm{cat}}}} \qquad (2.2.22)$$

where $T = L^2 / D$ (L is the effective diffuse layer thickness and D is the effective diffusion coefficient of a particle); R_{D} is the so-called limiting diffusion resistance as at very low frequencies Z' approaches R_{D} and Z'' tends to zero [1 - 5, 35 - 45]. It should be noted that the fractional exponent α_{cat} is equal to 0.5 in Eq. (2.2.22) in the case of finite length Warburg short circuit terminus model (FLW), which is the solution of the one-dimensional diffusion equation of a particle, being completely analogous to the wave transmission in a finite-length R,C transmission line model [1 – 5, 42 - 45].

According to the model developed by Wandlowski and de Levie [18 - 21], the isotropic two-dimensional cluster will mostly grow at its periphery where the rate of growth is proportional to the interfacial adsorbate concentration Γ on that part of the interface which is not yet covered by clusters, and on the periphery length $2\pi r$ with a proportionality constant k_{g} (i.e. k_{g} is the rate constant of the cluster growth). The rate constant of the reverse process (i.e. edge dissolution) is defined as k_{d}. However, the growth and dissolution of cluster will be assumed to have another pathway available as well, i.e. for the cluster | electrolyte interface

the rate constants k_g' and k_d' are assumed. Under these conditions the following expression for the cluster formation (rate) is valid

$$\frac{dS}{dt} = 2\pi r(k_g \Gamma - k_d) + \pi r^2 (k_g' c_{cat} - k_d') \qquad (2.2.23)$$

where S is the area of the cluster, t is time, Γ is the (absolute) interfacial excess, and c_{cat} is the adsorbate concentration, here assumed to be uniform up to the interface [20]. Thus, according to this model, the interface is composed of areas covered by clusters, and other areas not so covered, with the charge densities Q_1 and Q_0, respectively [20]. The charge density of the electrode, Q, is given by

$$Q = Q_0(1-\theta) + Q_1\theta \qquad (2.2.24)$$

Current density j is given by

$$j = dQ/dt = (Q_1 - Q_0)d\theta/dt + (1-\theta)dQ_0/dt + \theta\, dQ_1/dt \qquad (2.2.25)$$

As shown in [20], the first term of Eq. 2.2.25 describes the dominant features of the needle peak at low frequencies. The sinusoidal perturbation of the potential can be expressed as $E = E' + E''e^{jwt}$, the cluster radius as $r = r' + r''e^{jwt}$, the cluster area as $S = S' + S''e^{jwt}$, the interfacial adsorbate concentration as $\Gamma = \Gamma' + \Gamma''e^{jwt}$, the extended area fraction as $\theta_x = \theta_x' + \theta_x''e^{jwt}$, the area fraction as $\theta = \theta' + \theta''e^{jwt}$, and the current density as $j = j' + j''e^{jwt}$. Thus, according to [20] the current density of the needle adsorption-desorption peak is given as

$$j_n = j_n' + j_n''e^{jwt} \qquad (2.2.26)$$

and

$$\begin{aligned} j_n'' &= j\omega(Q_1 - Q_0)\theta'' = j\omega(Q_1 - Q_0)e^{-\theta_x'}\theta_x' \\ &= j\omega(Q_1 - Q_0)e^{-\theta_x'} 4\pi k_g (\partial\Gamma/\partial E)E''\textstyle\sum r' / (2j\omega - k_g' c + k_d') \end{aligned} \qquad (2.2.27)$$

from which the following impedance of the needle adsorption-desorption peak can be calculated [20]

$$Z_n = E/j_n'' = (2j\omega - k_g' c + k_d') \Big/ \left\{ j\omega(Q_1 - Q_0)e^{-\theta_x'} 4\pi k_g (\partial\Gamma/\partial E)\textstyle\sum r' \right\} \qquad (2.2.28)$$

Thus, impedance of the needle peak can be expressed by a series combination of formation resistance (R_n) and capacitance (C_n), of the needle peak (Fig. 5, circuit e)

$$R_n = 1 \Big/ \left\{ (Q_1 - Q_0)e^{-\theta_x'} 4\pi k_g (\partial\Gamma/\partial E)\textstyle\sum r' \right\} \qquad (2.2.29)$$

$$C_n = \left\{ (Q_1 - Q_0)e^{-\theta_x'} 4\pi k_g (\partial\Gamma/\partial E)\textstyle\sum r' \right\} \Big/ (k_d' - k_g' c) \qquad (2.2.30)$$

For dilute TBN^+ solutions, the diffusion effects are not yet completely negligible and

therefore it must be introduced the time-dependent interfacial concentration (i.e. surface concentration depends on ac frequency) in the form $c = c' + c''e^{jwt}$ and

$$\Gamma'' = (\partial\Gamma/\partial E)E'' + (\partial\Gamma/\partial c)c'' \quad (2.2.31)$$

Thus, there is a difficulty in that the boundary condition defining the interfacial flux will now be heterogeneous, and there is no exact solution for this non-trivial problem yet [20].

2.3 Adsorption of organic compounds at the electrode | base electrolyte interface

The adsorption of organic compound on the solid electrode | base electrolyte solution interface and the formation of EDL (electrical double layer) is determined by the interaction energies between the particles participated in the adsorption process (organic molecules, water molecules, base electrolyte ions, surface atoms of the electrode metal) [2,11,30 - 32].

The Gibbs adsorption energy for the uncharged organic compound adsorbed on the uncharged metal | electrolyte interface can be expressed as

$$\Delta G°_{ads} = \Delta G°_{air} + \Delta G°_{sol} + \Delta G°_{Me\text{-}A} - \Delta G°_{Me\text{-}water} \quad (2.3.1.)$$

where the Gibbs energy of the metal-water interaction $\Delta G°_{Me\text{-}water}$ (so- called hydrofilicity) corresponds to the model that the number of water clusters replaced by one adsorbed organic molecule, $n \approx 1$, $\Delta G°_{air}$ is the Gibbs adsorption energy of organic molecules on the air | solution interface, $\Delta G°_{sol}$ is the increase of the Gibbs energy of adsorbate caused by the so-called salting out effect (interaction between organic molecules and the base electrolyte ions) and $\Delta G°_{Me\text{-}A}$ is the Gibbs interaction energy between the adsorbed organic molecules and the electrode surface atoms [30].

The Gibbs energy of adsorption can be calculated as the sum of differences between the chemical potentials of adsorbate ($\mu°_{ads}$) and n solvent (water) molecules ($n\mu°_{water}$) at the surface of the electrode and in the bulk of a solution, respectively

$$\Delta G°_{ads} = (\mu°_{ads,\,s} - n\mu°_{water,\,s}) + (n\mu°_{water,\,b} - \mu°_{ads,\,b}) \quad (2.3.2)$$

where the second term is independent of the surface (metal) nature [30].

The value of $\Delta G°_{air}$ depends on the molar volume of the adsorbate, its molecular structure and on the presence of hydrophilic (polar) groups on it, because the solution of the organic compound in water (electrolyte solution) breaks the hydrogen bonds between the associated water molecules and therefore changes both the entropy and the internal energy of

water. In the case of linear aliphatic compounds (alcohols, esters, ketones, amines and carboxylic acids) the values of $\Delta G°_{air}$, to a first approximation, can be obtained by the following generalized correlation equation [25,30]

$$\Delta G°_{air} = -0.8\, R_A\, (1 - 2{,}5\times10^{-3}\, R_A) \qquad (2.3.3)$$

where the molecular refraction R_A of the organic compound is obtained as

$$R_A = M\,(n^2 - 1) / d\,(n^2 + 2) \qquad (2.3.4)$$

In Eq. (2.3.4) n is the refractive index, M is the molar mass and d is the density of organic compound. The dependence of the $\Delta G°_{air}$ on chemical nature of the linear aliphatic compound is very weak and, to a first approximation, it is independent of the chemical nature of the different functional groups in the adsorbate molecule [30].

The values of $\Delta G°_{sol}$ have been calculated according to the equation

$$\Delta G°_{sol} = -2.3RTc_{sol}lgK_{sol} \qquad (2.3.5)$$

where K_{sol} is the salting – out constant of adsorbate and is c_{sol} the concentration of the surface inactive electrolyte. According to the systematic analysis of the experimental data, to the first approximation, [25, 30] it can be concluded that the dependence of K_{sol} on the chemical nature of the aliphatic compound studied is weak and so the values of K_{sol} for the 0.1 M NaF and 0.05 M Na_2SO_4, established in [25, 30], can be used.

Comparison of the adsorption data for various aliphatic organic compounds shows that the value of $\Delta G°_{ads}$ increases in the order of electrodes Zn(2110)< Zn(1010)< Zn(0001)< Ag(110)< Ag(111)< Cd(1120)< Cd(1010)< Cd(0001)< Bi(111)< Bi(001)< Hg< Bi(211)< Bi(011)< Sb(111)< Sb(001)< Sb(211) as the hydrophilic properties of electrode surface decreases [25, 30 - 32].

2.4 Influence of the crystallographic structure of electrode surface on the adsorption of organic molecules

Electrochemical properties of a solid metal surface depend significantly not only on the chemical composition but also on the crystallographic structure of the surface of a metal studied [1 – 5, 11, 18, 23, 25, 30 - 33]. The discovery of the splitting effect of the adsorption – desorption maxima for organic compounds [16] played an important role in developing the theory of electric double layer and adsorption for the solid polycrystal surface [23, 27, 30-33, 46].

It was found [11,23, 28, 30 – 32, 50] that the shape of an adsorption isotherm is very sensitive to the crystallographic structure of the electrode surface. To obtain the share of the various single crystal planes at a polycrystal surface the linearised Frumkin isotherm in so-called logarithmic coordinates ($\ln[\theta/(1-\theta)c]$ vs. θ) can be used. According to the experimental data [25, 30 –32, 50] the isotherms for polycrystal electrodes are located between the partial isotherm for the less – active Bi(111) and more-active Bi(011) planes. The adsorption isotherms for polycrystal electrodes have very complicated shapes, being nonlinear in the whole region but sometimes there are small linear regions too, which characterize the microscopically homogenous areas on the macropolycrystalline electrode surface, as the adsorption activity of an organic compound is different on various monocrystal areas [30 –32, 50]. Therefore the shape of the adsorption isotherm can be a good polycrystallinity indicator [33, 50].

The potential of zero charge (pzc) of the single crystal electrodes depends noticeably on the homogeneity of the electrode surface i.e. on the crystallographic structure of the surface. According to the experimental results [30 –33, 50] for Bi (001), (011), (211) and (101) planes the difference of pzc is not more than 20 mV. The difference between pzc-s for Bi(111) and other Bi planes is approximately 60 mV and this is mainly caused by the specific electronic properties of Bi(111) plane. The influence of the solvent nature on the pzc values decreases in the following direction: AN>H_2O>MeOH>i-PrOH>EtOH, because of decreasing the specific interaction between the solvent molecules and the electrode surface atoms decreases in the same order [30 –33, 50].

Hydrophilicity of the Bi planes increases in the following order Bi(011) <Bi(211) < Bi(001) <Bi(111) and therefore the free energy of organic compound adsorption, ΔG_A, decreases in the same order of Bi planes [30 –33, 50]. The reticular density of the surface atoms increases and the free energy of adsorption ΔG_A decreases in the direction of Bi planes (011) < (211) < (001) < (111) [30 –33, 50]. The same behaviour was detected if the adsorption of n-ButOH, iso-ButOH, sec-ButOH, tert-ButOH, CH and PY (n-butanol - n-ButOH, iso-butanol -iso-ButOH, sec- butanol, sec-ButOH, tert-pantanol -tert-ButOH, cyclohexanol -CH and pyridine -PY) on the bismuth single crystal plane electrodes has been studied [30 –33]. Attraction coefficient a increases and the adsorption activity decreases in the following order of Bi planes (011) > (101) > (001) > (111) which may be caused by the more vertical orientation of the organic compounds on the more hydrofilic electrode surface.

2.5 Adsorption of tetraalkylammonium cations on Bi, Hg and Au electrodes.

The survey of earlier works on quaternary ammonium ions indicates that the adsorption of quaternary ammonium ions has been of interests to many workers, that anion co-adsorption may complicate the analysis data, and that slow interfacial kinetics may also be involved[15 - 21].

Organic cations which have been found specifically adsorbing tend to influence the process of electroreduction of ions. The reduction that is limited by the electron transfer is accelerated by inorganic cations as well as organic tetraalkylammonium cations (TAA^+) in entire region of potentials where the adsorption occures[27, 47 - 49]. The rate of reduction increases as the number of carbon atoms increases at tetraalkylammonium cation chains as their adsorbtivity increases[47]. The most likely to inorganic ions is the tetrametylammonium cation (Me_4N^+) as expected and its influence on the reduction of the anion is predicted by its charge. Also the second type of anions exists which rate of reduction is lowered by the TAA^+ [27, 47, 51]. The behaviour of TAA^+ on polycrystalline gold electrode have been found dependent on the number of carbons in alkyl chain[17]. Apart from the mercury and bismuth electrodes Me_4N^+will not adsorb on the surface of gold. This is in consistence with the fact that the capacitance minimum of the diffuse layer is independent from the concentration of the Me_4N^+in the solution[17]. The adsorption increases remarkably as the length of the carbon chain increases. The formation of the condensed layer is possible[17].

The experimental resalts reveal that the tetrabutylammonium cations do not interact specifically with the metal surface but they are expelled from the bulk of the solution. The capacity of the electric double layer depends noticeably on the metal of the electrode as tetrametyl and tetraetylammonium cations adsorb. In the case of the most strongly adsorbing tetrabutylammonium cations the capacitance does not depend on the metal nature [17]. The region of the adsorption of the TAA^+ decreases as the adsorbtion of the anions increases. In the case of gold the region of maximum adsorption decreases as the length of the carbon chain of TAA^+ increases. At strongly negative potentials the capacity is independent of the TAA^+ studied[32] and in the case of Bu_4N^+ and tetrapentylammonium cation (Pen_4N^+)the minimum of the capacitance of the diffuse layer will not appear. This is caused by the far stronger interaction with the metal. The same phenomenon has been found on mercury dropping electrode[18]. At far negative potentials the value of the capacitance remained the same in the case of the Bu_4N^+ solution if bismuth, gold or mercury electrodes were used. Accordingly Bu_4N^+ cations do not interact specifically with the surface.

The adsorption of TAA^+ is dependent of anion. If the anion is an halid the adsorption increases in the order F-<Cl-<Br-<I- [52 - 63]. Investigations of the system Hg|electrolyte water solution have revealed that the concentration of tetrapentylammonium bromide on the surface of the Hg is greater than in the saturated solution [53 - 54]. Damaskin et al [49] described it as the increase in the interaction between specifically adsorbed cations and halide anions.

The shape of the capacitance needle at negative potenetials depends on anion. In mixed electrolytes an additional sharp peak appears as the cations on the surface change [18]. On the process of the desorption of the Bu_4N^+ the cations of the electyrolyte adsorb.

The surface of the TAA^+ perchlorate- water /polycrystalline gold is described by the simple cirquit of active resistance and CPE element which are connected series [17].

Quaternary ammonium salts have been widely examined with the wide range of physical methods. These results show that TAA^+ cations cause different structure of water molecules in solution if the number of carbons in alkyl chain is greater than 3. These association effects depend on the hydrophobic properties of the cation and the anion. In the case of the quaternary ammonium salts the ion pairs situate in the lattices of the water molecules which are more structurated than in pure water[64 - 67]. These so called clatrate hydrates also exist on metal solution surfaces and their structure is dependent on the elecrical field of the double layer [68].

As supporting electrolytes commonly NaF, NaCl, NaBr, NaI, NaSCN, $NaClO_4$ and Na_2SO_4 were used [52 - 69]. Many features are strongly influenced by the nature of the supporting electrolyte anions. In general, the behavior in NaF and Na_2SO_4 solution differ from that in NaBr and NaI, while the other electrolytes exhibit intermediate behavior. The position of the adsorption desorption peak is independent of the nature of the electrolyte but its shape becomes sharper in the sequence SO_4^{2-}< F^-< Cl^-< Br^-< ClO_4^{2-}< SCN^-<I^-.

The pit capacitance is independent of the nature of the electrolyte anion used. The constancy of the pit capacitance in solutions of different electrolytes suggests that the compact layer in the pit region contains only tetrabutyl ammonium ions. This does not indicate weather water may be included in that layer[18]. In the presence of sufficiently high concentrations of Br^-, I^-, SCN^- and ClO_4^- ions the pit is metastable and gives way to another condensed phase which most likely contains anions.

In the highly concentrated Bu_4N^+ solutions in the presence of Br^-, I^-, SCN^- and ClO_4^- the capacitance of the pit is virtually the same as that of the film that replaces it so that it is no longer possible to distinguish between the two states from capacitance measurements. The

transition between those two states can be described as a process of nucleation and growth or an autocatalysis [19]. While substituting a cation and keeping an anion the same in C,E-curves have a pronounced effect on the position of the negative capacitance peak has been observed. The peak potential shifts towards more positive potential values in the order Li^+< Na^+<K^+< Rb^+<Cs^+. This is a result that common alkali metal ions (Na^+, K^+) are weakly specifically adsorbed at sufficiently negative potentials [19].

The complete desorption of Bu_4N^+ at sufficienly negative potentials demonstrates its ambivalent adsorption behavior. These results point to the formation of an adsorbed structure which involves co-adsorption of anions such as Br^-, SCN^-, ClO_4^- and I^-. Such anion co-adsorption, which may involve ion pairs of the type Bu_4NX and/or $(Bu_4)_2X^+$ and which may serve to reduce the electrostatic repulsion between the adsorbed cations, can persist at the most negative potentials of the adsorption region. Anion co-adsorption plays a significant role in the sudden desorption which gives rise to the needle peak [18 - 20].

For the dilute adsorbate concentrations $c<10^{-5}$M, the C-E curves exhibit a large scan rate and stirring dependant hysteresis, clearly associated with adsorbate mass transport. This hysteresis decreases as the concentration of Bu_4N^+ increases. [40]

As the narrow adsorption desorption peaks are also reported for some other neutral species their likely interpretation must be a general one, regardless of weather the adsorbate is a salt or a neutral species. [15 - 17]

In general , needle peaks are observed in solutions with quite high Bu_4N^+ concentrations, which makes it unlikely that they are predominantly controlled by diffusion like the more usual desad peaks [20].

The experimental data reveal that the interfacial admittance of the needle is well represented by the equivalent circuit of Fig. 5(e) in [20].

3 EXPERIMENTAL

The experimental procedure used in this work has been described in Refs. [1–5]. The final surface preparation of a Bi(hkl) electrode was obtained by electrochemical polishing in an aqueous KI + HCl solution. After that, the electrodes were carefully rinsed with ultra purified water and polarised at -1.0 V vs. Ag|AgCl|KCl (sat.) in H_2O (Ag|AgCl) in the working surface-inactive solution for 2 hours. The electric double layer impedance was measured using an Autolab PGSTAT 30 with a FRA 2 ($0.1 < f < 10000$ Hz, 5 mV modulation), and the system was calibrated using various standard equivalent circuits. The quality of the electrodes was tested by X-ray diffraction as well as AFM and STM methods [70].

Water for preparing the solutions was treated with the Milli Q+ purification system. Solutions were prepared volumetrically using Na_2SO_4 and $(C_4H_9)_4NI$ purified by triple recrystallization from water and treated in vacuum to dryness. Na_2SO_4 was calcined at 700°C immediately prior to the measurements. Electrolytic hydrogen was bubbled for 1–2 h through the electrolyte before the submersion of the electrode into the solution and temperature was kept at 298 ±1 K. [70]

4 RESULTS AND DISCUSSION

4.1 Cyclic voltammograms (CVs)

The CVs (scan rate 5 mV s^{-1}) were recorded in order to determine the quality of the surfaces investigated and the potential range in which the adsorption of tetrabutylammonium cation (TBN^+) occurred. The shape of the CV recorded for the supporting electrolyte was characteristic of the Bi($01\bar{1}$) plane in accordance with our previous studies [1–5, 70]. The cyclic voltammetry curves also indicate that the bismuth single crystal plane investigated is ideally polarizable within the potential region from -1.65 to -0.40 V (Ag|AgCl) in aqueous 0.05 M Na_2SO_4 solution. The same potential region of ideal polarizability was obtained according to the impedance data (Fig. 1). The noticeable increase in the current density for the solutions with addition of TBN^+ at E < -1.7 V (Ag|AgCl) is mainly caused by the weak

specific adsorption of TBN^+ ions at Bi($01\bar{1}$) (as the adsorption-desorption maxima have been established in the *C*,*E* curves (Fig. 2)) as well as by the shift of the zero charge potential toward less negative potentials, and by slow hydrogen evolution reaction at $E <$ -1.7 V (Ag|AgCl). It should be noted that the data measured at $E <$ -1.65 V have not been used for the quantitative analysis.

4.2 Complex plane (Z", Z') – plots

The complex plane plots [70] (so-called Nyquist plots, where the imaginary component $Z'' = 1/jC_s\omega$ ($j = \sqrt{-1}$, C_s is series resistance and angular frequency $\omega = 2\pi f$, where f is ac frequency, and Z' is the real part of the impedance) at different electrode potentials in the pure base electrolyte solution (Fig. 1) are in a good agreement with the data established in Refs [2,3]. The equivalent circuit parameters were calculated by fitting the impedance function to the measured spectra by a non-linear least squares fitting minimisation method [37,38], as well as by the "ZView for Windows (2.2)" program" [39, 70]. However, the results obtained using "ZView for Windows" will be discussed mainly in this paper.

The non-linear least square fitting data show that the *Z''*,*Z'*-curves (Fig. 1) for the Bi($01\bar{1}$) | base electrolyte interface can be described by the equivalent circuit which assumes that the interfacial impedance is in a form of the constant phase element (CPE) (the CPE impedance $Z_{CPE} = A^{-1}(j\omega)^{-\alpha}$, where A ($\mu F^{\alpha}\Omega^{\alpha-1}$ cm^{-2}) is a CPE coefficient and α is a fractional exponent (if $\alpha = 1.0$, then A simplifies to the double layer capacitance C_{dl})), R_{el} is the electrolyte resistance and R_{ad} is the adsorption (or partial charge transfer) resistance [1-5,35, 37, 40, 41]. According to the results of calculations, the value of R_{el} is practically independent of E but the values of α and A depend very slightly on E, and A has a small minimum at $E \sim$ -1.0 V (Ag|AgCl). The values of R_{ad} have a maximum in the region of $E \sim$ -1.0 V (Ag|AgCl), and R_{ad} decreases with the rise of the negative polarisation ($E <$ -1.65 V), which is caused by a slow cathodic process on the Bi planes (probably hydrogen evolution) at potentials more negative than -1.65 V. A small decrease of R_{ad} takes place in the region of positive polarisation ($E \geq$ -0.4 V), which is caused by the initial state of the surface oxidation of the Bi($01\bar{1}$) electrode. These potential regions ($E >$ -0.4 V and $E <$ -1.8 V) have not been used

for the quantitative analysis of the impedance data. According to Refs. [9-15, 35], R_{ad} in parallel to CPE means that a very slow adsorption-desorption process (i.e. a partial transfer process [1-5]) of the base electrolyte ions is possible. However, the very high R_{ad} values ($R_{ad} \geq 15000\ \Omega\ cm^2$) indicate that this process is very slow on Bi($01\bar{1}$) plane [1-5] and therefore the co-adsorption of the base electrolyte ions with TBN^+ cations can be neglected to a first approximation. On the other hand, R_{ad} in parallel to the double layer capacitance can also be traced back to a slow "true" heterogeneous charge transfer process not related to the adsorption-desorption process of the electrolyte ions [9,11-16]. However, the very low current density (j) values and very weak dependence of j on electrode potential, as well as very high R_{ad} values indicate the absence of quick "true" Faradaic reactions on the Bi single crystal plane | base electrolyte interface [1-5].

As for other real Bi single crystal plane electrodes [1-3], the impedance measured for Bi($01\bar{1}$) in the double layer region (no Faradaic current) follows a power law, such as that for the CPE [1-5, 33], with a value of the fractional exponent $\alpha \geq 0.96$, and the phase angle observed for the Bi single crystal planes is between -86° and -88°. To a first approximation, the values of α slightly lower than 1.0 can be explained by the very weak geometric and energetic inhomogeneities of the electrode surface (mainly on the nanoscopic and atomic scale) [1-5, 33]. Another explanation for the capacitance dispersion ($\alpha \leq 1.0$) would be the weak specific adsorption of the ions (mainly anions) as, due to the exponential dependence between the rate coefficient and adsorption activation energy, a relatively narrow distribution of surface energy (i.e. the weak energetic inhomogeneity of the solid surface) causes a broad distribution of the rate coefficients (or relaxation time constants) and, therefore, the more pronounced dependence of impedance on the ac frequency [1, 33, 35, 41]. However, the values of α obtained from 0.96 to 0.98 are practically independent of the electrode potential and can be explained mainly by the very weak geometric and energetic inhomogeneities of the Bi electrodes [1-5]. It should be noted that these conclusions are in a good agreement with the results in literature [33 – 37, 71] devoted to the conception of so-called "ideally polarizable electrode" [1-5]. The main results established can be reviewed as a conclusion that there is no ideally polarizable electrodes if $\alpha \neq 1.0$ [33, 70, 71]. Thus, from the physical point of view there are problems with the conception of "ideally polarizable electrode" for the solid electrodes but the classical conception takes into account only the fact that the Faradaic current has to be minimal [71]. It should be noted that the discussion of physical reasons for

the deviation of α from unity for the Bi($01\bar{1}$) | electrolyte interface is not a main aim of this paper.

The Z'',Z'-curves for the base electrolyte solution with various additions of TBN^+ ions are presented in Fig. 2 (points – experimental data, solid lines – calculations according to the Wandlowski-de Levie model, discussed later), and C,E-curves at constant ω (but at different concentrations of TBN^+, c_{cat}) are given in Fig. 3. In agreement with the Frumkin and Melik-Gaikazyan model [8-14], at constant potential, the values of C_s depend noticeably on ω in the region of the adsorption-desorption maxima E^{peak} as was found for CH, *tert*-PenOH, DDS and *n*-HepOH adsorption on Bi planes [1-5]. This is mainly caused by the dependence of surface coverage θ on E, i.e. by the dependence of $(\partial\theta/\partial E)_\mu$ on ω in a good agreement with the ideas of Refs. [8,9,11-14]. There is a weak dependence of C_s on f [15, 16, 70] in the region of maximal adsorption (E_{max}), where the very well pronounced capacitance depression takes place, characteristic of the adsorption of organic compounds and organic cations on the Hg, Au and Hg like metals [30-33]. In the region of maximal adsorption, C_s decreases with increasing c_{cat}. In the region of adsorption-desorption (E^{peak}), C_s rises with the increase of concentration of the adsorbate in the solution and there is a nearly linear dependence of C_s on $\omega^{1/2}$ in the region of moderate frequencies, characteristic of the mainly diffusion-limited process [1-8,11-14, 33]. At $E > E_{\sigma=0}$, adsorption of the I^- ions takes place at Bi($01\bar{1}$) like Hg, Au and polycrystalline Bi [30-32], but these data can not be used for the quantitative analysis, because the surface oxidation of the Bi($01\bar{1}$) plane is possible at E > -0.5 V (Ag|AgCl).

The dependences of R_s (series resistance) and R_p (parallel resistance) on $\omega^{1/2}$ at fixed electrode potentials and c_{cat} are given in Fig. 3 (b). According to these results, the values of R_s and R_p noticeably increase with decrease of ac frequency at E > -1.6 V (Ag|AgCl), and the very high R_s values at $\omega \to 0$ indicate that there is no quick Faradaic reactions at Bi($01\bar{1}$) | 0.5 M Na_2SO_4 + x M $(C_4H_9)_4NI$ solution interface. However, the noticeable difference between R_p and R_s values at more negative potentials ($E \leq$ -1.7 V) indicates that the partial charge transfer between Bi($01\bar{1}$) surface and TBN^+ ions or the "true" Faradaic processes are possible.

The shape of the Z'',Z'-plots depends noticeably on the electrode potential as well as somewhat on concentration of the TBN^+ ions in the solution (Fig. 2). Within the range of potentials $-1.65 \leq E \leq$ -1.45 V (Ag|AgCl), Z'',Z'-plots can be simulated, to a very rough approximation, by the depressed semicircles with the centre displaced below the real axis,

which indicates that the relaxation time τ is not a simple-valued quantity but is distributed continuously or discretely around a mean $\tau_m = \omega_m^{-1}$ value [37, 70] (more correct analysis of the *Z''*,*Z'*-data will be given later). On the other hand, these arcs can be substantially distorted by other relaxations whose mean time constants are within two orders of magnitude or less of that for the arc under consideration. Thus, according to the data in Fig. 2, two limiting stages (diffusion and adsorption or a (partial) charge transfer processes [1-5,9-4]) seem to be valid for the Bi($01\bar{1}$) | 0.05 M Na_2SO_4 + *x* M TBN^+ solution interface. The value of $Z'(\omega\rightarrow\infty) \equiv Z_\infty = R_\infty$ (Fig. 2) is practically independent of concentration of TBN^+ in the solution and the value of R_∞ can be taken equal to the electrolyte resistance R_{el}. However, the values of the heterogeneous relaxation time τ_m as well as Z''_{max} (imaginary impedance component *Z''* at τ_m) and the half-width of the arc on the real axis $(R_0 - R_\infty)/2$ (where R_0 is the real impedance component *Z'* as ω=0) as well as $Z'(\omega\rightarrow 0) \equiv R_0$ depend noticeably on concentration of the organic cation adsorbed (τ_m is proportional to c_{TBN^+}) and the adsorption resistance increases with increasing c_{TBN^+} in the solution.

According to the data in Fig. 2, at constant c_{TBN^+} and *Z'*, the value of |*Z''*| is maximal within the region of maximal adsorption (-1.2 < *E* < -0.65 V (Ag|AgCl)). The depression angle β' [8 – 14, 37, 70] has minimal and R_0 has maximal values in this region of potentials (the values of β' equal to 45° and 0° are characteristic of the purely diffusion limited process and heterogeneous charge transfer step, accordingly).

The dependence of phase angle δ (δ = arctan(|*Z''*|/*Z'*)) on log*f* has a minimum at $f \geq 2\times10^3$ Hz (Fig. 4 (a)) and the δ,log*f*-plots have very well exposed plateaus with $|\delta| \leq 80°$ at $f \leq 200$ Hz, characteristic of nearly pure capacitance behaviour ($|\delta| = -90°$). However, there is an additional maximum in the phase angle vs. log *f* plots for the data obtained in the region of maximal adsorption, which is probably due to the formation (or dissipating) of the two-dimensionally associated layers at some parts of the electrode surface. $|\delta|$ decreases somewhat at the negative potentials ($E \leq -1.45$ V) and at very low frequencies, which may be connected mainly with a partial charge transfer process or very slow Faradaic processes, occurring at very low frequencies [2-5, 70]. The shape of the δ,log*f*-curves is practically independent of electrode potential at $f \geq 100$ Hz (except $E \leq -1.65$ V and $E \geq -0.65$ V), but the region of intensive increase of $|\delta|$ with *f* (at constant $(\partial\delta/\partial f)_{c_{TBN^+}}$) is shifted toward lower values of *f* with the increase of negative polarisation, i.e. with the decrease of θ or Gibbs

adsorption Γ_{TBN^+}. The maximal values of $|\delta|$ increase very slightly with increasing c_{TBN^+} (Fig. 4 (c)), but the region of intensive increase of $|\delta|$ with *f* is noticeably shifted toward lower values of *f* with the decrease of c_{TBN^+}. The noticeable shift of δ,log*f* plot for *E* = -0.65 V can be explained by the specific adsorption of the I^- anions at the Bi($01\bar{1}$) surface in this potential region, and by the noticeably lower relaxation frequencies of the specifically adsorbed I^- anions [72].

4.3 Fitting of impedance data

The parameters for some systems, calculated by the "ZView for Windows 2.2" program, are given in Table 1.

Non-linear regression analysis [39] of the *Z*'',*Z*'-curves shows that in the region of potentials from –1.65 to –0.6 and at c_{TBN^+} less than 1×10^{-5} M, these data can be simulated with the classical Frumkin-Melik-Gaikazyan equivalent circuit presented in Fig. 5 (circuit b). The attempts to add some additional elements in this equivalent circuit (mainly an adsorption or charge transfer resistance R_{ad} (circuit c in Fig. 5)) did not give a better fit as it was found for Br^- adsorption on Au planes [35]. Thus, to a first approximation, in the case of less concentrated TBN^+ solutions it seems that the heterogeneous adsorption step of TBN^+ ions is comparatively quick and reversible at the Bi($01\bar{1}$) plane [17, 35]. This result is in a good agreement with the data for other aliphatic compound adsorption on the Bi planes studied [1-5]. The results of fitting by using the CPE instead of C_{dl} (circuit d in Fig. 5) did not give a noticeably better agreement of the calculated *Z*'',*Z*' plots with experimental ones and, for that reason, these results have not been discussed in more detail in this work [70]. Therefore, to a first approximation, the classical Frumkin-Melik-Gaikazyan circuit seems to be a more probable physical model for the adsorption layer formed at the Bi($01\bar{1}$) plane in the less concentrated TBN^+ solutions as it is the simplest circuit that gives a better fit to experimental results at potentials less negative than E^{peak}.

For the simulation of the Warburg-like diffusion impedance Z_W values, at first we used the classical Frumkin-Melik-Gaikazyan approximation, where diffusion of the molecules is assumed to be semi-infinite [1-5,8,9,11,13, 14, 37] with $\alpha_{cat} = 0.5$.
According to the data of simulations, there is a reasonable agreement of experimental results with the fitting data if α_{cat} has been fixed at 0.5 (Table 2).

For the better fit of the complex plane plots in the region of maximal adsorption (where a compact adsorption layer occurs at the some parts of the electrode surface), we have additionally used the ZView for Windows (Version 2.2) fitting program [39], with the generalised finite Warburg element (GFW). The results of simulation indicate that the χ^2-function as well as Δ^2 values decrease somewhat if the GFW element has been used, but the dependence of the other fitting parameters (C_{dl}, R_{el}, C_{ad}, R_{ad}) on the diffusion layer model selected is very weak. Thus, according to the suggestions given in Refs. [37 - 39], the GFW model is not very well justified for the Bi($01\bar{1}$) | $(C_4H_9)_4NI + Na_2SO_4$ aqueous solution interface and, for that reason, the dependence of the equivalent circuit element parameters on E and c_{cat}, obtained according to the classical Frumkin — Melik-Gaikszyan model [8, 9], will be discussed here.

The dependence of C_{dl} on the electrode potential is in a good agreement with the Frumkin-Damaskin adsorption theory for neutral organic compounds at ideally polarizable electrodes [8, 9,11,13]. C_{dl} has minimal values in the region of zero charge potential (in the region of maximal adsorption) and increases quickly with desorption of the organic compound from the electrode surface with increasingly negative polarisation of the electrode.

The adsorption capacitance (additional) values, C_{ad}, calculated according to Eqs. (2.2.20) and (2.2.21), are minimal at the potentials of maximal adsorption in a good agreement with the Frumkin-Damaskin adsorption theory for the neutral organic compounds at the ideally polarizable electrodes [7,11]. The C_{ad} values increase very quickly with the decrease of ω at $E \leq$ -1.45 V as well as at $E \geq$ -0.65 V, where the value of $\left(\partial\theta/\partial E\right)_{\mu}$ is high [70]. At very high frequencies as well as in the region of maximal adsorption, C_{ad} has a tendency to approach zero. At the potentials near E^{peak}, the values of C_{ad} rise with concentration of the tetrabutylammonium cation. Sometimes at peak potentials, there is instability in the fitting procedure caused by the very high values of C_{ad} at E^{peak} [2-5]. It should be noted that in the range of potentials from –1.65 to –1.5 V (Ag|AgCl), the error values for C_{ad} are very large and, therefore, the numerical values of C_{ad} established for this potential region have to be regarded with some caution.

The value of the electrolyte resistance R_{el} depends very slightly on the electrode potential ($\Delta R_{el} \leq 4\%$) as well as on c_{TBN^+} and this behaviour is characteristic of the ideally polarizable electrodes [2-5,7,11-13].

The values of the diffusion resistance, R_D, obtained according to Eqs. (2.2.20-2.2.22) are maximal in the region of maximal adsorption and R_D is practically independent of c_{TBN^+}. At the potentials near E^{peak}, R_D has minimal values, which are independent of c_{TBN^+}.

According to the results of simulations, based on the finite length Warburg short circuit terminus model (FLW), the fractional exponent α_{cat} values are slightly lower than 0.5 in the region of maximal adsorption [39]. At $E = E_{max}$, α is nearly equal to 0.5 in a reasonable agreement with the classical Frumkin-Melik-Gaikazyan semi-infinite diffusion model [9,11]. However, α_{cat} has minimal values at the potentials from –1.65 to -1.5 V (Ag|AgCl) in the case of more concentrated TBN^+ solutions, where the desorption of TBN^+ cations begin. Thus, the deviation of α_{cat} from 0.5 exists if the dependence of θ on E is high. This effect has been observed for more complicated systems and can probably be explained using the theory of the electrochemical impedance of anomalous diffusion [42 - 45] (i.e. using the anomalous diffusion model with the adsorbing interface in our case). Probably, to a first approximation, it can be concluded that the deviation of our system from the classical Frumkin — Melik-Gaikazyan model arises because of high surface coverage and compactness of the adsorption layer on some parts of the Bi($01\bar{1}$) surface [2-5].

The values of the parameter T, obtained at $\alpha_{cat} \neq 0.5$, (expressed as $T = L^2 / D$, where L is the effective diffuse layer thickness and D is the effective diffusion coefficient of a particle) are maximal in the region of maximum adsorption, but T approaches zero in the region of adsorption-desorption peaks. At E_{max}, the value of T increases with decreasing c_{TBN^+} [70]. The very low values of T indicate that thickness of the adsorption layer is very small or, in other words, the deviation of our system from the classical Frumkin — Melik-Gaikazyan model is unremarkable.

The values of α_{cat} unequal to 0.5 can be probably explained by the inhomogeneous adsorption layer structure, i.e. on some parts of the Bi($01\bar{1}$) plane, there is a very compact two-dimensionally associated adsorption layer (where no semi-infinite diffusion occurs) but at some parts, the adsorption rate is limited by the semi-infinite diffusion of the TBN^+ cations.

It is reasonable that the effect of diffusion is likely to be stronger for the non-covered interface than the covered part, because slow dissolution and growth are reducing its effects at the patches [20] (Fig. 5, circuit e). The impedance and capacitance data at low ac

frequency indicate that for more concentrated TBN^+ solutions, the two-dimensional cluster formation is possible in the limited region of the electrode surface [18 - 21].

The interfacial admittance can then be represented approximately by the equivalent circuit, where the Frumkin-Melik-Gaikazyan model for the interface non-covered by the two-dimensional compact cluster is valid. For less concentrated solutions the role of two-dimensional compact clusters is small and the circuit simplifies to the classical Frumkin-Melik-Gaikazyan model discussed in Refs. [1-5,9,11-14]. The results of simulations (Table 1 and Fig. 3) show that the addition of R_n and C_n into the equivalent circuit (circuit e in Fig. 5) increases noticeably the agreement of the experimental data with the fitted Z'',Z' plots for the more concentrated solutions ($c_{cat} > 5\times10^{-4}$ M). The values of C_n and R_n are comparatively low (Fig. 6 (a and b)). In the region of I^- adsorption (at $E > -0.65$ V) and TBN^+ adsorption, the noticeable decrease in the R_n values has been observed (Fig. 6 (b)). In the case of lower concentrations ($c_{cat} < 1\times10^{-5}$ M) the influence of C_n and R_n on the coincidence of fitted and experimental curves is very small. [70]

The double layer capacitance values C_{dl} are minimal in the regions of TBN^+ adsorption and increase with desorption of TBN^+ at $E < -1.65$ V or if the adsorption of I^- anions begins at $E > -0.65$ V (Fig. 6 (c)). The adsorption capacitance C_{ad} is very high in the region of adsorption-desorption peaks at $E < -1.65$ V (not shown in Fig. 6 (d)) and sometimes it is impossible to obtain the correct fitting data at $E \leq -1.65$ V. The diffusion resistance values R_D are maximal in the region of maximal adsorption (Fig. 7 (a)) and R_D decreases to zero at the potentials $E > -0.65$ and $E < -1.65$ V. The deviation of α_{cat} from 0.5 is remarkable only in the potential region near to the adsorption-desorption peaks (i.e. in the region where the desorption process starts). Comparison of C_{ad}, α_{cat}, R_D, C_{dl}, obtained using the equivalent circuits b and e shows that there is only a weak difference in the values of C_{dl} (C_{dl} is lower in the case of circuit e), but other values depend only weakly on the choice of the equivalent circuit used for fitting the complex plane plots for Bi($01\bar{1}$) | 0.05 M Na_2SO_4 + x M TBN^+ interface.

For obtaining the adsorption and diffusion relaxation times (τ_K and τ_D, respectively) we followed the expressions 2.2.3, 2.2.8, 2.2.11 and 2.2.12.

Eqs. (2.2.4) and (2.2.5) require that $(\omega R_p)^{-1}$,C_p dependence should take the form of a quarter-circle with the values of depression angle between the C_p axis and the radius of the arc $\beta = 45°$.[12, 70]The experimental results presented in Figs. 8 and 9 show that at less negative potentials ($E > -1.25$ V vs. Ag|AgCl), the TBN^+ adsorption is limited mainly by the rate of

diffusion ($\beta = 45°$). The values of β somewhat lower than 45° at more negative potentials than $E \leq 1.25$ V can be explained by the mixed kinetics of adsorption of TBN^+ cations from less concentrated solutions ($c_{TBN^+} \leq 5\times10^{-4}$ M). The values of β at $c_{TBN^+} \leq 5\times10^{-4}$ M are noticeably higher in the region of maximal adsorption than at $E \leq -1.65$ V, indicating that under these conditions the deviation from the diffusion-limiting step is small. The diffusion relaxation times obtained from the so-called high frequency region of the Cole-Cole plots are given in Table 2. Comparison of these data with the data for other organic compounds investigated [1-5] demonstrates comparatively quick mainly diffusion-limited process of TBN^+ cations. However, as for uracil and dodecylsulfate anion adsorption, there are noticeable deviations from the semicircle at lower frequency ($f < 50$ Hz), which can be explained by the diffusion-like process in the adsorption layer (formation of two-dimensionally ordered areas or restructuring of the adsorption layer) as in this region of the Cole-Cole plots, the linear dependence of $(\omega R_p)^{-1}$ on C_p with the slope value $\beta'' \sim 45°$ has been established The values of β' less than 45° established at more negative potentials than –1.05 V for less concentrated TBN^+ solutions can be explained by the mixed adsorption kinetics (slow diffusion and heterogeneous adsorption steps), and in these circumstances Eqs. 2.2.13 and 2.2.14 are valid. [70]

The values of relaxation frequency $\omega_{max} = 2\pi f_{max}$, corresponding to the maximum values of the angular frequency for the $(\omega R_p)^{-1}, C_p$ dependence determining the values of experimental relaxation time $\tau_{exp} = (\omega_{max})^{-1}$, given in Table 2), are practically independent of E at $E >$ -1.35 V (Ag|AgCl). The somewhat higher τ_{exp} values for the more concentrated TBN^+ solutions are probably mainly caused by the formation of the compact adsorption layer. At very low frequency, a noticeable increase of the $(\omega R_p)^{-1}$ values have been observed, which is caused by the slow reorganisation of the adsorption layer (two-dimensional association according to Lorenz and Möckel [22, 23]).

A better fit of $(\omega R_p)^{-1}$ versus log$f$ plots (Fig. 10) has been established if the mixed kinetics of adsorption was assumed, but the values of τ_K are very small (except $c_{TBN^+} = 5\times10^{-4}$M solutions at $E = -1.65$ V). [70] The values of the theoretical diffusion relaxation times obtained using Eq. (2.2.14), τ_D^{theor}, are practically independent of c_{TBN^+} but the values of τ_K^{theor} seem to increase with the surface coverage (i.e. with c_{TBN^+}). However, the

values of τ_D and τ_K (given in Table 2) indicate that diffusion is the main rate-determining step (except c_{TBN^+} = 5×10^{4}M solutions at E = -1.65 V).

For the frequency region from 50 to 6000 Hz, the $\cot\delta,\omega^{-1/2}$ plots are linear with the slope values $M = \sqrt{2D}/(\partial\Gamma/\partial c)_E$, given in Table 2. The slope value depends somewhat on c_{cat}, which can be explained by the dependence of $(\partial\Gamma/\partial c)_E$ on compactness of the adsorption layer (if we assume that D does not depend on c_{cat}). According to the data in Table 2, there is a noticeable dependence of M on E, which is caused by the dependence of θ on E. [70]

The noticeable deviations in the Cole-Cole plots (Fig. 9) established at low frequency can be explained by the two-dimensional association of molecules adsorbed in the interfacial region according to Refs. (11,22, 23, 70]. In this case, the value of $\cot\delta = R_p(\omega)\cdot C_{add}(\omega)\cdot\omega$ can be calculated using Eq. 2.2.19.

The results of theoretical simulations (non-linear regression analysis) of these data are given in Table 3 and Fig. 11. In spite of a small difference between the experimental and theoretical $\cot\delta,\omega^{-1/2}$-curves at E > -1.6 V (Ag|AgCl) in the region of low ac frequency, the Lorenz model [22, 29], taking into account the two-dimensional association in the adsorption layer, seems to be the only classical model which explains the behaviour of the Bi(01$\bar{1}$) | x M $(C_4H_9)_4NI$ + Na_2SO_4 aqueous solution interface at low frequencies. [70] The values of ω_0 increase with c_{cat} at fixed potential, but decrease with increasingly negative polarisation. ω_0 is higher for TBN^+ compared with dodecylsulfate and uracil [4,5], in a good agreement with the increase of the experimental characteristic relaxation frequency obtained from the Cole-Cole plots at f > 100 Hz. At $E \geq$ -1.6 V, the parameters k_1 and k_2 slightly decrease with increasing c_{cat}. At constant c_{cat}, the values of k_1 increase and k_2 decrease with increasing the negative polarisation (i.e. with decreasing the Gibbs adsorption). The values of k_3 are practically independent of c_{cat} and E. The values of k_1 and k_2 obtained for TBN^+ are noticeably lower than those for uracil, pentanol and dodecylsulfate anions [2,4,5]. Thus, at low frequencies, two-dimensional association is probable, and the exchange rate of this association is higher for TBN^+, compared with other compounds studied at Bi(01$\bar{1}$) plane. For a more detailed discussion, the experimental data for other experimental systems should be obtained and analysed. However, according to the data in Tables (1-3) and Figs. 9-11, the adsorption process of TBN^+ cations from dilute TBN^+ solutions to the Bi(01$\bar{1}$) plane is limited mainly by the rate of diffusion of the organic cations to the electrode surface, but the two-

dimensional association is possible at lower ac frequency values. The mixed kinetics of adsorption is possible at more negative potentials than –1.65 V (Ag|AgCl). [70]

5 CONCLUSION

Systematic analysis of the Cole-Cole, $(\omega R_p)^{-1}$,log$f$ and $\cot\delta,\omega^{-1/2}$ dependences for Bi($01\bar{1}$) | 0.05 M Na_2SO_4 + x M $(C_4H_9)_4NI$ + H_2O interface shows that for less concentrated $(C_4H_9)_4N^+$ solutions, the rate of adsorption of the $(C_4H_9)_4N^+$ cation is limited mainly by the rate of the diffusion step at potentials more positive than –1.25 V (Ag|AgCl), but at more negative potentials, there are small deviations from a purely diffusion-limited step toward mixed kinetics (slow diffusion and heterogeneous adsorption steps) at high ac frequencies. At very low frequencies, the two-dimensional association is possible. The analysis of complex plane plots demonstrates that for less concentrated $(C_4H_9)_4N^+$ solutions ($c_{TBN^+} < 1\times10^{-5}$ M), the impedance spectra for the system investigated can be simulated by the classical Frumkin — Melik-Gaikazyan model [8, 9]with the following parameters: electrolyte resistance (R_{el}), electrical double layer capacitance (C_{dl}), adsorption capacitance (C_{ad}) and Warburg-like diffusion impedance (Z_W). According to the non-linear least-square fitting data [70], C_{dl}, C_{ad} and diffusion resistance R_D depend on the electrode potential as well as on concentration of $(C_4H_9)_4N^+$cation, and are in a good agreement with the predictions of the adsorption theory of the organic compounds in the case of the ideally polarizable electrodes [8-11,23]. For the more concentrated $(C_4H_9)_4N^+$ solutions, the noticeable deviations toward the modified Frumkin — Melik-Gaikazyan model, including the generalised finite Warburg element (GFW) for a short circuit terminus model, are possible. [70] The better fit of the complex plane plots has been established if the Wandlowski – de Levie model [20], taking into account the inhomogeneous adsorption layer at the Bi($01\bar{1}$) surface, has been used. Comparison of the data obtained by using Wandlowski — de Levie model and Frumkin — Melik-Gaikazyan model shows that for dilute $(C_4H_9)_4N^+$ solutions in the region of moderate frequencies and electrode potentials, the deviation of the Bi($01\bar{1}$) | 0.05 M Na_2SO_4 + x M $(C_4H_9)_4NI$ + H_2O interface from the classical Frumkin — Melik-Gaikazyan model is weak. [8, 9, 70] For more concentrated $(C_4H_9)_4N^+$ solutions, the boundary conditions defining the interfacial flux of $(C_4H_9)_4N^+$ cations will be inhomogeneous as there are probably the compact two-dimensionally ordered clusters on some parts of the Bi($01\bar{1}$) surface but on the other surface parts there is no clusters and the semi-infinite diffusion of $(C_4H_9)_4N^+$ ions is possible. [70]

6 KOKKUVÕTE

Süstemaatiline adsorptsiooni kineetika andmete analüüs Cole-Cole, $(\omega R_p)^{-1}$,log$f$ ja $\cot\delta,\omega^{-1/2}$ sõltuvuste abil Bi$(01\bar{1})$ | 0.05 M Na_2SO_4 + x M $(C_4H_9)_4NI$ + H_2O piirpinna korral näitab, et vähem kontsentreeritud $(C_4H_9)_4N^+$ lahustes on $(C_4H_9)_4N^+$ katiooni adsorptsiooni kiirus limiteeritud põhiliselt difusioonilise staadiumiga sellistel potentsiaalidel, mis on positiivsemad kui –1.25 V (Ag|AgCl), aga negatiivsematel potentsiaalidel esineb kõrgetel vahelduvvoolu sagedustel teatavaid kõrvalekaldeid puhtalt difusioonilisest staadiumist segakineetilise adsorptsiooni staadiumi suunas (aeglase difusiooni ja heterogeense adsorptsiooni staadiumid). Väga madalatel sagedustel on võimalik adsorbaadi kahedimensionaalne assotsiatsioon. Komplekstasandi so. Nyqvisti graafikute analüüsist selgub, et vähemkontsentreeritud $(C_4H_9)_4N^+$ lahuste ($c_{TBN^+} < 1\times10^{-5}$ M) impedantsispektreid saab modelleerida kasutades klassikalist Frumkin — Melik-Gaikazyan mudelit [8, 9], milles on järgnevad ekvivalentsskeemi ja adsorptsiooni parameetrid: elektrolüüdi takistus (R_{el}), elektrilise kaksikkihi mahtuvus (C_{dl}), adsorptsiooniline mahtuvus(C_{ad}) ja Warburgi diffusiooniline impedats (Z_W). Vastavalt mittelineaarse vähimruutude meetodi analüüsi andmetele sõltuvad C_{dl}, C_{ad} ja difusiooniline takistus R_D elektroodi potentsiaalist ja $(C_4H_9)_4N^+$ katiooni kontsentratsioonist lahuses. Leitud andmed on heas vastavuses tulemustega, mida saadakse ideaalselt polaariseeritavate elektroodide orgaaniliste ühendite adsorptsiooniteooria abil [8-11,23]. Kontsentreeritumates $(C_4H_9)_4N^+$ katiooni lahustes annab paremaid tulemusi Frumkin — Melik-Gaikazyani mudel, kus on toimunud üldistatud piirilise Warburg elemendi (GFW) lisamine. Komplekstasandi graafikute parem kokkulangevus eksperimendi andmetega saadi, kui kasutati Wandlowski – de Levie mudelit[20], mis võtab arvesse mittehomogeense adsorptsioonilise kihi tekke Bi$(01\bar{1})$ elektroodi pinnal. Nende kahe mudeli alusel leitud andmete võrdlus selgitab, et lahjemates $(C_4H_9)_4N^+$ lahustes on keskmistel sagedustel ja elektroodi keskmistel potentsiaalidel Bi$(01\bar{1})$ | 0.05 M Na_2SO_4 + x M $(C_4H_9)_4NI$ + H_2O piirpinna andmete erinevus klassikalisest Frumkin — Melik-Gaikazyan mudelist väga väike. Kontsentreeritumates $(C_4H_9)_4N^+$ lahustes on piirilised tingimused erinevad kuna Bi$(01\bar{1})$ elektroodi mõningates piirkondades on tõenäoline kahedimensionaalsete klastrite teke, kuna teistel aladel neid ei moodustu. Seetõttu on seal tõenäoliselt võimalik $(C_4H_9)_4N^+$ ioonide klassikaline Ficki seadustele alluv difusiooniprotsess.

7 REFERENCES

[1] E.J. Lust, U.V. Palm, Sov. Electrochem. 24 (1988) 227, Engl. Tr.

[2] G. Nurk, A. Jänes, P. Miidla, K. Lust, E. Lust, J. Electroanal. Chem. 515 (2001) 17.

[3] A. Jänes, G. Nurk, K. Lust, E. Lust, J. Russ. Electrochem. 38 (2002) 11.

[4] H. Kasuk, G. Nurk, K. Lust, E. Lust, J. Electroanal. Chem. 550-551 (2003) 13.

[5] G. Nurk, H. Kasuk, K. Lust, A. Jänes, E. Lust, J. Electroanal. Chem. 553 (2003) 1.

[6] E. Lust, G. Nurk, A. Jänes, M. Arulepp, L. Permann, P. Nigu, P. Möller, Cond. Matter Physics 5 (2002) 307.

[7] E. Lust, G. Nurk, A. Jänes, M. Arulepp, P. Nigu, P. Möller, S. Kallip, V. Sammelselg, J. Solid State Electrochem. 7 (2003) 91.

[8] A.N. Frumkin, V.I. Melik-Gaikazyan, Dokl. Akad. Nauk USSR 77 (1951) 855.

[9] V.I. Melik-Gaikazyan, Zh. Fiz. Khim. 26 (1952) 560.

[10] K.S. Cole, R.H. Cole, J. Chem. Phys. 9 (1941) 341.

[11] A.N. Frumkin, B.B. Damaskin, in J.O'M. Bockris and B.E. Conway (Eds.), Modern Aspects of Electrochemistry, Vol. 3 (1964) p.149.

[12] R.D. Armstrong, W.P. Rice, H.R. Thirsk, J. Electroanal. Chem. 16 (1968) 517.

[13] M. Sluyters-Rehbach, J. Sluyters, in A. Bard (Ed.), Electroanalytical Chemistry, vol. 4, Marcel Dekker, New York, 1970, p.76.

[14] U. Retter, H. Jering, J. Electroanal. Chem. 46 (1973) 375.

[15] B. Damaskin, S. Karpov, S. Dyatkina, U. Palm, M. Salve, J. Electroanal. Chem. 136 (1982) 217.

[16] B. Damaskin, S. Karpov, S. Dyatkina, U. Palm, M. Salve, J. Electroanal. Chem. 189 (1983) 183.

[17] A. Tymosiak-Zielinska, Z. Borkowska, Electrochim. Acta 46 (2001) 3073.

[18] T. Wandlowski, R. de Levie, J. Electroanal. Chem. 329 (1992) 103.

[19] T. Wandlowski, R. de Levie, J. Electroanal. Chem.345 (1993) 413.

[20] T. Wandlowski, R. de Levie, J. Electroanal. Chem.352 (1993) 279.

[21] T. Wandlowski, R. de Levie, J. Electroanal. Chem. 380 (1995) 201.

[22] W. Lorenz, F. Möckel, Z. Elektrochem. 60 (1956) 507.

[23] B.B. Damaskin, O.A. Petrii, V.V. Batrakov, Adsorption of Organic Compounds on Electrodes, Plenum Press, New York, London, 1971, pp. 53-66.

[24] V. Brabec, S. D. Christian, G. Dryhurst, Biophys. Chem. 7 (1978) 253.

[25] E. Lust, A. Jänes, K. Lust, J. Ehrlich, Elecrochemica Acta 44 (1999) 4707.

[26] A. N. Frumkin, Z. Phys. Chem. 116 (1925) 446.

[27] B.B. Damaskin, L.N. Nekrassov, O.A. Petrii, B.I. Podlovchenko, E.V. Stenina, N.V. Fedorovich, in: B.B. Damaskin (Ed.), Electrochemical Properties in Organic Compound Solutions, Moscow University Press, Moscow, 1985, pp. 80–85 (in Russian).G. Brug, A. van der Eeden, M. Sluyters-Rehbach, J. Sluyters, J. Electroanal. Chem. 176 (1984) 275.

[28] G.A. Tedoradze, R.A. Arakelyan, Dokl. Akad. Nauk SSSR 156 (1964) 1170.

[29] W. Lorenz, Z. Elektrochem. 62 (1958) 192.

[30] E. Lust, A., Jänes, K. Lust, R. Pullerits, J. Electroanal. Chem. 431 (1997) 183.

[31] E. Lust, K. K. Lust, A. A.-J. Jänes, Russian J. Elecrochem. 31 (1995) 876.

[32] E. I. Lust, A. A.-J. Jänes, K. Lust, J.-J. Ehrlich, Russian J. Electroanal. Chem. 32 (1996) 597J.R. MacDonald (Ed.) Impedance Spectroscopy: Emphasizing Solid Materials and Systems, John Wiley & Sons, New York, 1987.

[33] S. Trasatti, E. Lust, in J.O'M. Bockris, R.E. White (Eds.), Modern Aspects of Electrochem., Vol. 33, Kluwer Academic / Plenum Publishers, New York, 1999, p.1.

[34]T.J. Van der Noot, J. Electroanal. Chem. 300 (1991) 199.

[35]T. Pajkossy, Th. Wandlowski, O.M. Kolb, J. Electroanal. Chem. 414 (1996) 209.

[36] G. Brug, A. van der Eeden, M. Sluyters-Rehbach, J. Sluyters, J. Electroanal. Chem. 176 (1984) 275.

[37] J.R. MacDonald (Ed.) Impedance Spectroscopy: Emphasizing Solid Materials and Systems, John Wiley & Sons, New York, 1987.

[38] B.A. Boukamp, J. Electrochem. Soc 142 (1995) 1885.

[39] ZView for Windows (version 2.2) fitting program, Scribner Inc., Souther Pines, NC, 1999.

[40] M. Sluyters-Rwhbach, Pure and Appl. Chem. 66 (1994) 1831.

[41] A. Lasia, in B.E. Conway, J.O'M. Bockris, R.E. White (Eds.), Modern Aspects of Electrochem., Vol. 32, Kluwer Academic, New York, 1999, Ch. 2.

[42]T. Jacobsen, K. West, Electrochim. Acta 40 (1995) 233.

[43]A. Compte, Phys. Rev. E 53 (1996) 4191.

[44]A. Compte, R. Metzlek, J. Phys. A: Math. Gen. 30 (1997) 7277.

[45]J. Bisquert and A. Compte, J. Electroanal. Chem. 499 (2001) 112.

[46] M. Salve, A. Alumaa, U. Palm, Trans. Tartu State Univ. 289 (1971) 54.

[47] E. E. Ferapontova J. Electroanal. Chem 476 (1999) 37-35.

[48] O. A. Petrii, N. V. Nikolaeva-Fedorovich, Zhurn. Fiz. Khim. 35 (1961) 1999.

[49] N. V. Nikolaeva-Fedorovich, B. B. Damaskin, O. A. Petrii, Collect. Czech. Chem. Commun. 25 (1960) 2982.B.A. Boukamp, Equivalent Circuit User's Manual, University of Twente, 1989.

[50]E. Lust, A. Jänes, M. Väärtnõu, K. Lust Electrochimica Acta (1997)

[51] N. V. Fedorovich, Ross. Khim. Zhurn. (Mendeleev Chem. J.) 2 (1996) 86.

[52]G. H. Naficy, The`se de 3e Cycle, Montpellier, 1972.

[53] E. Verdier, G.H. Naficy, P. Vanel, J. Chim. Phys., 70 (1973) 160.

[54] J. Piro, R. Bennes, E. Bou Karam, J. Electroanal. Chem., 57 (1974) 399.

[55] E. Bou Karam, R. Bennes, D. Bellostas, J. Electroanal. Chem., 84 (1977) 21.

[56] M. A. V. Devanathan, M. J. Fernando, Trans. Faraday soc., 58 (1962) 368.

[57] F. M. Kimmerle, H. Menard, J. Electroanal. Chem., 54 (1974) 101.

[58] H. Menard, F. M. Kimmerle, Can. J. Chem., 54 (1976) 2488.

[59] J. Bisquert, G. Garcia-Belmonte, P.R. Bueno, E. Longo, L.O.S. Bulhões, J. Electroanal. Chem. 452 (1998) 229.

[60]K. Tamaki, Bull. Chem. Soc. Japan, 47 (1974) 2764.

[61] B. B. Damaskin, R. I. Kaganovich, V. M. Gerovich, S. L. Dyatkina, Elektrokhimiya, 5 (1967) 507.

[62] J. Kuta, I. Smoler, Coll. Czech. Chem. Commun., 40 (1975) 225.

[63] P. Vanel, The`se de Doctorat es Sciences, Montpellier, 1975.

[64]W. Y. Wen, J. Solution Chem., 2 (1973) 253.

[65] B. S. Krumgals, J. Gen. Chem. (U.S.S.R.), 44 (1974) 1385.

[66] K. P. Mishchenko, G. M. Poltoratsky, Thermodynamique et Structure des Solutions Aqueuses et Non Aqueuses d'Electrolytes, Izel Khim, Leningrad, 1976, p.293.

[67] R. M. Diamond, J. Phys. Chem., 67 (1963) 2513.ZView for Windows (version 2.2) fitting program, Scribner Inc., Souther Pines, NC, 1999.

[68]P. Vanel, D. Schumann, J. Electroanal. Chem., 87 (1978) 119.

[69] A. Losurdo, H. E. Wirth, J. Phys. Chem., 76 (1972) 130, 1333.

[70] K. Laes, G. Nurk, M. Väärtnõu, K. Lust, A. Jänes, E. Lust J. Electroanal. Chem (in press)

[71]A.N. Frumkin, Potentsyaly nulevogo zaryada (Potentials of zero charge), Nauka, Moscow, (1979).

[72] M. Väärtnõu, E. Lust, J. Electroanal. Chem. 533 (2002) 107.

8 LEGENDS OF FIGURES

Fig. 1. Complex plane plots for Bi($01\bar{1}$) in 0.05 M Na_2SO_4 aqueous solution at different electrode potentials E (V vs. Ag|AgCl): -0.6 (1); -1.5 (2); -1. 7 (3). Inset: the equivalent circuit used for fitting of the experimental data (R_{el} – electrolyte resistance; CPE – constant phase element; and R_{ad} – adsorption or partial charge transfer resistance).

Fig. 2. Complex plane plots for the Bi($01\bar{1}$) plane in 0.05 M Na_2SO_4 solutions with addition of 5×10^{-4} M (a) and 5×10^{-2} M (b) $(C_4H_9)_4N^+$ cation at different electrode potentials E (V vs. Ag|AgCl): -0.65 (1); -0.85 (2); -1.05 (3); -1.45 (4) and –1.65 (5) (points – experimental data; solid lines – fitting according to Wandlowski – de Levie model).

Fig. 3. Differential capacitance vs. electrode potential curves (a) (at ac frequency f = 210 Hz) for Bi($01\bar{1}$) in the 0.05 M Na_2SO_4 electrolyte (1) and with additions of $(C_4H_9)_4N^+$ (M): (2) – 1×10^{-8}; (3) – 1×10^{-7}; (4) – 5×10^{-7}; (5) –1×10^{-6}; (6) –5×10^{-6}; (7) –1×10^{-5}; (8) –5×10^{-5}; (9) –1×10^{-4}; (10) –5×10^{-4}; and (11) –1×10^{-3} . R_s (1,3) and R_p (2,4) vs. $\omega^{1/2}$ dependences (b) for the Bi($01\bar{1}$) | 1×10^{-3} M $(C_4H_9)_4N^+$ + 0.05 M Na_2SO_4 aqueous solution interface at the potentials (V vs. Ag|AgCl): -1.2 (1,2); and –1.7 (3,4).

Fig. 4. Dependence of the phase angle (δ) on ac frequency for Bi($01\bar{1}$) in 0.05 M Na_2SO_4 solution with addition of 5×10^{-4} M (a) and 5×10^{-2} M (b) $(C_4H_9)_4N^+$ at different electrode potentials, E (V vs. Ag|AgCl) (a): -0.65 (1); -0.85 (2) ; -1-05 (3); -1.25 (4); -1.45 (5); and -1.65 (6); and at constant E = -0.65 V (Ag|AgCl) (c) for various $c_{(C_4H_9)_4N^+}$ (M): (1) – 5×10^{-2}; (2) – 5×10^{-3}; and (3) – 5×10^{-4}.

Fig. 5. Equivalent circuits of an electrode in the presence of organic cation adsorption: (a) Randles circuit; (b) Frumkin — Melik–Gaikazyan circuit, (c) combined Frumkin — Melik-Gaikazyan — Randles circuit; (d) Frumkin — Melik-Gaikazyan circuit with CPE instead of C_{dl}; and (e) Wandlowski — de Levie circuit (R_{el} – electrolyte solution resistance; C_{dl} – double layer capacitance; C_{ad} – adsorption capacitance; R_{ad} - adsorption

or partial charge transfer resistance; Z_w –Warburg-like diffusion impedance; CPE – constant phase element; C_n and R_n – capacitance and resistance of the formation of the two-dimensionally associated layer (i.e. the capacitance and resistance of the "needle" peak formation).

Fig. 6. Dependence of the so called needle peak capacitance C_n (a); and resistance R_n (b); double layer ("true") capacitance C_{dl} (c); and adsorption capacitance C_{ad} (d) on the electrode potential for Bi($01\bar{1}$) in the 0.05 M Na_2SO_4 aqueous solution with additions of $(C_4H_9)_4N^+$ (M): (1) – 5×10^{-2}; and (2) – 5×10^{-4}.

Fig. 7. Dependence of diffusion resistance R_D (a) and the fractional exponent α_{cat} (Eq. 3) (b) on the electrode potential for Bi($01\bar{1}$) in the 0.05 M Na_2SO_4 aqueous solution with additions of $(C_4H_9)_4N^+$ (M): (1) – 5×10^{-2}; and (2) – 5×10^{-4}.

Fig. 8. Cole-Cole (complex admittance) plots for the Bi($01\bar{1}$) | 0.05 M Na_2SO_4 + 5×10^{-4} M $(C_4H_9)_4N^+$ solution interface at the electrode potentials, E (V vs. Ag|AgCl): -1.35 (1); -1.05 (2); and –1.65 (3).

Fig. 9. Cole-Cole (complex admittance) plots for Bi($01\bar{1}$)| 0.05 M Na_2SO_4 + 5×10^{-2} M $(C_4H_9)_4N^+$ solution interface at the electrode potentials, E (V vs. Ag|AgCl): -1.65 (1); -1.35 (2); and –1.25 (3).

Fig. 10. $(\omega R_p)^{-1}$,log$f$ plots for Bi($01\bar{1}$) in the 0.05 M Na_2SO_4 aqueous solution with addition of 5×10^{-2} M $(C_4H_9)_4N^+$ at E = -1.65 V (Ag|AgCl) (experimental data (1) and fitted data according to Eq. (15 b) (2); and Eq. (16 b) (3) at the values of τ_D^{theor} and τ_K^{theor}, presented in Table 2).

Fig. 11. $\cot\delta,\omega^{-1/2}$ plots for Bi($01\bar{1}$) in the 0.05 M Na_2SO_4 aqueous solution with additions of $(C_4H_9)_4N^+$ (M): 5×10^{-4} (a); and 5×10^{-2} (b) at the electrode potentials (V vs. Ag|AgCl): -1.05 (1); -1.35 (2); and –1.65 (3) (filled marks – experimental data; open marks –data calculated according to Eq. (18) at the values of ω_0, k_1, k_2 and k_3, presented in Table 3).

Table 1. Results of non-linear least squares fitting for Bi($01\bar{1}$) | 0.05 M Na_2SO_4 + *x* M $(C_4H_9)_4N^+$ + H_2O interface.

c_{cat}/ M	E / V vs. Ag|AgCl	Parameter	Frumkin — Melik-Gaikazyan model (circuit b)	Wandlowski-De Levie model (at $\alpha \neq 0.5$) (circuit e)
5×10^{-4}	-1.05	χ^2	6.7×10^{-3}	5.4×10^{-4}
		Δ^2	0.65	0.053
		R_{el} / Ω cm^2	18.9 (2.3%)	10.7 (4.3%)
		C_{dl} / μF cm^{-2}	5.6 (1.1%)	2.9 (5.0%)
		R_D / Ω cm^2	106510 (15%)	104980 (2.7%)
		T / s	8.82 (27.6%)	7.32 (5.9%)
		α_{cat}	0.5 (fixed)	0.48 (0.71%)
		C_{ad} / μF cm^{-2}	179 (20.8%)	154 (15.7%)
		C_n / μF cm^{-2}	-	3.0 (4.3%)
		R_n / Ω cm^2	-	46.5 (6.1%)
5×10^{-4}	-1.45	χ^2	1.19×10^{-2}	5.7×10^{-4}
		Δ^2	1.30	0.06
		R_{el} / Ω cm^2	19.2 (2.8%)	12.1 (3.8%)
		C_{dl} / μF cm^{-2}	7.6 (1.8%)	3.9 (4.8%)
		R_D / Ω cm^2	8875 (2.0 %)	10870 (1.2%)
		T / s rad^{-1}	0.23 (5.8 %)	0.53 (5.6%)
		α_{cat}	0.5 (fixed)	0.42 (1.4%)
		C_{ad} / μF cm^{-2}	780 (19.3 %)	2917 (21.8%)
		C_n / μF cm^{-2}	-	5.1 (3.6%)
		R_n / Ω cm^2	-	37.7 (5.0%)
5×10^{-2}	-1.05	χ^2	3.4×10^{-3}	2.2×10^{-4}
		Δ^2	0.35	0.022
		R_{el} / Ω cm^2	13.7 (2.0%)	8.3 (4.2%)
		C_{dl} / μF cm^{-2}	5.4 (0.7%)	3.4 (3.9%)
		R_D / Ω cm^2	93788 (9.1%)	71690 (4.0%)
		T / s rad^{-1}	6.40 (17.3%)	5.17 (5.0%)
		α_{cat}	0.5 (fixed)	0.46 (1.1%)
		C_{ad} / μF cm^{-2}	285 (23.8%)	124 (8.8%)
		C_n / μF cm^{-2}	-	2.4(5.4%)
		R_n / Ω cm^2	-	49.5(8.3%)

χ^2 – chi-square function; Δ^2 – weighted sum of squares; R_{el} –electrolyte resistance; C_{dl} – double layer capacitance; R_D –limiting diffusion resistance; $T = L^2/D$ (L is the effective diffuse layer thickness; D is the effective diffusion coefficient of a cation); α_{cat} – fractional exponent; C_{ad} – adsorption capacitance; R_n and C_n – "needle" peak formation resistance and capacitance [42]; c_{cat} – concentration of the $(C_4H_9)_4N^+$ cations

Table 2. Experimental and calculated diffusion and adsorption relaxation times for Bi($01\bar{1}$) | 0.05 M Na_2SO_4 + *x* M $(C_4H_9)_4N^+$ + H_2O interface.

c_{cat} / M	*E* / V vs. Ag|AgCl	$10^4\ \tau_{exp}$ / s	β / deg	*M* (Eq. 17)	$10^4\ \tau_D^{theor}$ / s (Eq. (15 b))	$10^4\ \tau_D^{theor}$ / s (Eq. (16 b)	$10^7\ \tau_K^{theor}$ / s (Eq. 16 b)
5×10^{-4}	-1.05	0.98	39	156	1.5	0.9	0.1
	-1.35	0.98	31	140	1.6	1.2	1.0
	-1.65	1.35	23	37	16.0	7.0	10000
5×10^{-2}	-1.05	1.40	47	199	0.90	0.60	10.0
	-1.35	1.60	47	200	0.97	0.85	100
	-1.65	9.80	47	143	1.20	0.80	10.0

c_{cat} – concentration of the $(C_4H_9)_4N^+$ cations;
τ_{exp} – experimental relaxation time obtained from the Cole-Cole plot;
β – angle between C_p axis and the radius of the aec of the Cole-Cole (ωR_p^{-1} vs. C_p) plot.

Table 3. Non-linear regression analysis data for Bi($01\bar{1}$) | 0.05 M Na_2SO_4 + x M $(C_4H_9)_4N^+$ + H_2O interface.

x / M	E / V vs Ag|AgCl	$10^{-4}\ \omega_0$ / s^{-1} (Eq. 18)	$10^4\ k_1$ (Eq. 18)	$10^3\ k_2$ (Eq. 18)	k_3 (Eq. 18)	R^2
5×10^{-4}	-1.05	1.89±0.65	7.9±3.0	6.9±3.1	0.78±0.08	0.88
	-1.35	1.17±0.35	12.2±4.0	6.6±2.9	0.84±0.08	0.91
	-1.65	0.28±0.03	114.5±16.9	-28.6±4.6	0.62±0.05	0.94
$5x10^{-2}$	-1.05	2.83±1.07	6.8±2.8	4.7±2.3	0.81±0.09	0.88
	-1.35	2.84±0.99	6.6±2.5	3.3±1.6	0.79±0.08	0.90
	-1.65	0.87±0.10	101.1±13.2	-6.4±1.3	1.38±0.10	0.97

R^2 – the correlation coefficient

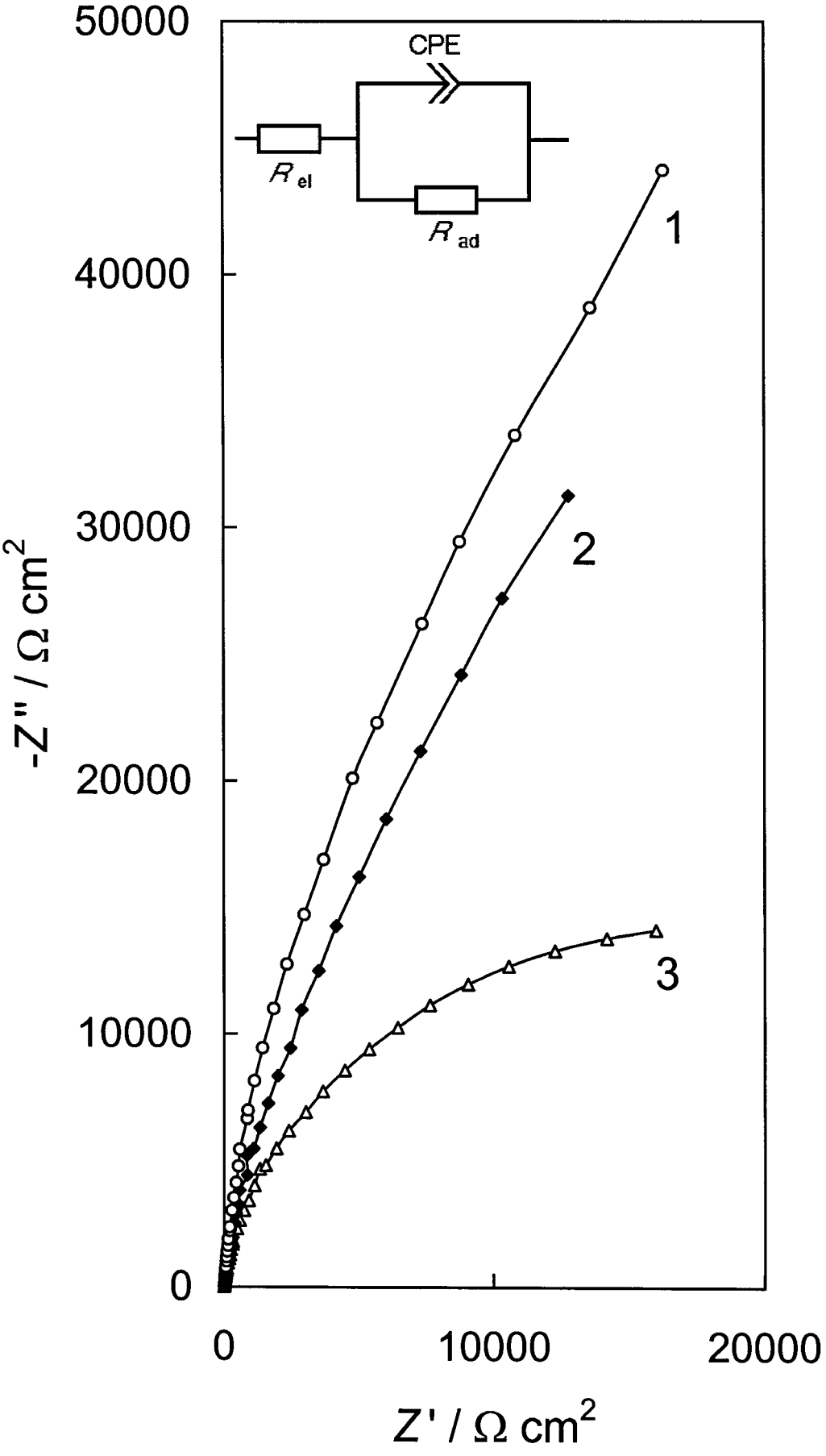
50000
40000
30000
20000
10000
0
-Z'' / Ω cm2
0
10000
20000
Z' / Ω cm2
CPE
Rel
Rad
1
2
3

Fig. 1.

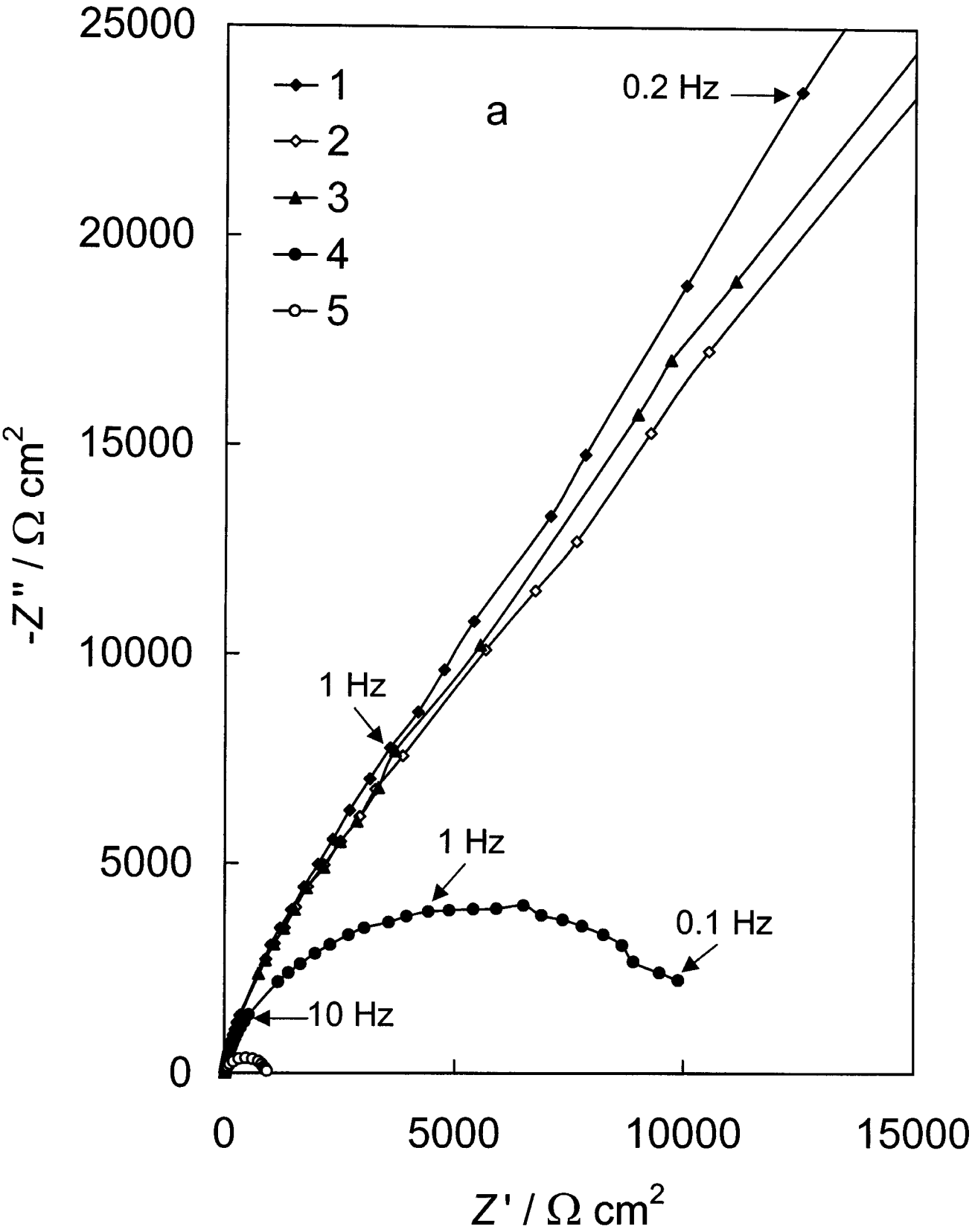
25000
20000
15000
10000
5000
0
-Z'' / Ω cm2
0
5000
10000
15000
Z' / Ω cm2
1
2
3
4
5
a
0.2 Hz
1 Hz
1 Hz
0.1 Hz
10 Hz

Fig. 2a.

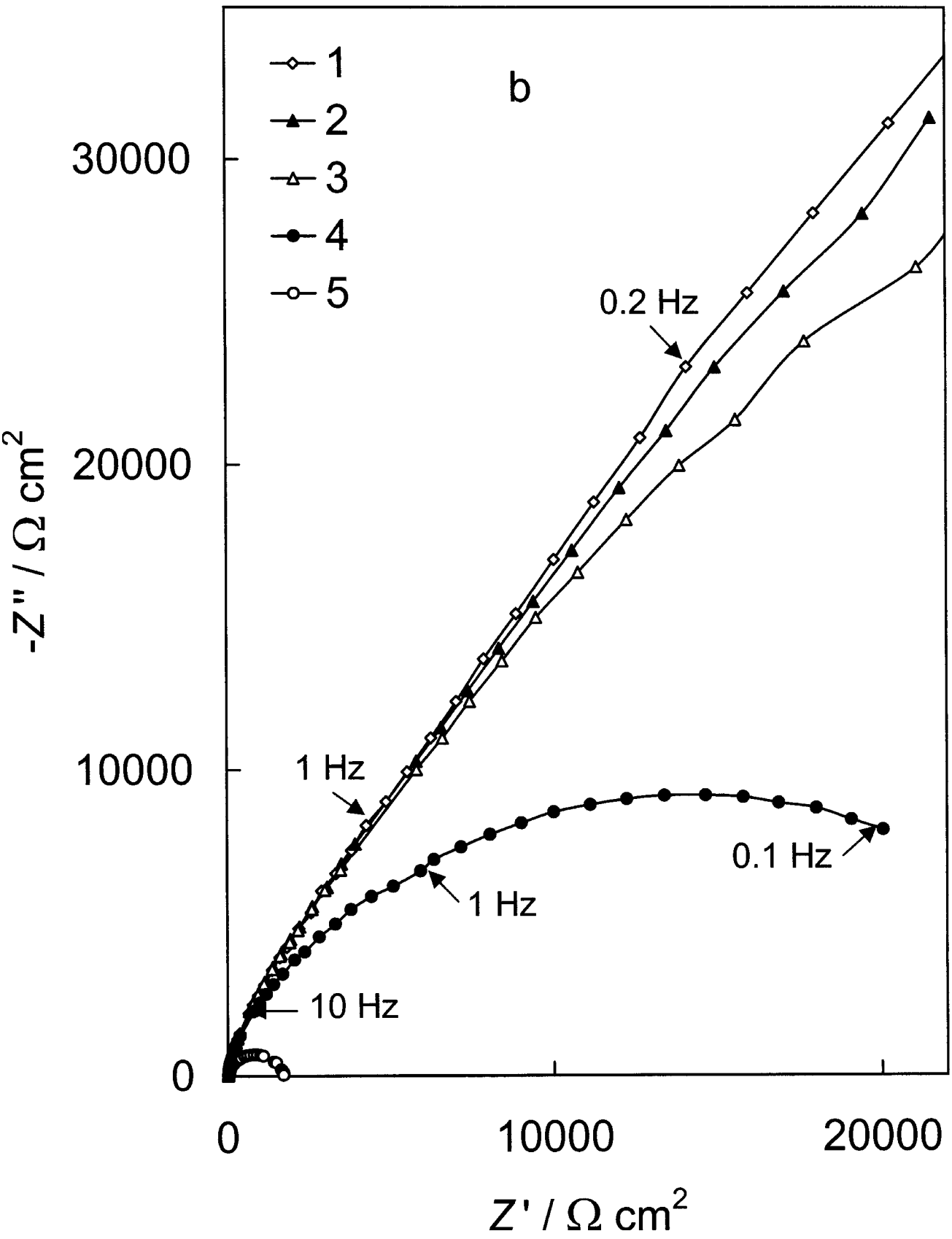
b
1
2
3
4
5
0.2 Hz
1 Hz
0.1 Hz
1 Hz
10 Hz
30000
20000
10000
0
0
10000
20000
-Z'' / Ω cm2
Z' / Ω cm2

Fig. 2b.

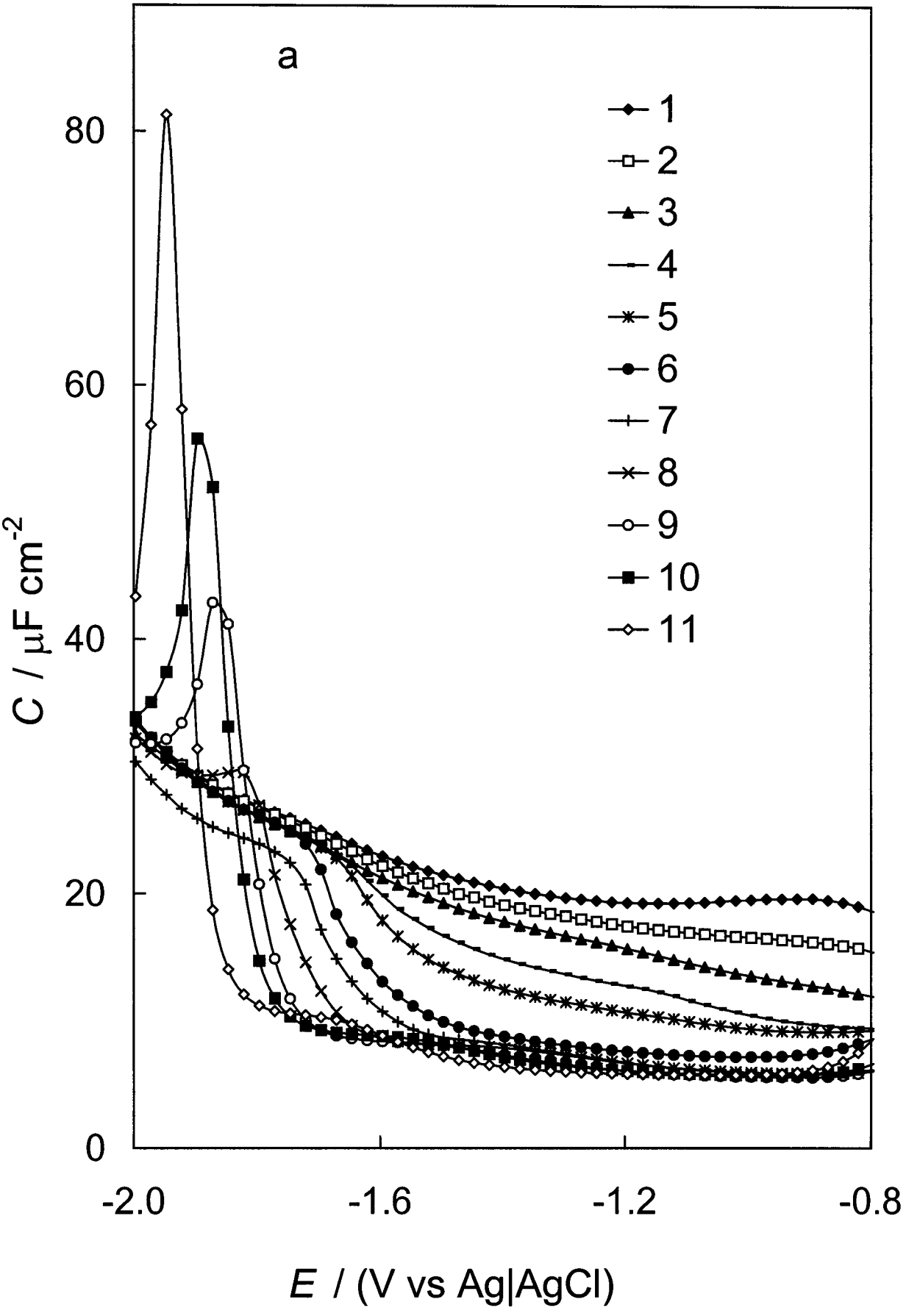

Fig. 3a.

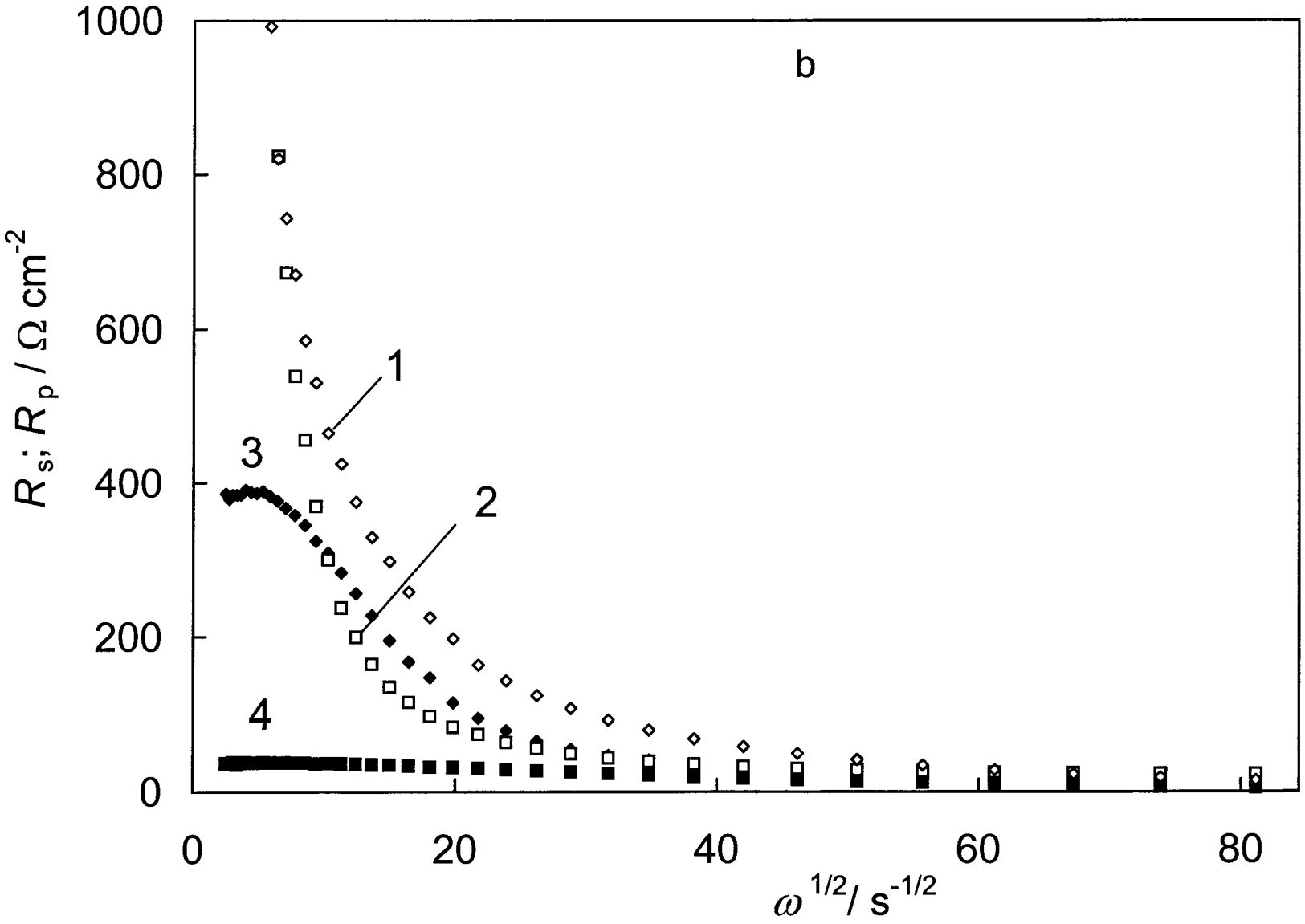

Fig. 3b.

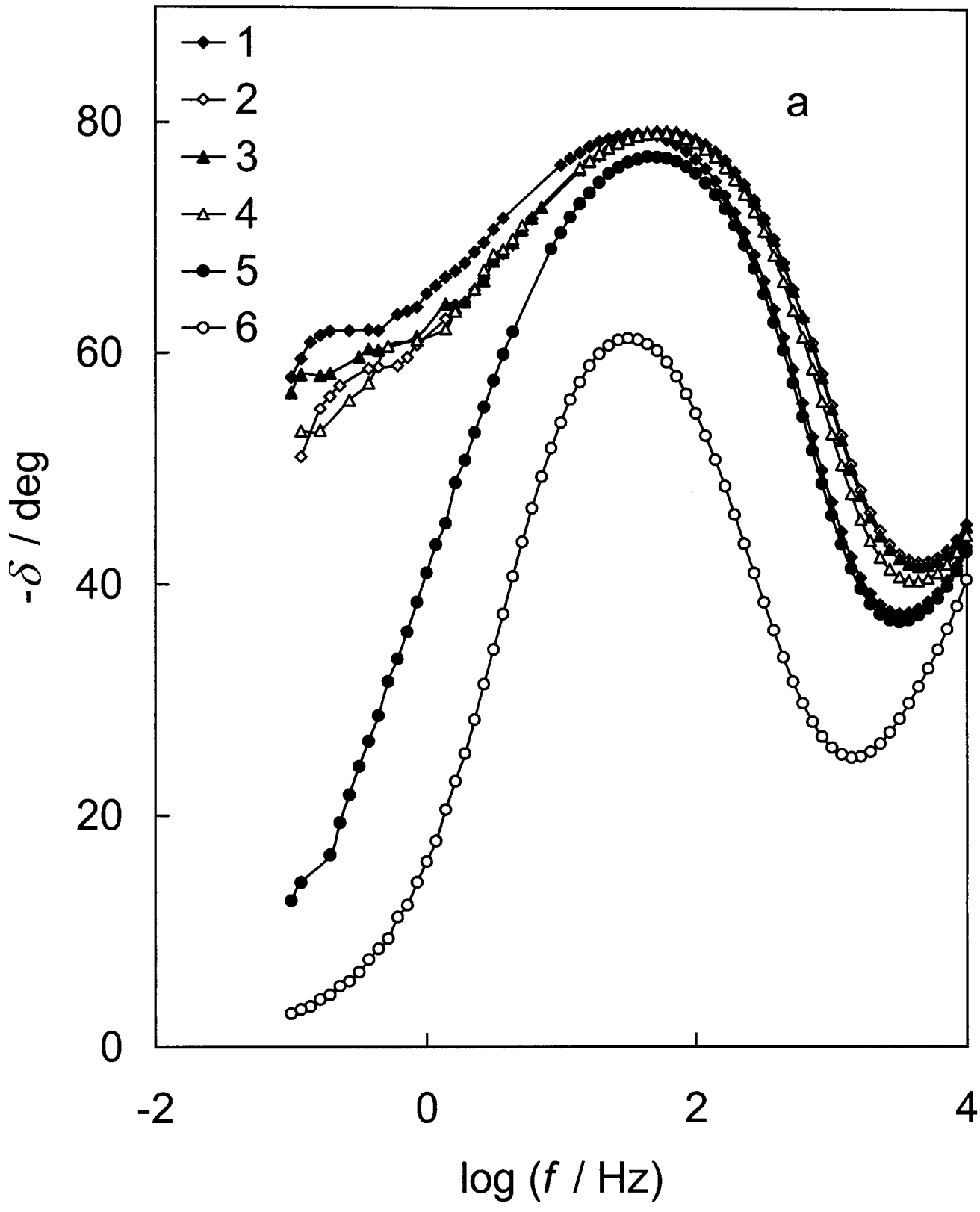

Fig. 4a.

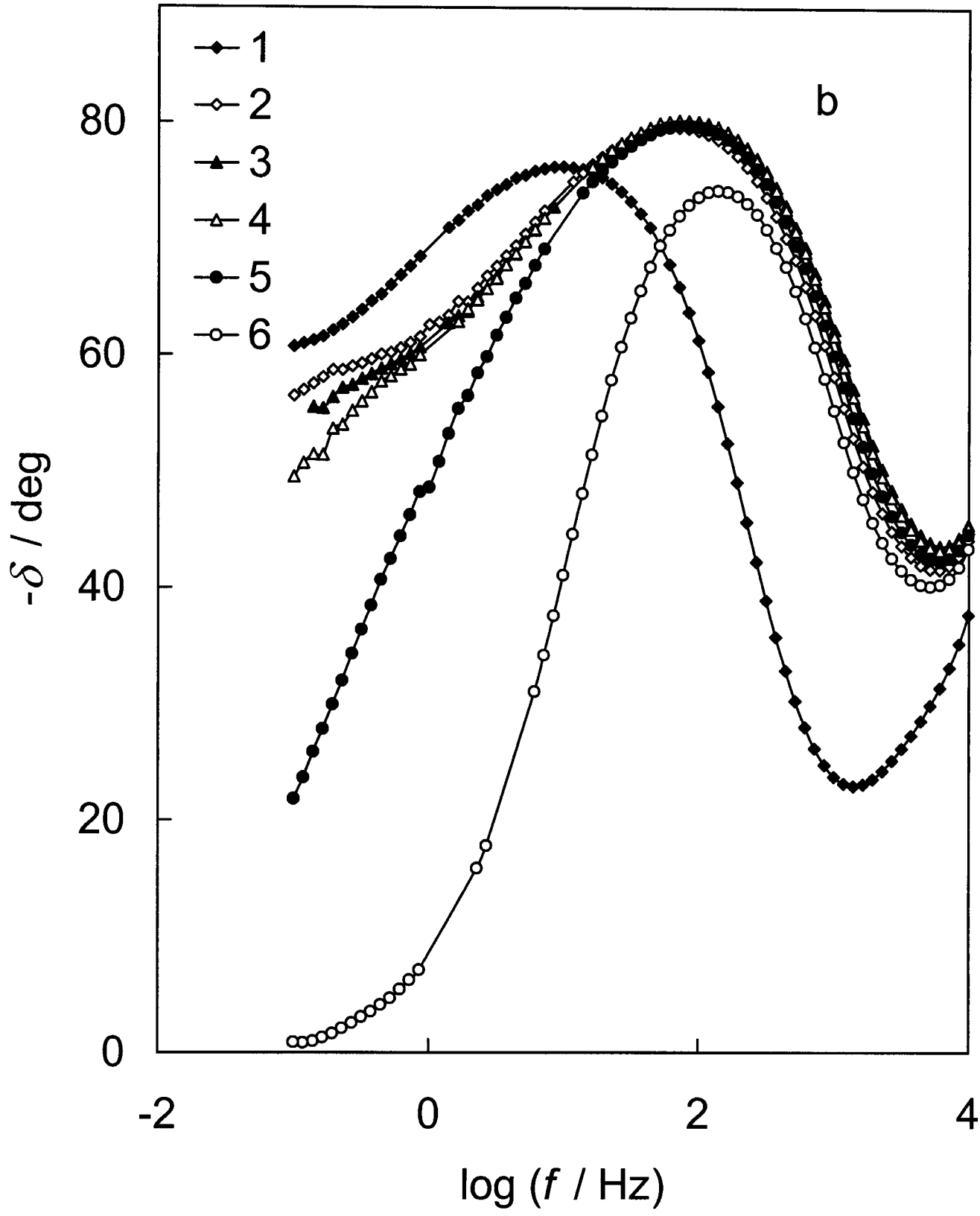

Fig. 4b.

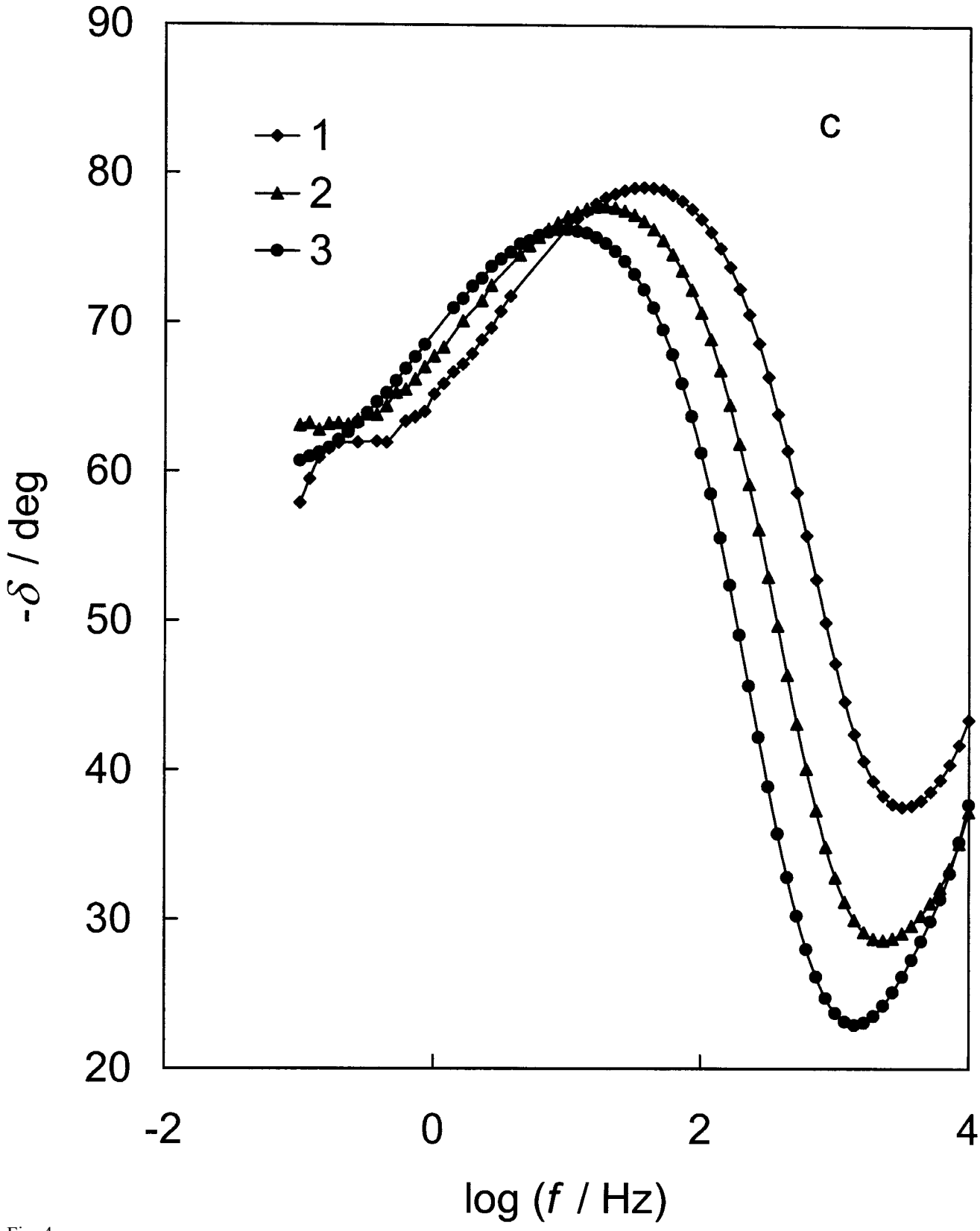

Fig. 4c.

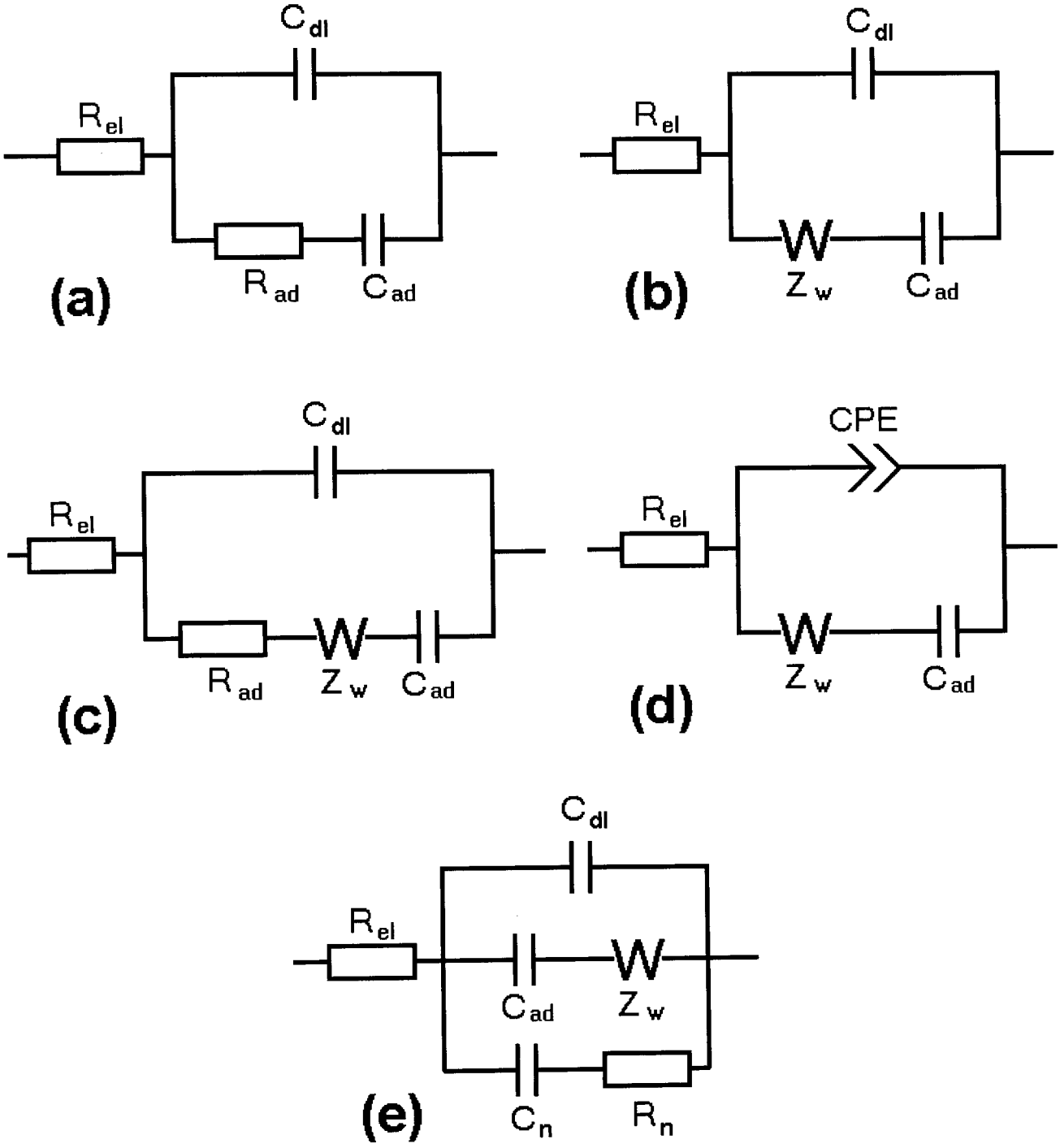
C dl
R el
R ad
C ad
(a)
C dl
R el
W
Z w
C ad
(b)
C dl
R el
R ad
W
Z w
C ad
(c)
CPE
R el
W
Z w
C ad
(d)
C dl
R el
C ad
W
Z w
C n
R n
(e)

Fig. 5.

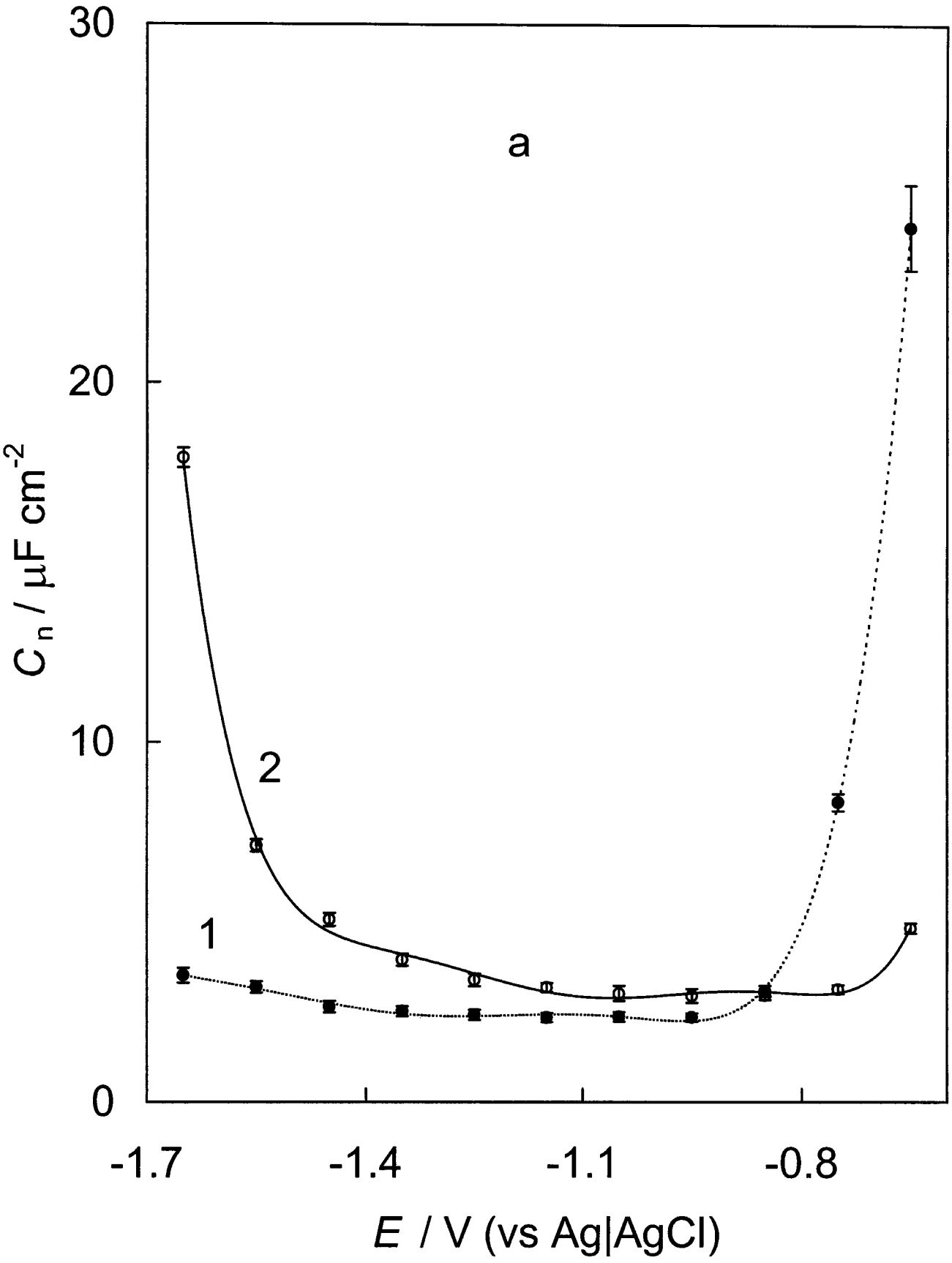

Fig. 6a.

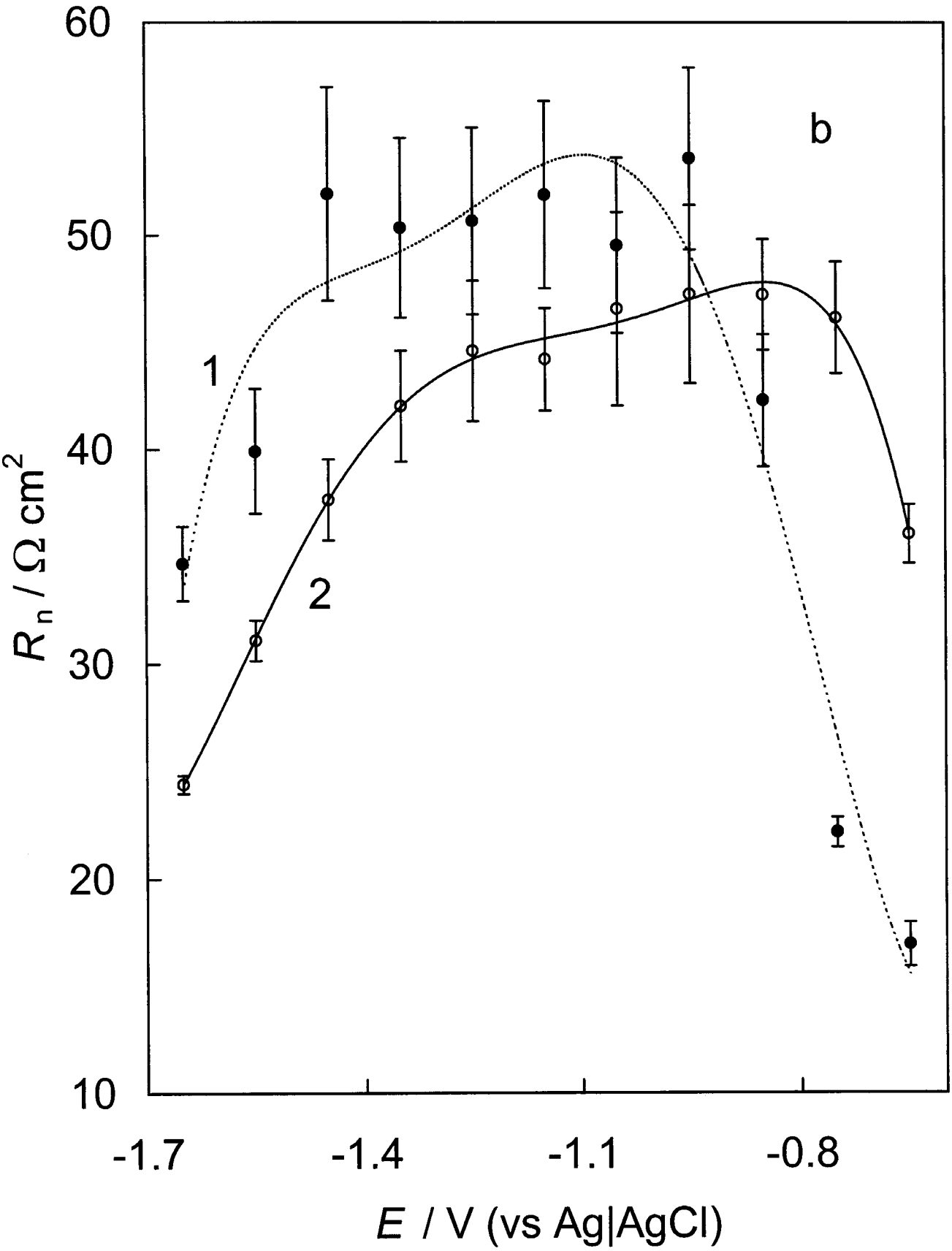

Fig. 6b.

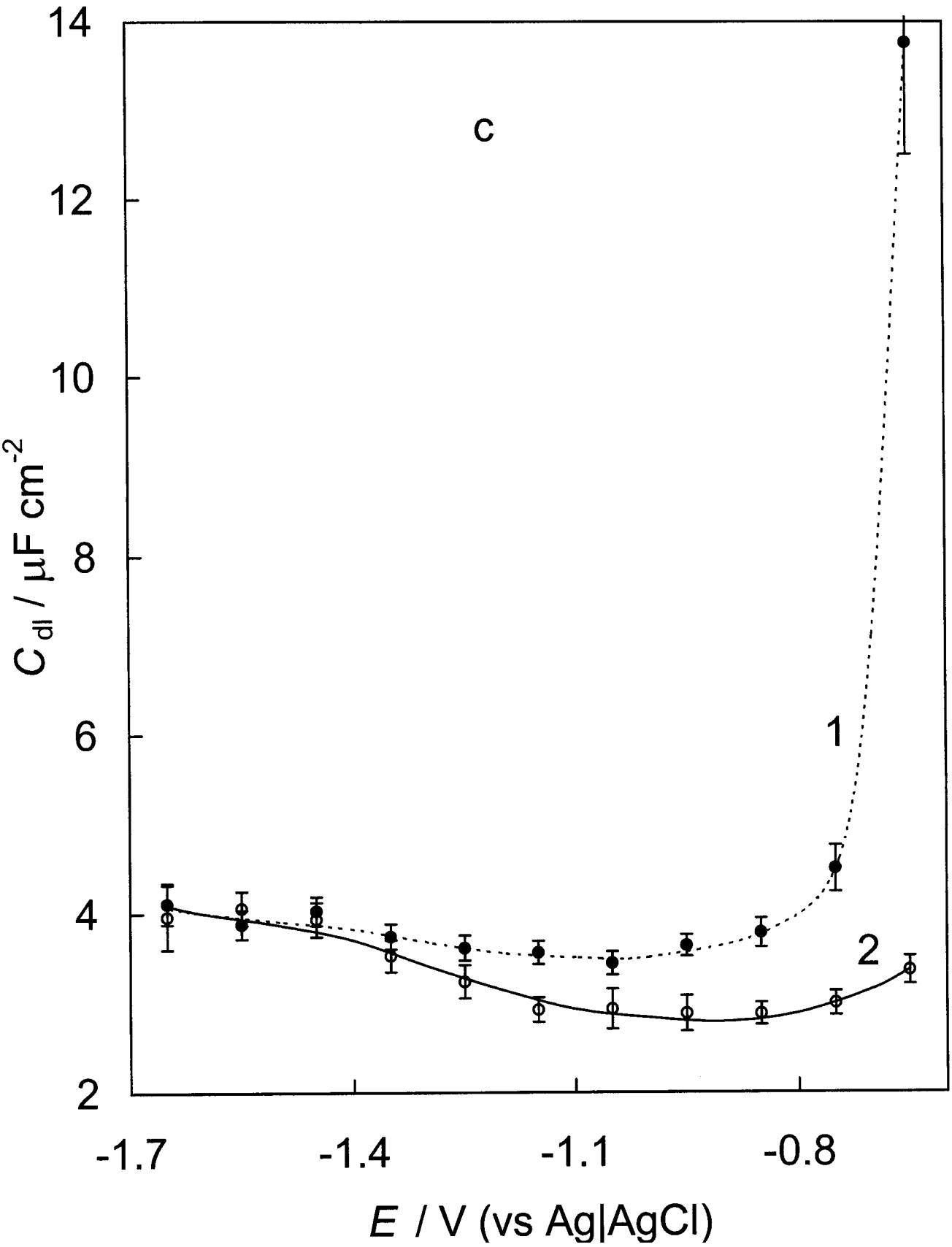

Fig. 6c.

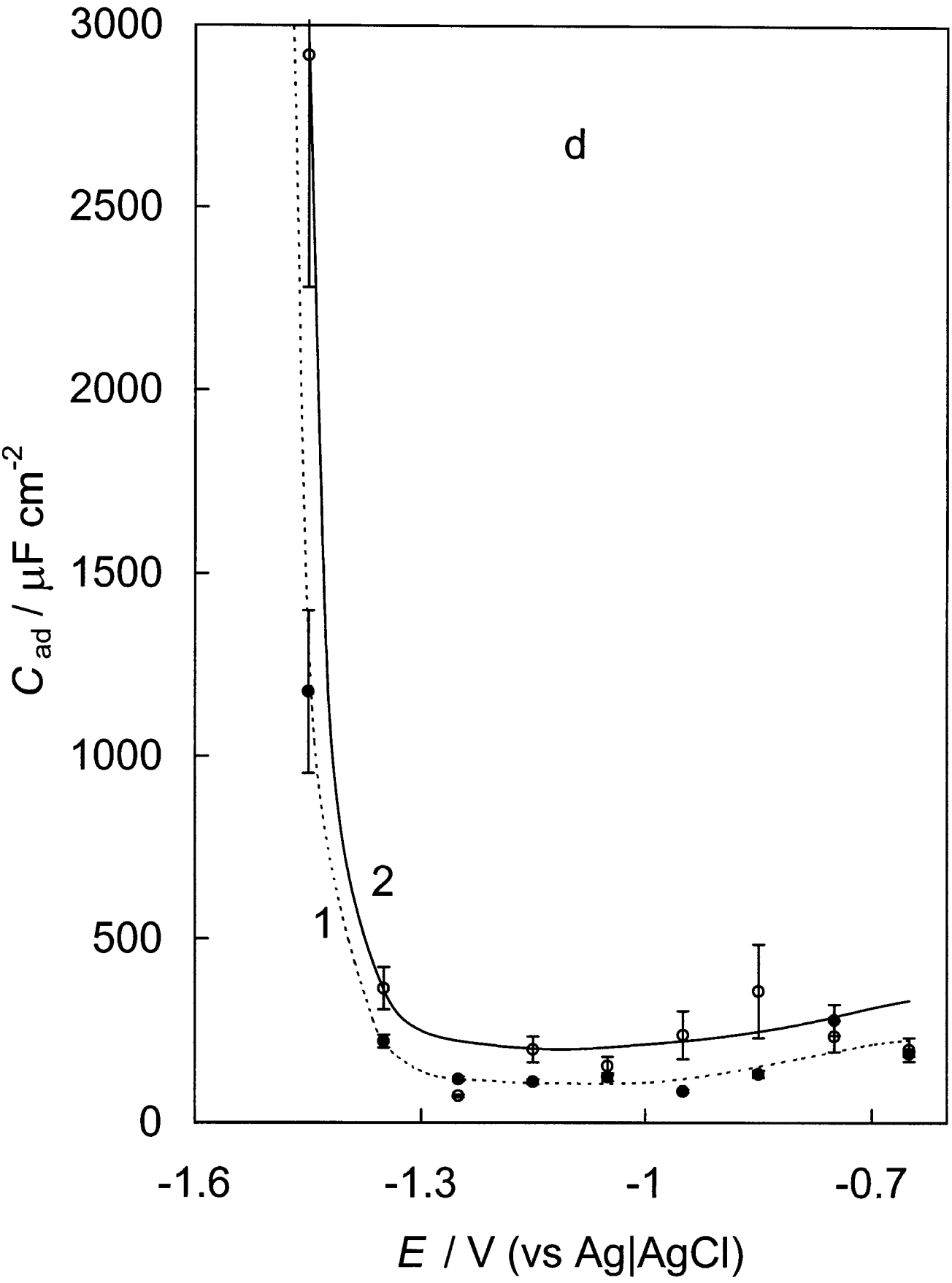
3000
2500
2000
1500
1000
500
0
d
2
1
C_{ad} / μF cm^{-2}
-1.6
-1.3
-1
-0.7
E / V (vs Ag|AgCl)

Fig. 6d.

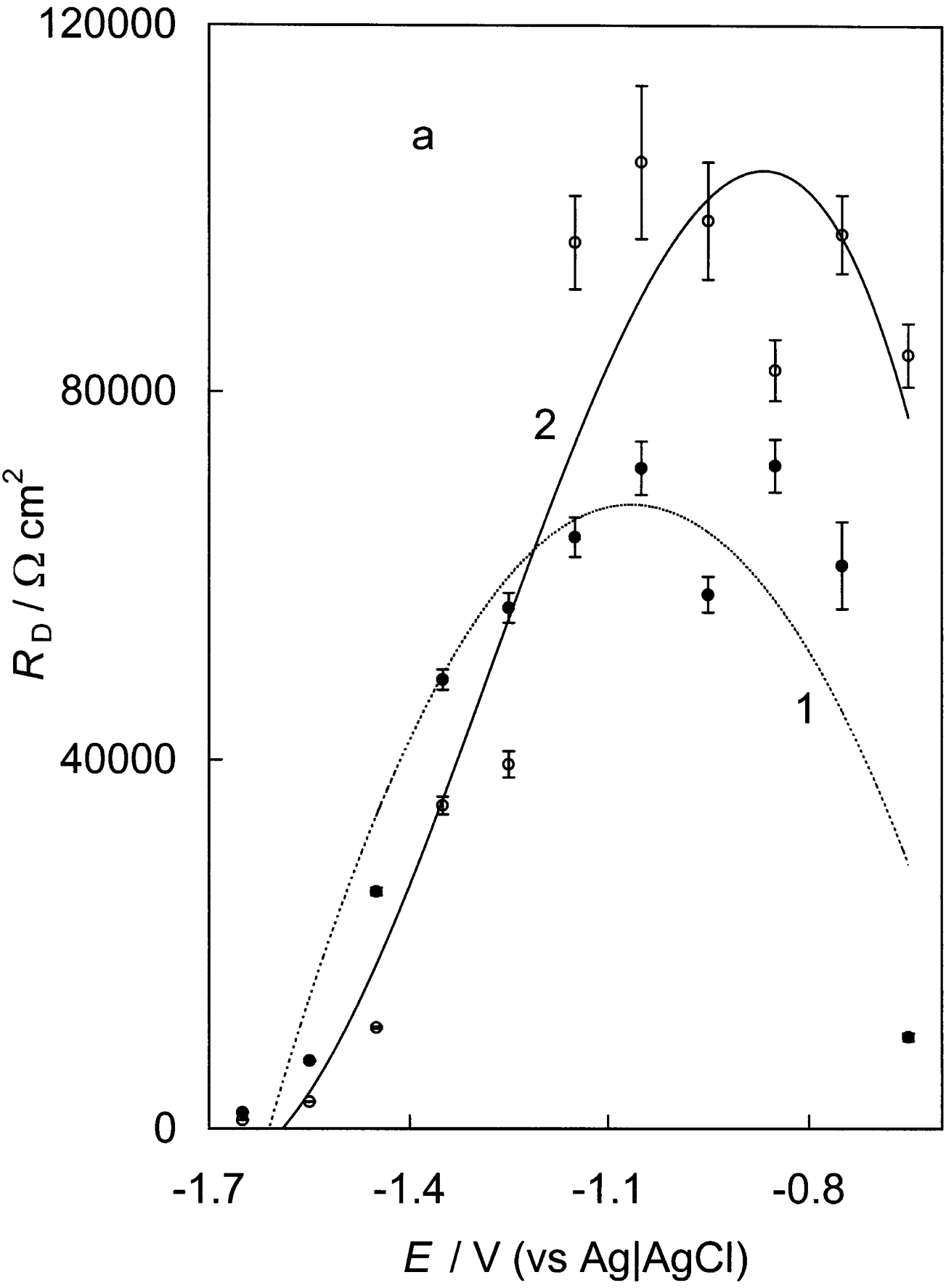

Fig. 7a.

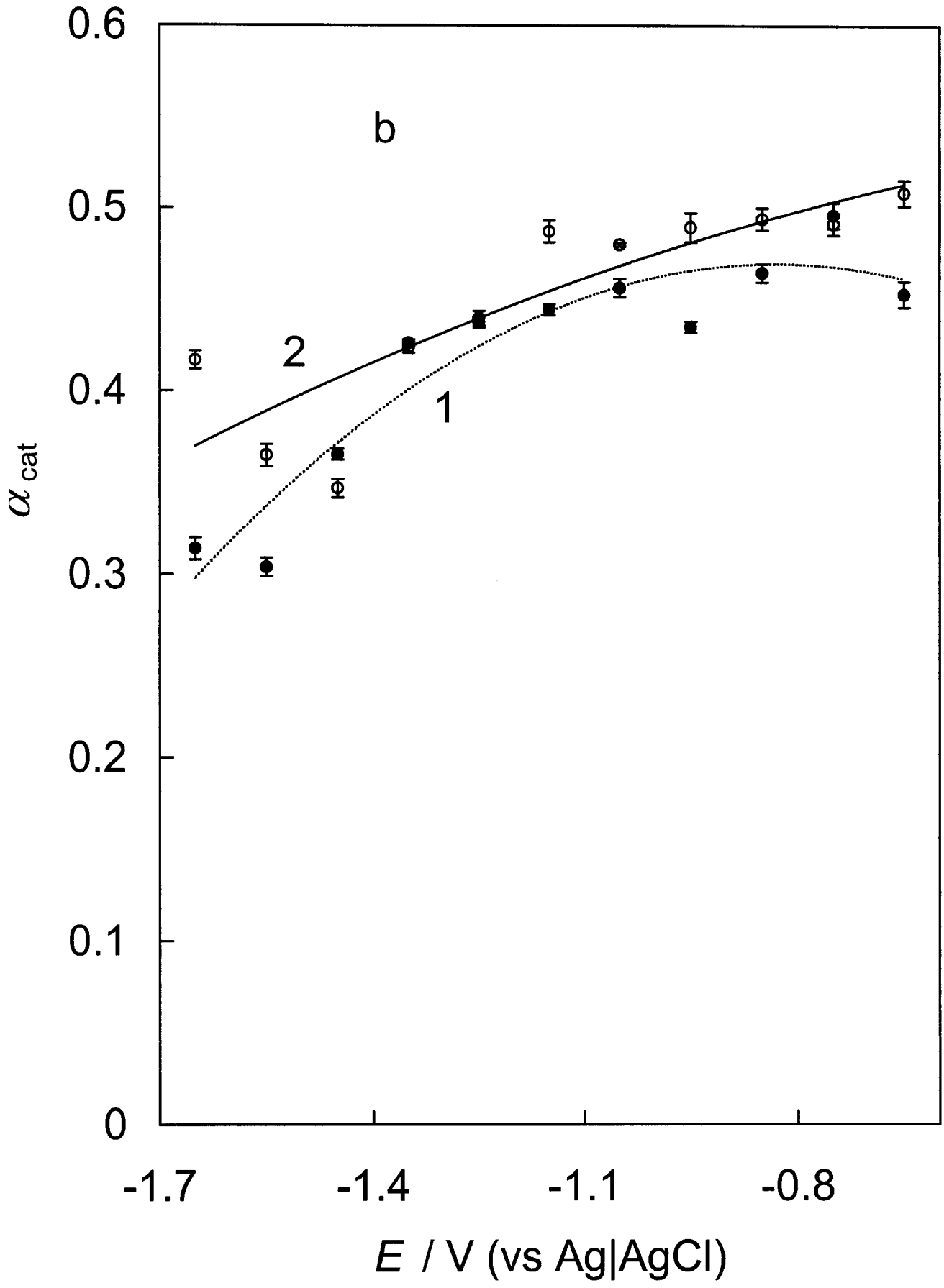

Fig. 7b.

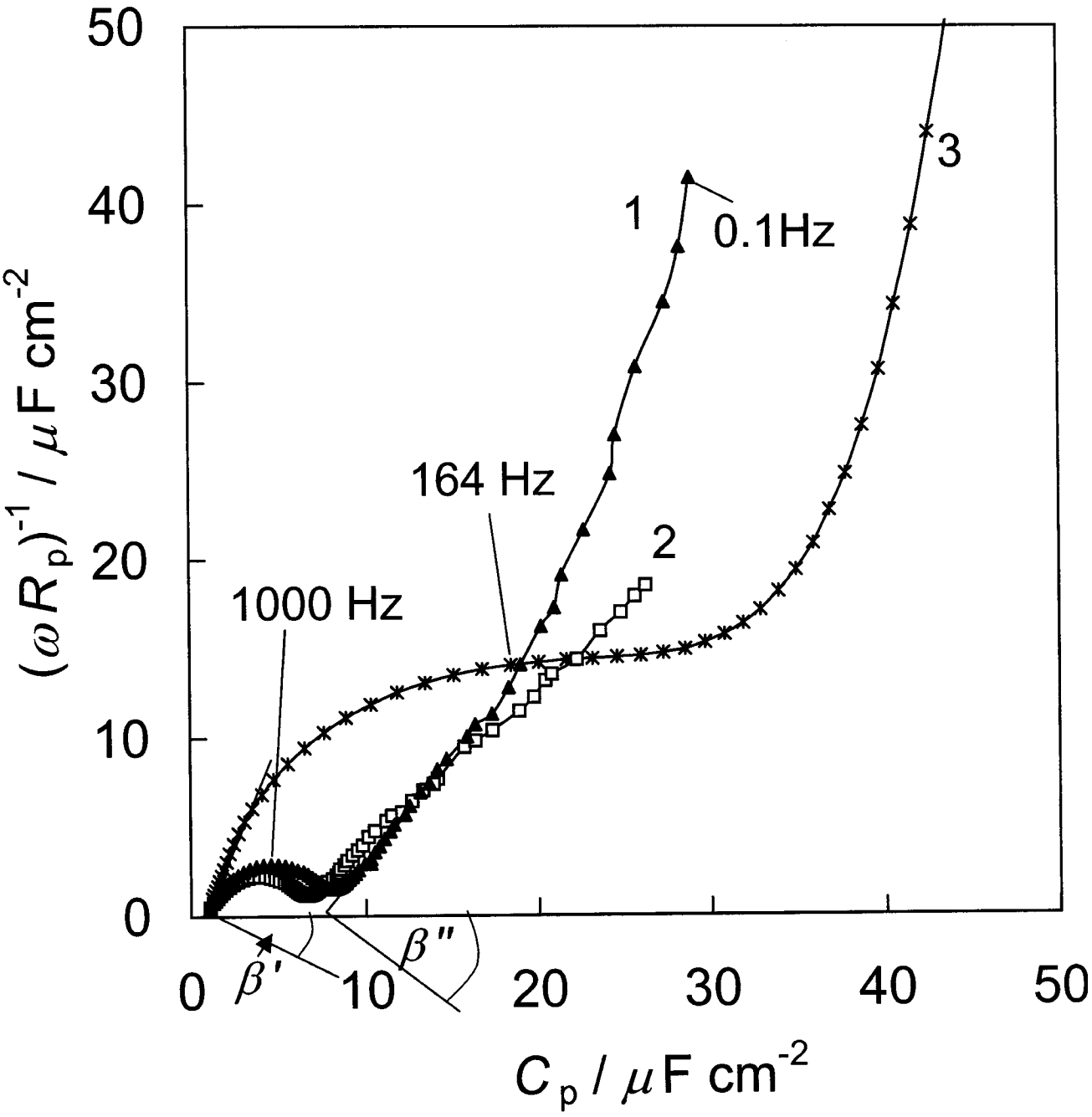
50
40
30
20
10
0
0
10
20
30
40
50
$(\omega R_p)^{-1}$ / μF cm^{-2}
C_p / μF cm^{-2}
1
2
3
0.1Hz
164 Hz
1000 Hz
β'
β''

Fig. 8.

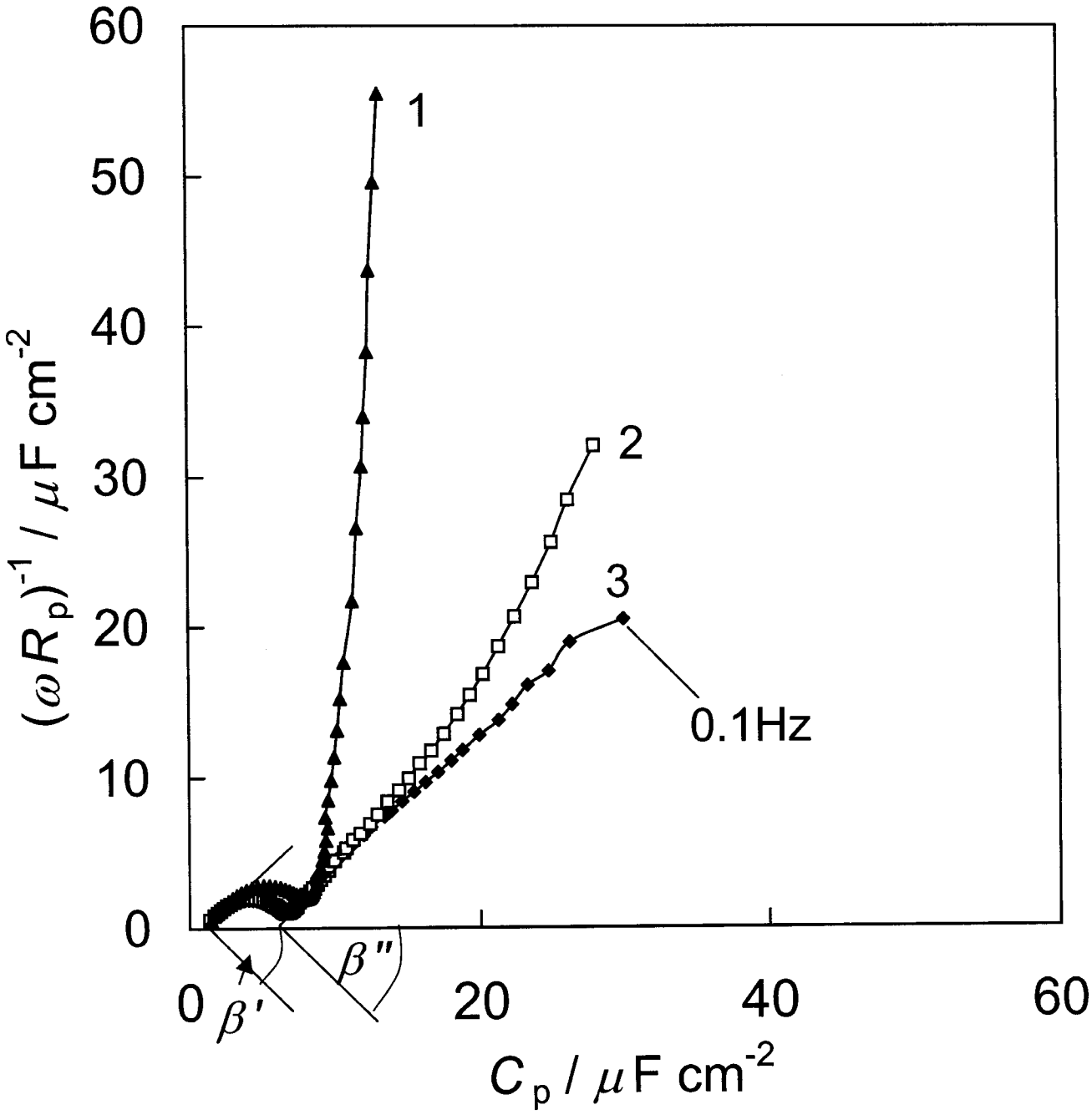

Fig. 9.

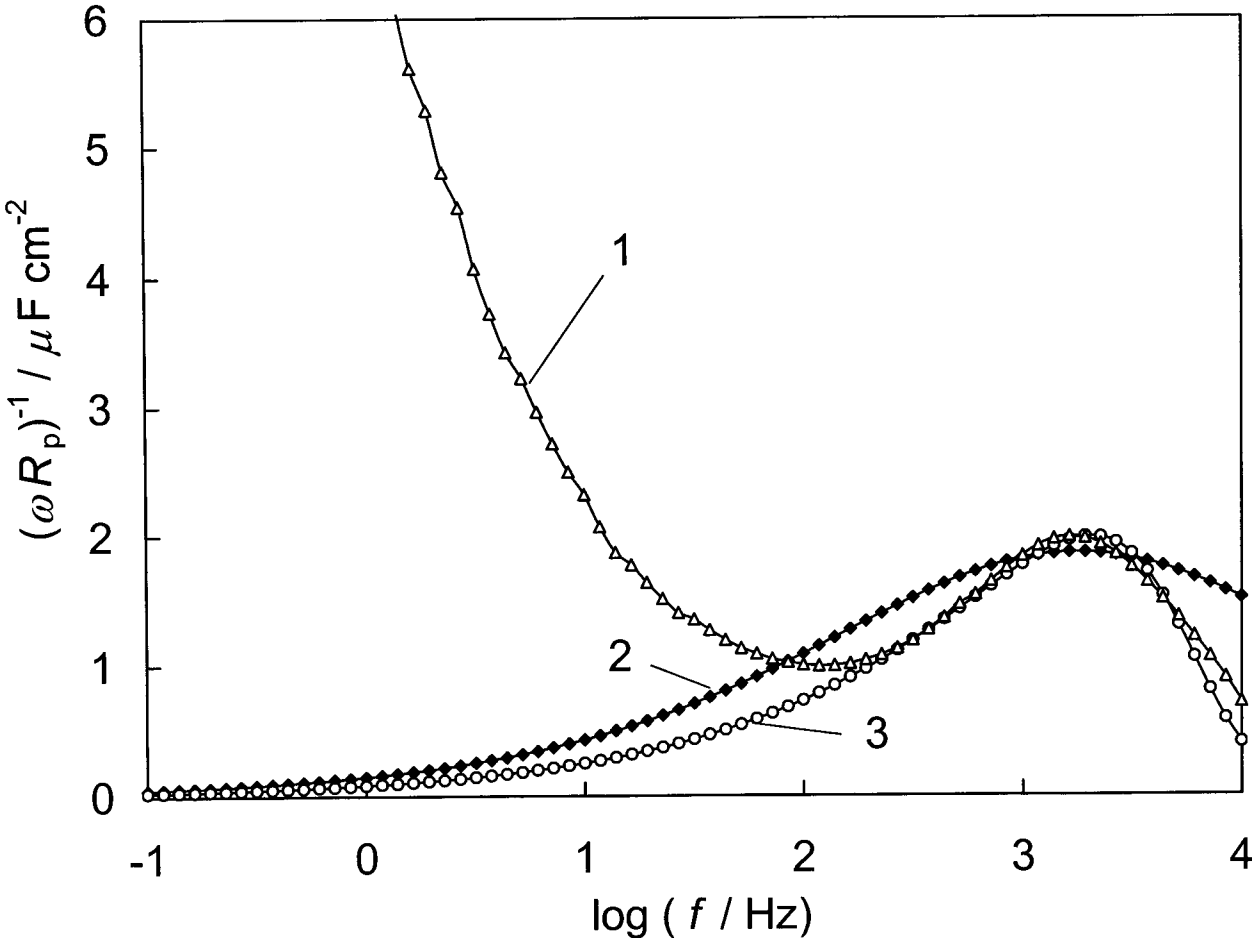

Fig. 10.

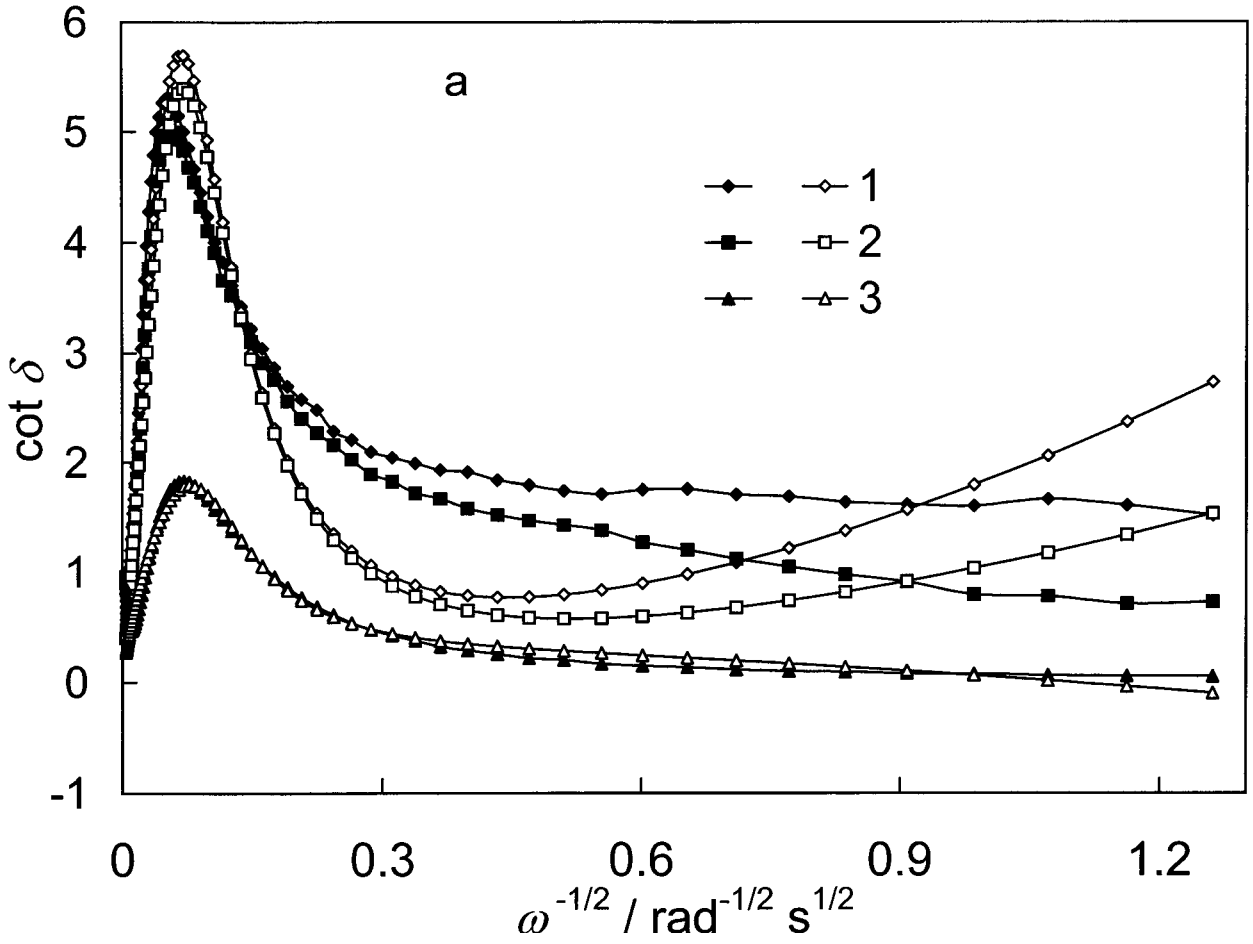

Fig. 11a.

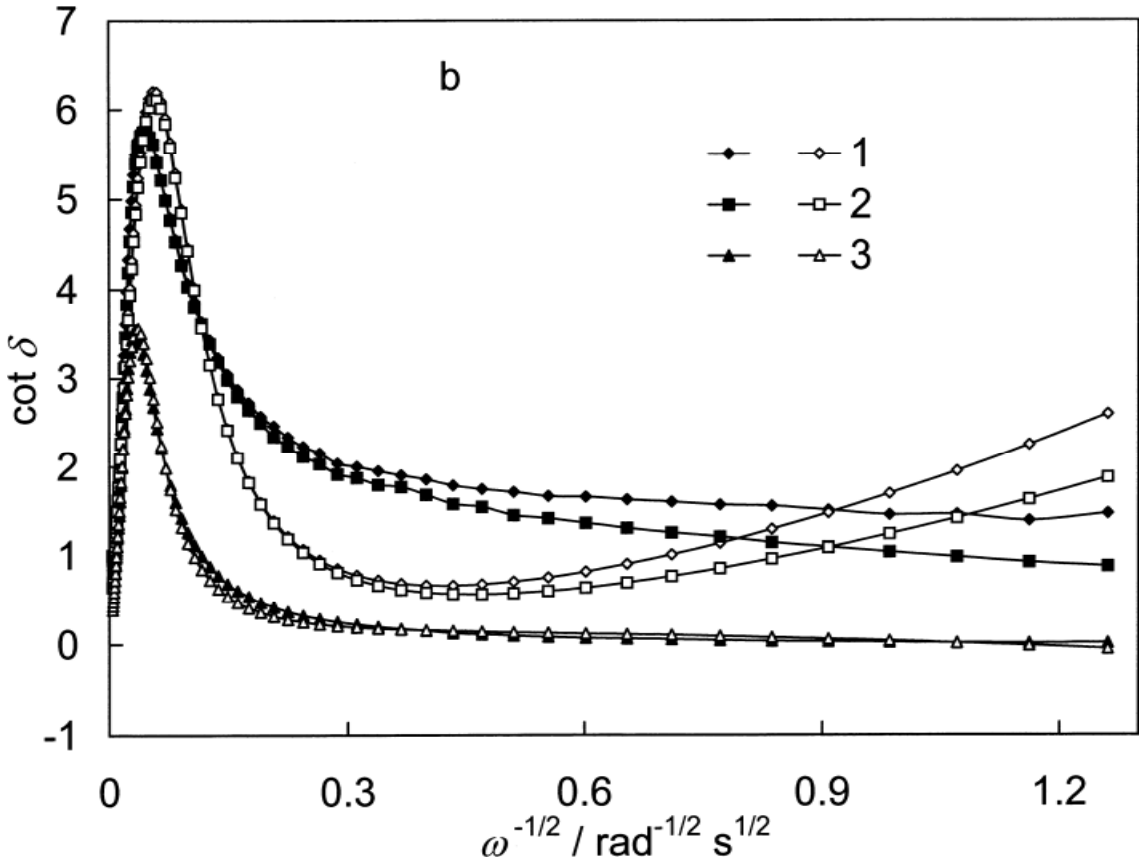

Fig. 11b.

Adsorption kinetics of tetrabutylammonium cations on Bi($01\bar{1}$) plane

K. Laes, G. Nurk, M. Väärtnõu, K. Lust, A. Jänes and E. Lust[*1]

Institute of Physical Chemistry, University of Tartu, 2 Jakobi Street, 51014 Tartu, Estonia

Abstract

Electrochemical impedance spectroscopy has been employed for the study of adsorption kinetics of the tetrabutylammonium cations (TBN^+) at the Bi($01\bar{1}$) | 0.05 M Na_2SO_4 aqueous solution interface. Nonlinear regression analysis has been used for fitting the experimental complex plane (Z'',Z') plots and it was found that the Frumkin—Melik-Gaikazyan equivalent circuit can be used with a good accuracy to describe the experimental data for less concentrated TBN^+ solution. Other more complicated equivalent circuits have been used for interpretation of the experimental impedance data for more concentrated TBN^+ solutions. However, the influence of their elements (charge transfer resistance, resistance and capacitance of the formation of compact two-dimensional adsorption layers at some parts of the electrode) is comparatively small. Analysis of the Cole-Cole and other dependences shows that diffusion of TBN^+ to the Bi($01\bar{1}$) electrode surface is probably the rate-determining step of the adsorption process (for less concentrated TBN^+ solutions) in the region of maximal adsorption potential and at moderate ac frequency. At lower frequency, the two-dimensional association process of TBN^+ is possible. Within the region of adsorption-desorption peaks, the mixed kinetic mechanism (slow diffusion and adsorption steps with the relaxation time constants τ_D and τ_K ($\tau_D > \tau_K$)) has been established.

Keywords: tetrabutylammonium cation, adsorption, impedance, adsorption kinetics, single crystal, bismuth

1. Introduction

This work is a part of the project devoted to the study of the influence of the crystallographic structure of bismuth on the adsorption kinetics of neutral organic molecules and ions at the Bi | solution interface [1-5]. Analysis of the impedance data demonstrates that the adsorption process of 2-methyl-2-butanol (*tert*-PenOH), cyclohexanol (CH) and normal heptanol (*n*-HepOH) is mainly limited by the rate of diffusion of the organic molecules to the electrode surface [1-3]. However, at small frequencies and higher concentrations of *tert*-

[*] Corresponding author (e-mail: enn@chem.ut.ee, fax: +372 7 375160)

PenOH, CH, uracil, dodecyl sulfate anions (DDS) and *n*-HepOH noticeable deviations of the system from a purely diffusion-limited mechanism have been established [1-5]. These deviations are mainly caused by the two-dimensional association of the molecules adsorbed in the adsorption layer and by formation of the two-dimensional clusters at some regions of the adsorption layer. The adsorption kinetics of various tetraalkylammonium ions at an electrode surface is a very important problem as these cations in combination with various anions are widely used in the electrochemical double layer (edl) capacitors and the electrochemical behaviour of these cations (i.e. adsorption and diffusion relaxation times) determines the characteristic frequencies (i.e. charging and discharging times) of the edl capacitors. The impedance studies of the nanoporous carbon | non-aqueous tetrabutylammonium salt systems show very complicated kinetic behaviour [6,7] and, for that reason, the results for nearly ideally flat electrode are inevitable for the better understanding of the mechanism of processes, occurring at the surface of the nanoporous carbon electrode.

It should be noted that Frumkin and Melik-Gaikazyan first observed the frequency-dependence of the impedance of an Hg electrode adsorbing neutral organic molecules [8] and the detailed discussion of the theoretic background of this problem is given in Refs. [8-16].

The main aim of this work was to establish the nature of the limiting stage and to obtain the kinetic parameters of tetrabutylammonium cation adsorption on the Bi($01\bar{1}$) plane surface.

2. Experimental

The experimental procedure used in this work has been described in Refs. [1–5]. The final surface preparation of a Bi(hkl) electrode was obtained by electrochemical polishing in an aqueous KI + HCl solution. After that, the electrodes were carefully rinsed with ultra purified water and polarised at -1.0 V vs. Ag|AgCl|KCl (sat.) in H_2O (Ag|AgCl) in the working surface-inactive solution for 2 hours. The electric double layer impedance was measured using an Autolab PGSTAT 30 with a FRA 2 ($0.1 < f < 10000$ Hz, 5 mV modulation), and the system was calibrated using various standard equivalent circuits. The quality of the electrodes was tested by X-ray diffraction as well as AFM and STM methods [1-5].

Water for preparing the solutions was treated with the Milli Q+ purification system. Solutions were prepared volumetrically using Na_2SO_4 and $(C_4H_9)_4NI$ purified by triple recrystallization from water and treated in vacuum to dryness. Na_2SO_4 was calcined at 700°C immediately prior to the measurements. Electrolytic hydrogen was bubbled for 1–2 h through the electrolyte before the submersion of the electrode into the solution and temperature was kept at 298 ±1 K.

3. Results and discussion

3.1. Cyclic voltammograms (CVs)

The CVs (scan rate 5 mV s^{-1}) were recorded in order to determine the quality of the surfaces investigated and the potential range in which the adsorption of tetrabutylammonium cation (TBN^+) occurred. The shape of the CV recorded for the supporting electrolyte was characteristic of the Bi($01\bar{1}$) plane in accordance with our previous studies [1–5]. The cyclic voltammetry curves also indicate that the bismuth single crystal plane investigated is ideally polarizable within the potential region from -1.65 to -0.40 V (Ag|AgCl) in aqueous 0.05 M Na_2SO_4 solution. The same potential region of ideal polarizability was obtained according to the impedance data (Fig. 1). The noticeable increase in the current density for the solutions with addition of TBN^+ at $E <$ -1.7 V (Ag|AgCl) is mainly caused by the weak specific adsorption of TBN^+ ions at Bi($01\bar{1}$) (as the adsorption-desorption maxima have been established in the *C*,*E* curves (Fig. 2)) as well as by the shift of the zero charge potential toward less negative potentials, and by slow hydrogen evolution reaction at $E <$ -1.7 V (Ag|AgCl). It should be noted that the data measured at $E <$ -1.65 V have not been used for the quantitative analysis.

3.1. Complex plane (Z", Z') – plots

The complex plane plots (so-called Nyquist plots, where the imaginary component $Z'' = 1/jC_s\omega$ ($j = \sqrt{-1}$, C_s is serious resistance and angular frequency $\omega = 2\pi f$, where f is ac frequency, and Z' is the real part of the impedance) at different electrode potentials in the

pure base electrolyte solution (Fig. 1) are in a good agreement with the data established in Refs [2,3]. The equivalent circuit parameters were calculated by fitting the impedance function to the measured spectra by a non-linear least squares fitting minimisation method [17,18], as well as by the "ZView for Windows (2.2)" program" [19,20,21]. However, the results obtained using "ZView for Windows" will be discussed mainly in this paper.

The non-linear least square fitting data show that the *Z''*,*Z'*-curves (Fig. 1) for the Bi($01\bar{1}$) | base electrolyte interface can be described by the equivalent circuit which assumes that the interfacial impedance is in a form of the constant phase element (CPE) (the CPE impedance $Z_{CPE} = A^{-1}(j\omega)^{-\alpha}$, where A ($\mu F^{\alpha}\Omega^{\alpha-1}$ cm^{-2}) is a CPE coefficient and α is a fractional exponent (if $\alpha = 1.0$, then A simplifies to the double layer capacitance C_{dl})), R_{el} is the electrolyte resistance and R_{ad} is the adsorption (or partial charge transfer) resistance [1-5,13,15,16,20,21]. According to the results of calculations, the value of R_{el} is practically independent of E but the values of α and A depend very slightly on E, and A has a small minimum at $E \sim$ -1.0 V (Ag|AgCl). The values of R_{ad} have a maximum in the region of $E \sim$ -1.0 V (Ag|AgCl), and R_{ad} decreases with the rise of the negative polarisation ($E <$ -1.65 V), which is caused by a slow cathodic process on the Bi planes (probably hydrogen evolution) at potentials more negative than -1.65 V. A small decrease of R_{ad} takes place in the region of positive polarisation ($E \geq$ -0.4 V), which is caused by the initial state of the surface oxidation of the Bi($01\bar{1}$) electrode. These potential regions ($E >$ -0.4 V and $E <$ -1.8 V) have not been used for the quantitative analysis of the impedance data. According to Refs. [9-15,20,21], R_{ad} in parallel to CPE means that a very slow adsorption-desorption process (i.e. a partial transfer process [1-5]) of the base electrolyte ions is possible. However, the very high R_{ad} values ($R_{ad} \geq 15000\ \Omega$ cm^2) indicate that this process is very slow on Bi($01\bar{1}$) plane [1-5] and therefore the co-adsorption of the base electrolyte ions with TBN^+ cations can be neglected to a first approximation. On the other hand, R_{ad} in parallel to the double layer capacitance can also be traced back to a slow "true" heterogeneous charge transfer process not related to the adsorption-desorption process of the electrolyte ions [9,11-16]. However, the very low current density (j) values and very weak dependence of j on electrode potential, as well as very high R_{ad} values indicate the absence of quick "true" Faradaic reactions on the Bi single crystal plane | base electrolyte interface [1-5].

As for other real Bi single crystal plane electrodes [1-3], the impedance measured for Bi($01\bar{1}$) in the double layer region (no Faradaic current) follows a power law, such as that for the CPE [1-5,15,16,20-27], with a value of the fractional exponent $\alpha \geq 0.96$, and the

phase angle observed for the Bi single crystal planes is between -86° and -88°. To a first approximation, the values of α slightly lower than 1.0 can be explained by the very weak geometric and energetic inhomogeneities of the electrode surface (mainly on the nanoscopic and atomic scale) [1-5,15-27]. Another explanation for the capacitance dispersion ($\alpha \leq 1.0$) would be the weak specific adsorption of the ions (mainly anions) as, due to the exponential dependence between the rate coefficient and adsorption activation energy, a relatively narrow distribution of surface energy (i.e. the weak energetic inhomogeneity of the solid surface) causes a broad distribution of the rate coefficients (or relaxation time constants) and, therefore, the more pronounced dependence of impedance on the ac frequency [15,16,20,21]. However, the values of α obtained from 0.96 to 0.98 are practically independent of the electrode potential and can be explained mainly by the very weak geometric and energetic inhomogeneities of the Bi electrodes [1-5]. It should be noted that these conclusions are in a good agreement with the results in literature [22-27] devoted to the conception of so-called "ideally polarizable electrode" [1-5, 15,16,28]. The main results established can be reviewed as a conclusion that there is no ideally polarizable electrodes if $\alpha \neq 1.0$ [22,24-27]. Thus, from the physical point of view there are problems with the conception of "ideally polarizable electrode" for the solid electrodes but the classical conception takes into account only the fact that the Faradaic current has to be minimal [23,25,28,29]. It should be noted that the discussion of physical reasons for the deviation of α from unity for the Bi$(01\bar{1})$ | electrolyte interface is not a main aim of this paper and therefore the more detailed analysis will be given in our next publication.

The Z'',Z'-curves for the base electrolyte solution with various additions of TBN^+ ions are presented in Fig. 3 (points – experimental data, solid lines – calculations according to the Wandlowski-de Levie model, discussed later), and C,E-curves at constant ω (but at different concentrations of TBN^+, c_{cat}) are given in Fig. 2. In agreement with the Frumkin and Melik-Gaikazyan model [8-15], at constant potential, the values of C_s depend noticeably on ω in the region of the adsorption-desorption maxima E^{peak} as was found for CH, *tert*-PenOH, DDS and *n*-HepOH adsorption on Bi planes [1-5]. This is mainly caused by the dependence of surface coverage θ on E, i.e. by the dependence of $(\partial\theta/\partial E)_\mu$ on ω in a good agreement with the ideas of Refs. [8,9,11-16]. There is a weak dependence of C_s on f [30-32] in the region of maximal adsorption (E_{max}), where the very well pronounced capacitance depression takes place, characteristic of the adsorption of organic compounds and organic cations on the Hg, Au and Hg like metals [30-32]. In the region of maximal adsorption, C_s decreases with

increasing c_{cat}. In the region of adsorption-desorption (E^{peak}), C_s rises with the increase of concentration of the adsorbate in the solution and there is a nearly linear dependence of C_s on $\omega^{1/2}$ in the region of moderate frequencies, characteristic of the mainly diffusion-limited process [1-8,11-16]. At $E > E_{\sigma=0}$, adsorption of the I^- ions takes place at Bi($01\bar{1}$) like Hg, Au and polycrystalline Bi [30-32], but these data can not be used for the quantitative analysis, because the surface oxidation of the Bi($01\bar{1}$) plane is possible at E > -0.5 V (Ag|AgCl).

The dependences of R_s (series resistance) and R_p (parallel resistance) on $\omega^{1/2}$ at fixed electrode potentials and c_{cat} are given in Fig. 2 (b). According to these results, the values of R_s and R_p noticeably increase with decrease of ac frequency at E > -1.6 V (Ag|AgCl), and the very high R_s values at $\omega \to 0$ indicate that there is no quick Faradaic reactions at Bi($01\bar{1}$) | 0.5 M Na_2SO_4 + x M $(C_4H_9)_4NI$ solution interface. However, the noticeable difference between R_p and R_s values at more negative potentials ($E \leq$ -1.7 V) indicates that the partial charge transfer between Bi($01\bar{1}$) surface and TBN^+ ions or the "true" Faradaic processes are possible.

The shape of the *Z''*,*Z'*-plots depends noticeably on the electrode potential as well as somewhat on concentration of the TBN^+ ions in the solution (Fig. 3). Within the range of potentials $-1.65 \leq E \leq$ -1.45 V (Ag|AgCl), *Z''*,*Z'*-plots can be simulated, to a very rough approximation, by the depressed semicircles with the centre displaced below the real axis, which indicates that the relaxation time τ is not a simple-valued quantity but is distributed continuously or discretely around a mean $\tau_m = \omega_m^{-1}$ value [16] (more correct analysis of the *Z''*,*Z'*-data will be given later). On the other hand, these arcs can be substantially distorted by other relaxations whose mean time constants are within two orders of magnitude or less of that for the arc under consideration. Thus, according to the data in Fig. 3, two limiting stages (diffusion and adsorption or a (partial) charge transfer processes [1-5,9-16]) seem to be valid for the Bi($01\bar{1}$) | 0.05 M Na_2SO_4 + x M TBN^+ solution interface. The value of $Z'(\omega\to\infty) \equiv Z_\infty = R_\infty$ (Fig. 3) is practically independent of concentration of TBN^+ in the solution and the value of R_∞ can be taken equal to the electrolyte resistance R_{el}. However, the values of the heterogeneous relaxation time τ_m as well as Z''_{max} (imaginary impedance component Z'' at τ_m) and the half-width of the arc on the real axis $(R_0 - R_\infty)/2$ (where R_0 is the real impedance component Z' as ω=0) as well as $Z'(\omega\to0) \equiv R_0$ depend noticeably on concentration of the organic cation adsorbed (τ_m is proportional to c_{TBN^+}) and the adsorption resistance increases with increasing c_{TBN^+} in the solution.

According to the data in Fig. 3, at constant c_{TBN^+} and Z', the value of $|Z''|$ is maximal within the region of maximal adsorption (-1.2 < E < -0.65 V (Ag|AgCl)). The depression angle β' [15,16] has minimal and R_0 has maximal values in this region of potentials (the values of β' equal to 45° and 0° are characteristic of the purely diffusion limited process and heterogeneous charge transfer step, accordingly).

The dependence of phase angle δ ($\delta = \arctan(|Z''|/Z')$) on log$f$ has a minimum at $f \geq 2\times10^3$ Hz (Fig. 4 (a)) and the δ,log$f$-plots have very well exposed plateaus with $|\delta| \leq 80°$ at $f \leq 200$ Hz, characteristic of nearly pure capacitance behaviour ($|\delta| = -90°$). However, there is an additional maximum in the phase angle vs. log f plots for the data obtained in the region of maximal adsorption, which is probably due to the formation (or dissipating) of the two-dimensionally associated layers at some parts of the electrode surface. $|\delta|$ decreases somewhat at the negative potentials ($E \leq -1.45$ V) and at very low frequencies, which may be connected mainly with a partial charge transfer process or very slow Faradaic processes, occurring at very low frequencies [2-5]. The shape of the δ,log$f$-curves is practically independent of electrode potential at $f \geq 100$ Hz (except $E \leq -1.65$ V and $E \geq -0.65$ V), but the region of intensive increase of $|\delta|$ with f (at constant $\left(\partial\delta/\partial f\right)_{c_{TBN^+}}$) is shifted toward lower values of f with the increase of negative polarisation, i.e. with the decrease of θ or Gibbs adsorption Γ_{TBN^+}. The maximal values of $|\delta|$ increase very slightly with increasing c_{TBN^+} (Fig. 4 (c)), but the region of intensive increase of $|\delta|$ with f is noticeably shifted toward lower values of f with the decrease of c_{TBN^+}. The noticeable shift of δ,log$f$ plot for E = -0.65 V can be explained by the specific adsorption of the I^- anions at the Bi($01\bar{1}$) surface in this potential region, and by the noticeably lower relaxation frequencies of the specifically adsorbed I^- anions [27].

3.3 Fitting of impedance data

Experimental impedance data were mainly analysed using the equivalent circuits illustrated in Fig. 5, where R_{el} is the electrolyte resistance, C_{dl} and C_{ad} are the double layer and adsorption capacitances, respectvely; CPE is the constant phase element; Z_W is Warburg-like diffusion impedance and R_{ad} is the adsorption or partial charge transfer resistance [1-5,9,11-21]. C_n and R_n are the capacitance and resistance of the "needle" adsorption-desorption peak formation discussed later in more detail. The value of C_{dl} characterises the

capacitance of the metal | electrolyte interface at ac $f \to \infty$; and C_{ad} is caused by the dependence of the electrode surface coverage θ on the electrode potential E. Studying the difference between five equivalent circuits presented in Fig. 5, there are two accurate ways to obtain an indication of how well the modelling function reproduces the experimental data set: (1) observing the parameter values and their relative error estimates (in %); (2) the chi-square function (χ^2) and the weighted sum of the squares (Δ^2) also give a good indication about the quality of the fit [2-5,17-19]. The parameters for some systems, calculated by the "ZView for Windows 2.2" program, are given in Table 1.

Non-linear regression analysis [19] of the Z'',Z'-curves shows that in the region of potentials from –1.65 to –0.6 and at c_{TBN^+} less than 1×10^{-5} M, these data can be simulated with the classical Frumkin-Melik-Gaikazyan equivalent circuit presented in Fig. 5 (circuit b). In this case, the specific impedance and capacitance functions have the following forms

$$Z(\omega) = R_{el} + \frac{1}{j\omega C_{dl} + \dfrac{1}{\dfrac{\sigma_{ad}}{\sqrt{j\omega}} + \dfrac{1}{j\omega C_{ad}}}} \qquad (1)$$

and

$$C(\omega) = \frac{1}{j\omega[Z(\omega) - R_{el}]} = C_{dl} + \frac{C_{ad}}{1 + \sigma_{ad} C_{ad} \sqrt{j\omega}} \qquad (2)$$

where $\sigma_{ad}(j\omega)^{-1/2}$ represents the diffusion (Warburg-like) impedance Z_W with its coefficient σ_{ad}. The replacement of Warburg-like diffusion impedance by the adsorption or partial charge transfer resistance R_{ad} in this equivalent circuit (circuit I) did not give a better fit of the experimental resultswith the calculated data. (It should be noted that the value of χ^2 function should decrease by tenfold if a new circuit element is introduced into the equivalent circuit system, and the simplest equivalent circuit should be taken as a more reliable model of the interface if the values of χ^2 function are comparable [16-19].) The attempts to add some additional elements in this equivalent circuit (mainly an adsorption or charge transfer resistance R_{ad} (circuit c in Fig. 5)) did not give a better fit as it was found for Br^- adsorption on Au planes [32]. Thus, to a first approximation, in the case of less concentrated TBN^+ solutions it seems that the heterogeneous adsorption step of TBN^+ ions is comparatively quick and reversible at the Bi($01\bar{1}$) plane [32,33]. This result is in a good agreement with the data for other aliphatic compound adsorption on the Bi planes studied [1-5]. The results of fitting by using the CPE instead of C_{dl} (circuit d in Fig. 5) did not give a noticeably better

agreement of the calculated Z'',Z' plots with experimental ones and, for that reason, these results have not been discussed in more detail in this work. Therefore, to a first approximation, the classical Frumkin-Melik-Gaikazyan circuit seems to be a more probable physical model of the adsorption layer formed at the Bi($01\bar{1}$) plane in the less concentrated TBN^+ solutions as it is the simplest circuit that gives a better fit to experimental results at potentials less negative than E^{peak}.

For the simulation of the Warburg-like diffusion impedance Z_W values, at first we used the classical Frumkin-Melik-Gaikazyan approximation, where diffusion of the molecules is assumed to be semi-infinite [1-5,8,9,11,13-16] with $\alpha_{cat} = 0.5$. According to the data of simulations, there is a reasonable agreement of experimental results with the fitting data if α_{cat} has been fixed at 0.5 (Table 2). For the better fit of the complex plane plots in the region of maximal adsorption (where a compact adsorption layer occurs at the some parts of the electrode surface), we have additionally used the ZView for Windows (Version 2.2) fitting program [19], where the generalised finite Warburg element (GFW) for a short circuit terminus model is expressed as

$$Z_{GFW} = \frac{R_D \tanh\left[(jT\omega)^{\alpha_{cat}}\right]}{(jT\omega)^{\alpha_{cat}}} \qquad (3)$$

where $T = L^2 / D$ (L is the effective diffuse layer thickness and D is the effective diffusion coefficient of a particle); R_D is the so-called limiting diffusion resistance as at very low frequencies Z' approaches R_D and Z'' tends to zero [16-19,35-39]. It should be noted that the fractional exponent α_{cat} is equal to 0.5 in Eq. (3) in the case of finite length Warburg short circuit terminus model (FLW), which is the solution of the one-dimensional diffusion equation of a particle, being completely analogous to the wave transmission in a finite-length R,C transmission line model [35-39]. The results of simulation indicate that the χ^2-function as well as Δ^2 values decrease somewhat if the GFW element has been used, but the dependence of the other fitting parameters (C_{dl}, R_{el}, C_{ad}, R_{ad}) on the diffusion layer model selected is very weak. Thus, according to the suggestions given in Refs. [16-19], the GFW model is not very well justified for the Bi($01\bar{1}$) | $(C_4H_9)_4NI + Na_2SO_4$ aqueous solution interface and, for that reason, the dependence of the equivalent circuit element parameters on E and c_{cat}, obtained according to the classical Frumkin — Melik-Gaikszyan model, will be discussed here.

The dependence of C_{dl} on the electrode potential is in a good agreement with the Frumkin-Damaskin adsorption theory for neutral organic compounds at ideally polarizable

electrodes [7,11,13]. C_{dl} has minimal values in the region of zero charge potential (in the region of maximal adsorption) and increases quickly with desorption of the organic compound from the electrode surface with increasingly negative polarisation of the electrode.

The adsorption capacitance (additional) values, C_{ad}, calculated according to Eqs. (1) and (2), are minimal at the potentials of maximal adsorption in a good agreement with the Frumkin-Damaskin adsorption theory for the neutral organic compounds at the ideally polarizable electrodes [7,11]. The C_{ad} values increase very quickly with the decrease of ω at $E \leq$ -1.45 V as well as at $E \geq$ -0.65 V, where the value of $(\partial\theta/\partial E)_{\mu}$ is high. At very high frequencies as well as in the region of maximal adsorption, C_{ad} has a tendency to approach zero. At the potentials near E^{peak}, the values of C_{ad} rise with concentration of the tetrabutylammonium cation. Sometimes at peak potentials, there is instability in the fitting procedure caused by the very high values of C_{ad} at E^{peak} [2-5]. It should be noted that in the range of potentials from –1.65 to –1.5 V (Ag|AgCl), the error values for C_{ad} are very large and, therefore, the numerical values of C_{ad} established for this potential region have to be regarded with some caution.

The value of the electrolyte resistance R_{el} depends very slightly on the electrode potential ($\Delta R_{el} \leq 4\%$) as well as on c_{TBN^+} and this behaviour is characteristic of the ideally polarizable electrodes [2-5,7,11-13].

The values of the diffusion resistance, R_D, obtained according to Eqs. (1-3) are maximal in the region of maximal adsorption and R_D is practically independent of c_{TBN^+}. At the potentials near E^{peak}, R_D has minimal values, which are independent of c_{TBN^+}.

According to the results of simulations, based on the finite length Warburg short circuit terminus model (FLW), the fractional exponent α_{cat} values are slightly lower than 0.5 in the region of maximal adsorption. At $E = E_{max}$, α is nearly equal to 0.5 in a reasonable agreement with the classical Frumkin-Melik-Gaikazyan semi-infinite diffusion model [9,11]. However, α_{cat} has minimal values at the potentials from –1.65 to -1.5 V (Ag|AgCl) in the case of more concentrated TBN^+ solutions, where the desorption of TBN^+ cations begin. Thus, the deviation of α_{cat} from 0.5 exists if the dependence of θ on E is high. This effect has been observed for more complicated systems and can probably be explained using the theory of the electrochemical impedance of anomalous diffusion [35-39] (i.e. using the anomalous diffusion model with the adsorbing interface in our case). Probably, to a first approximation, it can be concluded that the deviation of our system from the classical Frumkin — Melik-

Gaikazyan model arises because of high surface coverage and compactness of the adsorption layer on some parts of the Bi($01\bar{1}$) surface [2-5].

The parameter T, obtained at $\alpha_{cat} \neq 0.5$, is expressed as $T = L^2 / D$, where L is the effective diffuse layer thickness and D is the effective diffusion coefficient of a particle. The values of T are maximal in the region of maximum adsorption, but T approaches zero in the region of adsorption-desorption peaks. At E_{max}, the value of T increases with decreasing c_{TBN^+}. The very low values of T indicate that thickness of the adsorption layer is very small or, in other words, the deviation of our system from the classical Frumkin — Melik-Gaikazyan model is unremarkable. The values of α_{cat} unequal to 0.5 can be probably explained by the inhomogeneous adsorption layer structure, i.e. on some parts of the Bi($01\bar{1}$) plane, there is a very compact two-dimensionally associated adsorption layer (where no semi-infinite diffusion occurs) but at some parts, the adsorption rate is limited by the semi-infinite diffusion of the TBN^+ cations.

The impedance and capacitance data at low ac frequency indicate that for more concentrated TBN^+ solutions, the two-dimensional cluster formation is possible in the limited region of the electrode surface [40-43]. According to the model developed by Wandlowski and de Levie [40-43], the isotropic two-dimensional cluster will mostly grow at its periphery where the rate of growth is proportional to the interfacial adsorbate concentration Γ on that part of the interface which is not yet covered by clusters, and on the periphery length $2\pi r$ with a proportionality constant k_g (i.e. k_g is the rate constant of the cluster growth). The rate constant of the reverse process (i.e. edge dissolution) is defined as k_d. However, the growth and dissolution of cluster will be assumed to have another pathway available as well, i.e. for the cluster | electrolyte interface the rate constants k_g' and k_d' are assumed. Under these conditions the following expression for the cluster formation (rate) is valid [42]

$$\frac{dS}{dt} = 2\pi r(k_g \Gamma - k_d) + \pi r^2 (k_g' c_{cat} - k_d') \qquad (4)$$

where S is the area of the cluster, t is time, Γ is the (absolute) interfacial excess, and c_{cat} is the adsorbate concentration, here assumed to be uniform up to the interface. Thus, according to this model, the interface is composed of areas covered by clusters, and other areas not so covered, with the charge densities Q_1 and Q_0, respectively [42]. The charge density of the electrode, Q, is given by

$$Q = Q_0(1-\theta) + Q_1\theta \qquad (5)$$

Current density j is given by

$$j = \mathrm{d}Q/\mathrm{d}t = (Q_1 - Q_0)\,\mathrm{d}\theta/\mathrm{d}t + (1-\theta)\,\mathrm{d}Q_0/\mathrm{d}t + \theta\,\mathrm{d}Q_1/\mathrm{d}t \qquad (6)$$

As shown in [42], the first term of Eq. 6 describes the dominant features of the needle peak at low frequencies. The sinusoidal perturbation of the potential can be expressed as $E = E' + E''\mathrm{e}^{\mathrm{j}wt}$, the cluster radius as $r = r' + r''\mathrm{e}^{\mathrm{j}wt}$, the cluster area as $S = S' + S''\mathrm{e}^{\mathrm{j}wt}$, the interfacial adsorbate concentration as $\Gamma = \Gamma' + \Gamma''\mathrm{e}^{\mathrm{j}wt}$, the extended area fraction as $\theta_\mathrm{x} = \theta_\mathrm{x}' + \theta_\mathrm{x}''\mathrm{e}^{\mathrm{j}wt}$, the area fraction as $\theta = \theta' + \theta''\mathrm{e}^{\mathrm{j}wt}$, and the current density as $j = j' + j''\mathrm{e}^{\mathrm{j}wt}$. Thus, according to [42] the current density of the needle adsorption-desorption peak is given as

$$j_\mathrm{n} = j_\mathrm{n}' + j_\mathrm{n}''\mathrm{e}^{\mathrm{j}wt} \qquad (7)$$

and

$$\begin{aligned} j_\mathrm{n}'' &= \mathrm{j}\omega(\mathrm{Q}_1 - Q_0)\theta'' = \mathrm{j}\omega(\mathrm{Q}_1 - Q_0)\mathrm{e}^{-\theta_\mathrm{x}'}\theta_x' \\ &= \mathrm{j}\omega(\mathrm{Q}_1 - Q_0)\mathrm{e}^{-\theta_\mathrm{x}'}\,4\pi k_\mathrm{g}(\partial\Gamma/\partial E)E''\textstyle\sum r'/\left(2\mathrm{j}\omega - k_\mathrm{g}'c + k_d'\right) \end{aligned} \qquad (8)$$

from which the following impedance of the needle adsorption-desorption peak can be calculated [42]

$$Z_\mathrm{n} = E/j_\mathrm{n}'' = \left(2\mathrm{j}\omega - k_\mathrm{g}'c + k_d'\right)/\left\{\mathrm{j}\omega(\mathrm{Q}_1 - Q_0)\mathrm{e}^{-\theta_\mathrm{x}'}\,4\pi k_\mathrm{g}(\partial\Gamma/\partial E)\textstyle\sum r'\right\} \qquad (9)$$

Thus, impedance of the needle peak can be expressed by a series combination of formation resistance (R_n) and capacitance (C_n), of the needle peak (Fig. 5, circuit e)

$$R_\mathrm{n} = 1/\left\{(\mathrm{Q}_1 - Q_0)\mathrm{e}^{-\theta_\mathrm{x}'}\,4\pi k_\mathrm{g}(\partial\Gamma/\partial E)\textstyle\sum r'\right\} \qquad (10)$$

$$C_\mathrm{n} = \left\{(\mathrm{Q}_1 - Q_0)\mathrm{e}^{-\theta_\mathrm{x}'}\,4\pi k_\mathrm{g}(\partial\Gamma/\partial E)\textstyle\sum r'\right\}/\left(k_d' - k_\mathrm{g}'c\right) \qquad (11)$$

For dilute TBN^+ solutions, the diffusion effects are not yet completely negligible and therefore it must be introduced the time-dependent interfacial concentration (i.e. surface concentration depends on ac frequency) in the form $c = c' + c''\mathrm{e}^{\mathrm{j}wt}$ and

$$\Gamma'' = (\partial\Gamma/\partial E)E'' + (\partial\Gamma/\partial c)c'' \qquad (12)$$

Thus, there is a difficulty in that the boundary condition defining the interfacial flux will now be heterogeneous, and there is no exact solution for this non-trivial problem yet [42]. It is reasonable that the effect of diffusion is likely to be stronger for the non-covered interface than the covered part, because slow dissolution and growth are reducing its effects at the patches [42] (Fig. 5, circuit e). The interfacial admittance can then be represented approximately by the equivalent circuit, where the Frumkin-Melik-Gaikazyan model for the interface non-covered by the two-dimensional compact cluster is valid. For less concentrated solutions the role of two-dimensional compact clusters is small and the circuit simplifies to the classical Frumkin-Melik-Gaikazyan model discussed in Refs. [1-5,9,11-15]. The results

of simulations (Table 1 and Fig. 3) show that the addition of R_n and C_n into the equivalent circuit (circuit e in Fig. 5) increases noticeably the agreement of the experimental data with the fitted Z'',Z' plots for the more concentrated solutions ($c_{cat} > 5\times10^{-4}$ M). The values of C_n and R_n are comparatively low (Fig. 6 (a and b)). In the region of I^- adsorption (at E > -0.65 V) and TBN^+ adsorption, the noticeable decrease in the R_n values has been observed (Fig. 6 (b)). In the case of lower concentrations ($c_{cat} < 1\times10^{-5}$ M) the influence of C_n and R_n on the coincidence of fitted and experimental curves is very small.

The double layer capacitance values C_{dl} are minimal in the regions of TBN^+ adsorption and increase with desorption of TBN^+ at E < -1.65 V or if the adsorption of I^- anions begins at E > -0.65 V (Fig. 6 (c)). The adsorption capacitance C_{ad} is very high in the region of adsorption-desorption peaks at E < -1.65 V (not shown in Fig. 6 (d)) and sometimes it is impossible to obtain the correct fitting data at $E \leq$ -1.65 V. The diffusion resistance values R_D are maximal in the region of maximal adsorption (Fig. 7 (a)) and R_D decreases to zero at the potentials E > –0.65 and E < –1.65 V. The deviation of α_{cat} from 0.5 is remarkable only in the potential region near to the adsorption-desorption peaks (i.e. in the region where the desorption process starts). Comparison of C_{ad}, α_{cat}, R_D, C_{dl}, obtained using the equivalent circuits b and e shows that there is only a weak difference in the values of C_{dl} (C_{dl} is lower in the case of circuit e), but other values depend only weakly on the choice of the equivalent circuit used for fitting the complex plane plots for Bi($01\bar{1}$) | 0.05 M Na_2SO_4 + x M TBN^+ interface.

For obtaining the adsorption and diffusion relaxation times (τ_K and τ_D, respectively) expressed as

$$\tau_D = \left(\frac{\partial \Gamma}{\partial c}\right)_E^2 \Big/ D; \quad \tau_D = \Gamma_m^2 \theta^2 (1-\theta)^2 \Big/ \left\{c^2 D[1-2a\theta(1-\theta)]^2\right\} \qquad (13)$$

$$\tau_K = \left(\frac{\partial \Gamma}{\partial v}\right)_{E,c}; \quad \tau_K = \Gamma_m \theta(1-\theta)/\{v_0[1-2a\theta(1-\theta)]\} \qquad (14)$$

the Cole-Cole plots (frequency-related admittance of the electrode), presented in Figs. 8 and 9, have been calculated. In Eqs. (13) and (14) Γ_m is Gibbs maximal adsorption; v (in mol cm^{-2} s^{-1}) is the net rate of adsorption and the adsorption exchange rate is defined as v_0; a is the attraction interaction coefficient in the Frumkin isotherm [1-5,7,11,14]. In the case of adsorption kinetics controlled entirely by the rate of diffusion the frequency-related admittance of an electrode is expressed as

$$C_p = C_{dl} + \frac{C_{ad}\left[1 + (0.5\omega\tau_D)^{1/2}\right]}{1 + (2\omega\tau_D)^{1/2} + \omega\tau_D} \qquad (15a)$$

$$\frac{1}{\omega R_p} = \frac{C_{ad}(0.5\omega\tau_D)^{1/2}}{1 + (2\omega\tau_D)^{1/2} + \omega\tau_D} \qquad (15b)$$

Eqs. (15a) and (15b) require that $(\omega R_p)^{-1}$,C_p dependence should take the form of a quarter-circle with the values of depression angle between the C_p axis and the radius of the arc $\beta = 45°$.The experimental results presented in Figs. 8 and 9 show that at less negative potentials (E > -1.25 V vs. Ag|AgCl), the TBN^+ adsorption is limited mainly by the rate of diffusion ($\beta = 45°$). The values of β somewhat lower than 45° at more negative potentials than $E \leq 1.25$ V can be explained by the mixed kinetics of adsorption of TBN^+ cations from less concentrated solutions ($c_{TBN^+} \leq 5\times10^{-4}$ M). The values of β at $c_{TBN^+} \leq 5\times10^{-4}$ M are noticeably higher in the region of maximal adsorption than at $E \leq$ -1.65 V, indicating that under these conditions the deviation from the diffusion-limiting step is small. The diffusion relaxation times obtained from the so-called high frequency region of the Cole-Cole plots are given in Table 2. Comparison of these data with the data for other organic compounds investigated [1-5] demonstrates comparatively quick mainly diffusion-limited process of TBN^+ cations. However, as for uracil and dodecylsulfate anion adsorption, there are noticeable deviations from the semicircle at lower frequency (f < 50 Hz), which can be explained by the diffusion-like process in the adsorption layer (formation of two-dimensionally ordered areas or restructuring of the adsorption layer) as in this region of the Cole-Cole plots, the linear dependence of $(\omega R_p)^{-1}$ on C_p with the slope value $\beta'' \sim 45°$ has been established The values of β' less than 45° established at more negative potentials than –1.05 V for less concentrated TBN^+ solutions can be explained by the mixed adsorption kinetics (slow diffusion and heterogeneous adsorption steps), and in these circumstances the following expressions for the frequency-related admittance have been established by Lorenz and Möckel [44,45]

$$C_p = C_{dl} + \frac{C_{ad}\left[1 + (0.5\omega\tau_D)^{1/2}\right]}{\left[(0.5\omega\tau_D)^{1/2} + \omega\tau_K\right]^2 + \left[(0.5\omega\tau_D)^{1/2} + 1\right]^2} \qquad (16a)$$

$$\frac{1}{\omega R_p} = \frac{C_{ad}\left[(0.5\omega\tau_D)^{1/2} + \omega\tau_K\right]}{\left[(0.5\omega\tau_D)^{1/2} + \omega\tau_K\right]^2 + \left[(0.5\omega\tau_D)^{1/2} + 1\right]^2} \qquad (16b)$$

The values of relaxation frequency $\omega_{max} = 2\pi f_{max}$, corresponding to the maximum values of the angular frequency for the $(\omega R_p)^{-1}$,C_p dependence determining the values of experimental

relaxation time $\tau_{exp} = (\omega_{max})^{-1}$, given in Table 2), are practically independent of E at $E >$ -1.35 V (Ag|AgCl). The somewhat higher τ_{exp} values for the more concentrated TBN^+ solutions are probably mainly caused by the formation of the compact adsorption layer. At very low frequency, a noticeable increase of the $(\omega R_p)^{-1}$ values have been observed, which is caused by the slow reorganisation of the adsorption layer (two-dimensional association according to Lorenz and Möckel [44]).

A better fit of $(\omega R_p)^{-1}$ versus log$f$ plots (Fig. 10) has been established if the mixed kinetics of adsorption was assumed, but the values of τ_K are very small (except $c_{TBN^+} = 5\times10^{-4}$M solutions at E = -1.65 V). The values of the theoretical diffusion relaxation times obtained using Eq. (16b), τ_D^{theor}, are practically independent of c_{TBN^+} but the values of τ_K^{theor} seem to increase with the surface coverage (i.e. with c_{TBN^+}). However, the values of τ_D and τ_K (given in Table 2) indicate that diffusion is the main rate-determining step (except $c_{TBN^+} = 5\times10^{4}$M solutions at E = -1.65 V).

If at constant frequency the adsorption process is characterised by the additional capacitance $C_{add}(\omega)$ and $R_p(\omega)$, assumed to be parallel in the equivalent circuit, then for a slow diffusion step $\cot\delta$ can be calculated as

$$\cot\delta = \omega R_p(\omega) C_{add}(\omega) = 1 + \sqrt{2D}\left[(\partial\Gamma/\partial c)_E \sqrt{\omega}\right]^{-1} = 1 + M\omega^{-1/2} \qquad (17)$$

For the frequency region from 50 to 6000 Hz, the $\cot\delta, \omega^{-1/2}$ plots are linear with the slope values $M = \sqrt{2D}/(\partial\Gamma/\partial c)_E$, given in Table 2. M depends somewhat on c_{cat}, which can be explained by the dependence of $(\partial\Gamma/\partial c)_E$ on compactness of the adsorption layer (if we assume that D does not depend on c_{cat}). According to the data in Table 2, there is a noticeable dependence of M on E, which is caused by the dependence of θ on E.

The noticeable deviations in the Cole-Cole plots (Fig. 9) established at low frequency can be explained by the two-dimensional association of molecules adsorbed in the interfacial region according to Refs. (11,44,45]. In this case, the value of $\cot\delta = R_p(\omega)\cdot C_{add}(\omega)\cdot\omega$ can be calculated as

$$\cot\delta = \frac{k_1\left(k_2 + k_1\frac{\sqrt{\omega}}{M}\right) + \left(\frac{\omega}{\omega_0}\right)^2\left(k_3 + \frac{\sqrt{\omega}}{M}\right)}{\left[k_1^2 + \left(\frac{\omega}{\omega_0}\right)^2\right]\left(\frac{\omega}{\omega_0} + \frac{\sqrt{\omega}}{M}\right) + \frac{\omega}{\omega_0}\left(k_1k_3 - k_2\right)} \quad (18)$$

where ω_0 is the exchange rate of the two-dimensional association, and k_1, k_2 and k_3 are certain constants characterising the process of two-dimensional association [11,44,45]. The results of theoretical simulations (non-linear regression analysis) of these data are given in Table 3 and Fig. 11. In spite of a small difference between the experimental and theoretical $\cot\delta,\omega^{-1/2}$-curves at $E >$ -1.6 V (Ag|AgCl) in the region of low ac frequency, the Lorenz model [44], taking into account the two-dimensional association in the adsorption layer, seems to be the only classical model which explains the behaviour of the Bi($01\bar{1}$) | x M $(C_4H_9)_4NI + Na_2SO_4$ aqueous solution interface at low frequencies. The values of ω_0 increase with c_{cat} at fixed potential, but decrease with increasingly negative polarisation. ω_0 is higher for TBN^+ compared with dodecylsulfate and uracil [4,5], in a good agreement with the increase of the experimental characteristic relaxation frequency obtained from the Cole-Cole plots at $f >$ 100 Hz. At $E \geq$ -1.6 V, the parameters k_1 and k_2 slightly decrease with increasing c_{cat}. At constant c_{cat}, the values of k_1 increase and k_2 decrease with increasing the negative polarisation (i.e. with decreasing the Gibbs adsorption). The values of k_3 are practically independent of c_{cat} and E. The values of k_1 and k_2 obtained for TBN^+ are noticeably lower than those for uracil, *tert*-pentanol and dodecylsulfate anions [2,4,5]. Thus, at low frequencies, two-dimensional association is probable, and the exchange rate of this association is higher for TBN^+, compared with other compounds studied at Bi($01\bar{1}$) plane. For a more detailed discussion, the experimental data for other experimental systems should be obtained and analysed. However, according to the data in Tables (1-3) and Figs. 9-11, the adsorption process of TBN^+ cations from dilute TBN^+ solutions to the Bi($01\bar{1}$) plane is limited mainly by the rate of diffusion of the organic cations to the electrode surface, but the two-dimensional association is possible at lower ac frequency values. The mixed kinetics of adsorption is possible at more negative potentials than –1.65 V (Ag|AgCl).

3. Conclusion

Systematic analysis of the Cole-Cole, $(\omega R_p)^{-1}$,log$f$ and $\cot\delta,\omega^{-1/2}$ dependences for Bi($01\bar{1}$) | 0.05 M Na_2SO_4 + x M $(C_4H_9)_4NI$ + H_2O interface shows that for less concentrated $(C_4H_9)_4N^+$ solutions, the rate of adsorption of the $(C_4H_9)_4N^+$ cation is limited mainly by the rate of the diffusion step at potentials more positive than –1.25 V (Ag|AgCl), but at more negative potentials, there are small deviations from a purely diffusion-limited step toward mixed kinetics (slow diffusion and heterogeneous adsorption steps) at high ac frequencies. At very low frequencies, the two-dimensional association is possible. The analysis of complex plane plots demonstrates that for less concentrated $(C_4H_9)_4N^+$ solutions ($c_{TBN^+} < 1\times10^{-5}$ M), the impedance spectra for the system investigated can be simulated by the classical Frumkin — Melik-Gaikazyan model with the following parameters: electrolyte resistance (R_{el}), electrical double layer capacitance (C_{dl}), adsorption capacitance (C_{ad}) and Warburg-like diffusion impedance (Z_W). According to the non-linear least-square fitting data, C_{dl}, C_{ad} and diffusion resistance R_D depend on the electrode potential as well as on concentration of $(C_4H_9)_4N^+$, and are in a good agreement with the predictions of the adsorption theory of the organic compounds in the case of the ideally polarizable electrodes [8-11,45]. For the more concentrated $(C_4H_9)_4N^+$ solutions, the noticeable deviations toward the modified Frumkin — Melik-Gaikazyan model, including the generalised finite Warburg element (GFW) for a short circuit terminus model, are possible. The better fit of the complex plane plots has been established if the Wandlowski – de Levie model [42], taking into account the inhomogeneous adsorption layer at the Bi($01\bar{1}$) surface, has been used. Comparison of the data obtained by using Wandlowski — de Levie model and Frumkin — Melik-Gaikazyan model shows that for dilute $(C_4H_9)_4N^+$ solutions in the region of moderate frequencies and electrode potentials, the deviation of the Bi($01\bar{1}$) | 0.05 M Na_2SO_4 + x M $(C_4H_9)_4NI$ + H_2O interface from the classical Frumkin — Melik-Gaikazyan model is weak. For more concentrated $(C_4H_9)_4N^+$ solutions, the boundary conditions defining the interfacial flux of $(C_4H_9)_4N^+$ cations will be inhomogeneous as there are probably the compact two-dimensionally ordered clusters on some parts of the Bi($01\bar{1}$) surface but on the other surface parts there is no clusters and the semi-infinite diffusion of $(C_4H_9)_4N^+$ ions is possible.

Acknowledgements – This work was supported in part by the Estonian Science Foundation under Projects 4568 and 5213.

References

[73] E.J. Lust, U.V. Palm, Sov. Electrochem. 24 (1988) 227, Engl. Tr.

[74] G. Nurk, A. Jänes, P. Miidla, K. Lust, E. Lust, J. Electroanal. Chem. 515 (2001) 17.

[75] A. Jänes, G. Nurk, K. Lust, E. Lust, J. Russ. Electrochem. 38 (2002) 11.

[76] H. Kasuk, G. Nurk, K. Lust, E. Lust, J. Electroanal. Chem. 550-551 (2003) 13.

[77] G. Nurk, H. Kasuk, K. Lust, A. Jänes, E. Lust, J. Electroanal. Chem. 553 (2003) 1.

[78] E. Lust, G. Nurk, A. Jänes, M. Arulepp, L. Permann, P. Nigu, P. Möller, Cond. Matter Physics 5 (2002) 307.

[79] E. Lust, G. Nurk, A. Jänes, M. Arulepp, P. Nigu, P. Möller, S. Kallip, V. Sammelselg, J. Solid State Electrochem. 7 (2003) 91.

[80] A.N. Frumkin, V.I. Melik-Gaikazyan, Dokl. Akad. Nauk USSR 77 (1951) 855.

[81] V.I. Melik-Gaikazyan, Zh. Fiz. Khim. 26 (1952) 560.

[82] K.S. Cole, R.H. Cole, J. Chem. Phys. 9 (1941) 341.

[83] A.N. Frumkin, B.B. Damaskin, in J.O'M. Bockris and B.E. Conway (Eds.), Modern Aspects of Electrochemistry, Vol. 3 (1964) p.149.

[84] R.D. Armstrong, W.P. Rice, H.R. Thirsk, J. Electroanal. Chem. 16 (1968) 517.

[85] M. Sluyters-Rehbach, J. Sluyters, in A. Bard (Ed.), Electroanalytical Chemistry, vol. 4, Marcel Dekker, New York, 1970, p.76.

[86] U. Retter, H. Jering, J. Electroanal. Chem. 46 (1973) 375.

[87] G. Brug, A. van der Eeden, M. Sluyters-Rehbach, J. Sluyters, J. Electroanal. Chem. 176 (1984) 275.

[88] J.R. MacDonald (Ed.) Impedance Spectroscopy: Emphasizing Solid Materials and Systems, John Wiley & Sons, New York, 1987.

[89] B.A. Boukamp, Equivalent Circuit User's Manual, University of Twente, 1989.

[90] B.A. Boukamp, J. Electrochem. Soc 142 (1995) 1885.

[91] ZView for Windows (version 2.2) fitting program, Scribner Inc., Souther Pines, NC, 1999.

[92] M. Sluyters-Rwhbach, Pure and Appl. Chem. 66 (1994) 1831.

[93] A. Lasia, in B.E. Conway, J.O'M. Bockris, R.E. White (Eds.), Modern Aspects of Electrochem., Vol. 32, Kluwer Academic, New York, 1999, Ch. 2.

[94] P. Zoltowski, J. Electroanal. Chem. 443 (1998) 149.

[95] G. Lang, K.E. Heusler, J. Electroanal. Chem. 457 (1998) 257.

[96] A. Sadkowski, J. Electroanal. Chem.481 (2000) 222.

[97] G. Lang, K.E. Heusler, J. Electroanal. Chem. 482 (2000) 227.

[98] P. Zoltowski, J. Electroanal. Chem. 481 (2000) 230.

[99] M. Väärtnõu, E. Lust, J. Electroanal. Chem. 533 (2002) 107.

[100] A.N. Frumkin, Potentsyaly nulevogo zaryada (Potentials of zero charge), Nauka, Moscow, (1979).

[101] S. Trasatti, E. Lust, in J.O'M. Bockris, R.E. White (Eds.), Modern Aspects of Electrochem., Vol. 33, Kluwer Academic / Plenum Publishers, New York, 1999, p.1.

[102] B. Damaskin, S. Karpov, S. Dyatkina, U. Palm, M. Salve, J. Electroanal. Chem. 136 (1982) 217.

[103] B. Damaskin, S. Karpov, S. Dyatkina, U. Palm, M. Salve, J. Electroanal. Chem. 189 (1983) 183.

[104] A. Tymosiak-Zielinska, Z. Borkowska, Electrochim. Acta 46 (2001) 3073.
[105] T. Pajkossy, Th. Wandlowski, O.M. Kolb, J. Electroanal. Chem. 414 (1996) 209.
[106] Z. Kerner, T. Pajkossy, Electrochim. Acta 47 (2002) 2025.
[107] T. Jacobsen, K. West, Electrochim. Acta 40 (1995) 233.
[108] A. Compte, Phys. Rev. E 53 (1996) 4191.
[109] A. Compte, R. Metzlek, J. Phys. A: Math. Gen. 30 (1997) 7277.
[110] J. Bisquert, G. Garcia-Belmonte, P.R. Bueno, E. Longo, L.O.S. Bulhões, J. Electroanal. Chem. 452 (1998) 229.
[111] J. Bisquert and A. Compte, J. Electroanal. Chem. 499 (2001) 112.
[112] T. Wandlowski, R. de Levie, J. Electroanal. Chem. 329 (1992) 103.
[113] T. Wandlowski, R. de Levie, J. Electroanal. Chem.345 (1993) 413.
[114] T. Wandlowski, R. de Levie, J. Electroanal. Chem.352 (1993) 279.
[115] T. Wandlowski, R. de Levie, J. Electroanal. Chem. 380 (1995) 201.
[116] W. Lorenz, F. Möckel, Z. Elektrochem. 60 (1956) 507.
[117] B.B. Damaskin, O.A. Petrii, V.V. Batrakov, Adsorption of Organic Compounds on Electrodes, Plenum Press, New York, London, 1971, pp. 53-66.

8 LEGENDS OF FIGURES

Fig. 1. Complex plane plots for Bi($01\bar{1}$) in 0.05 M Na_2SO_4 aqueous solution at different electrode potentials E (V vs. Ag|AgCl): -0.6 (1); -1.5 (2); -1. 7 (3). Inset: the equivalent circuit used for fitting of the experimental data (R_{el} – electrolyte resistance; CPE – constant phase element; and R_{ad} – adsorption or partial charge transfer resistance).

Fig. 2. Differential capacitance vs. electrode potential curves (a) (at ac frequency f = 210 Hz) for Bi($01\bar{1}$) in the 0.05 M Na_2SO_4 electrolyte (1) and with additions of $(C_4H_9)_4N^+$ (M): (2) – 1×10^{-8}; (3) – 1×10^{-7}; (4) – 5×10^{-7}; (5) –1×10^{-6}; (6) –5×10^{-6}; (7) –1×10^{-5}; (8) –5×10^{-5}; (9) –1×10^{-4}; (10) –5×10^{-4}; and (11) –1×10^{-3} . R_s (1,3) and R_p (2,4) vs. $\omega^{1/2}$ dependences (b) for the Bi($01\bar{1}$) | 1×10^{-3} M $(C_4H_9)_4N^+$ + 0.05 M Na_2SO_4 aqueous solution interface at the potentials (V vs. Ag|AgCl): -1.2 (1,2); and –1.7 (3,4).

Fig. 3. Complex plane plots for the Bi($01\bar{1}$) plane in 0.05 M Na_2SO_4 solutions with addition of 5×10^{-4} M (a) and 5×10^{-2} M (b) $(C_4H_9)_4N^+$ cation at different electrode potentials E (V vs. Ag|AgCl): -0.65 (1); -0.85 (2); -1.05 (3); -1.45 (4) and –1.65 (5) (points – experimental data; solid lines – fitting according to Wandlowski – de Levie model).

Fig. 4. Dependence of the phase angle (δ) on ac frequency for Bi($01\bar{1}$) in 0.05 M Na_2SO_4 solution with addition of 5×10^{-4} M (a) and 5×10^{-2} M (b) $(C_4H_9)_4N^+$ at different electrode potentials, E (V vs. Ag|AgCl) (a): -0.65 (1); -0.85 (2) ; -1-05 (3); -1.25 (4); -1.45 (5); and -1.65 (6); and at constant E = -0.65 V (Ag|AgCl) (c) for various $c_{(C_4H_9)_4N^+}$ (M): (1) – 5×10^{-2}; (2) – 5×10^{-3}; and (3) – 5×10^{-4}.

Fig. 5. Equivalent circuits of an electrode in the presence of organic cation adsorption: (a) Randles circuit; (b) Frumkin — Melik–Gaikazyan circuit, (c) combined Frumkin — Melik-Gaikazyan — Randles circuit; (d) Frumkin — Melik-Gaikazyan circuit with CPE instead of C_{dl}; and (e) Wandlowski — de Levie circuit (R_{el} – electrolyte solution resistance; C_{dl} – double layer capacitance; C_{ad} – adsorption capacitance; R_{ad} - adsorption or partial charge transfer resistance; Z_w –Warburg-like diffusion impedance; CPE – constant phase element; C_n and R_n – capacitance and resistance of the formation of the two-dimensionally associated layer (i.e. the capacitance and resistance of the "needle" peak formation).

Fig. 6. Dependence of the so called needle peak capacitance C_n (a); and resistance R_n (b); double layer ("true") capacitance C_{dl} (c); and adsorption capacitance C_{ad} (d) on the electrode potential for Bi($01\bar{1}$) in the 0.05 M Na_2SO_4 aqueous solution with additions of $(C_4H_9)_4N^+$ (M): (1) – 5×10^{-2}; and (2) – 5×10^{-4}.

Fig. 7. Dependence of diffusion resistance R_D (a) and the fractional exponent α_{cat} (Eq. 3) (b) on the electrode potential for Bi($01\bar{1}$) in the 0.05 M Na_2SO_4 aqueous solution with additions of $(C_4H_9)_4N^+$ (M): (1) – 5×10^{-2}; and (2) – 5×10^{-4}.

Fig. 8. Cole-Cole (complex admittance) plots for the Bi($01\bar{1}$) | 0.05 M Na_2SO_4 + 5×10^{-4} M $(C_4H_9)_4N^+$ solution interface at the electrode potentials, E (V vs. Ag|AgCl): -1.35 (1); -1.05 (2); and –1.65 (3).

Fig. 9. Cole-Cole (complex admittance) plots for Bi($01\bar{1}$)| 0.05 M Na_2SO_4 + 5×10^{-2} M $(C_4H_9)_4N^+$ solution interface at the electrode potentials, E (V vs. Ag|AgCl): -1.65 (1); -1.35 (2); and –1.25 (3).

Fig. 10. $(\omega R_p)^{-1}$,log$f$ plots for Bi($01\bar{1}$) in the 0.05 M Na_2SO_4 aqueous solution with addition of 5×10^{-2} M $(C_4H_9)_4N^+$ at E = -1.65 V (Ag|AgCl) (experimental data (1) and fitted data according to Eq. (15 b) (2); and Eq. (16 b) (3) at the values of τ_D^{theor} and τ_K^{theor}, presented in Table 2).

Fig. 11. $\cot\delta,\omega^{1/2}$ plots for Bi($01\bar{1}$) in the 0.05 M Na_2SO_4 aqueous solution with additions of $(C_4H_9)_4N^+$ (M): 5×10^{-4} (a); and 5×10^{-2} (b) at the electrode potentials (V vs. Ag|AgCl): -1.05 (1); -1.35 (2); and –1.65 (3) (filled marks – experimental data; open marks –data calculated according to Eq. (18) at the values of ω_0, k_1, k_2 and k_3, presented in Table 3).

Table 1. Results of non-linear least squares fitting for Bi($01\bar{1}$) | 0.05 M Na_2SO_4 + *x* M $(C_4H_9)_4N^+$ + H_2O interface.

c_{cat}/ M	E / V vs. Ag|AgCl	**9** PARAMETER	Frumkin — Melik-Gaikazyan model (circuit b)	Wandlowski-De Levie model (at $\alpha \neq 0.5$) (circuit e)
5×10^{-4}	-1.05	χ^2	6.7×10^{-3}	5.4×10^{-4}
		Δ^2	0.65	0.053
		R_{el} / Ω cm^2	18.9 (2.3%)	10.7 (4.3%)
		C_{dl} / μF cm^{-2}	5.6 (1.1%)	2.9 (5.0%)
		R_D / Ω cm^2	106510 (15%)	104980 (2.7%)
		T / s	8.82 (27.6%)	7.32 (5.9%)
		α_{cat}	0.5 (fixed)	0.48 (0.71%)
		C_{ad} / μF cm^{-2}	179 (20.8%)	154 (15.7%)
		C_n / μF cm^{-2}	-	3.0 (4.3%)
		R_n / Ω cm^2	-	46.5 (6.1%)
5×10^{-4}	-1.45	χ^2	1.19×10^{-2}	5.7×10^{-4}
		Δ^2	1.30	0.06
		R_{el} / Ω cm^2	19.2 (2.8%)	12.1 (3.8%)
		C_{dl} / μF cm^{-2}	7.6 (1.8%)	3.9 (4.8%)
		R_D / Ω cm^2	8875 (2.0 %)	10870 (1.2%)
		T / s rad^{-1}	0.23 (5.8 %)	0.53 (5.6%)
		α_{cat}	0.5 (fixed)	0.42 (1.4%)
		C_{ad} / μF cm^{-2}	780 (19.3 %)	2917 (21.8%)
		C_n / μF cm^{-2}	-	5.1 (3.6%)
		R_n / Ω cm^2	-	37.7 (5.0%)
5×10^{-2}	-1.05	χ^2	3.4×10^{-3}	2.2×10^{-4}
		Δ^2	0.35	0.022
		R_{el} / Ω cm^2	13.7 (2.0%)	8.3 (4.2%)
		C_{dl} / μF cm^{-2}	5.4 (0.7%)	3.4 (3.9%)
		R_D / Ω cm^2	93788 (9.1%)	71690 (4.0%)
		T / s rad^{-1}	6.40 (17.3%)	5.17 (5.0%)
		α_{cat}	0.5 (fixed)	0.46 (1.1%)
		C_{ad} / μF cm^{-2}	285 (23.8%)	124 (8.8%)
		C_n / μF cm^{-2}	-	2.4(5.4%)
		R_n / Ω cm^2	-	49.5(8.3%)

χ^2 – chi-square function; Δ^2 – weighted sum of squares; R_{el} –electrolyte resistance; C_{dl} – double layer capacitance; R_D –limiting diffusion resistance; $T = L^2/D$ (L is the effective diffuse layer thickness; D is the effective diffusion coefficient of a cation); α_{cat} – fractional exponent; C_{ad} – adsorption capacitance; R_n and C_n – "needle" peak formation resistance and capacitance [42]; c_{cat} – concentration of the $(C_4H_9)_4N^+$ cations

Table 2. Experimental and calculated diffusion and adsorption relaxation times for Bi($01\bar{1}$) | 0.05 M Na_2SO_4 + *x* M $(C_4H_9)_4N^+$ + H_2O interface.

c_{cat} / M	*E* / V vs. Ag|AgCl	$10^4\ \tau_{exp}$ / s	β / deg	*M* (Eq. 17)	$10^4\ \tau_D^{theor}$ / s (Eq. (15 b))	$10^4\ \tau_D^{theor}$ / s (Eq. (16 b)	$10^7\ \tau_K^{theor}$ / s (Eq. 16 b)
5×10^{-4}	-1.05	0.98	39	156	1.5	0.9	0.1
	-1.35	0.98	31	140	1.6	1.2	1.0
	-1.65	1.35	23	37	16.0	7.0	10000
5×10^{-2}	-1.05	1.40	47	199	0.90	0.60	10.0
	-1.35	1.60	47	200	0.97	0.85	100
	-1.65	9.80	47	143	1.20	0.80	10.0

c_{cat} – concentration of the $(C_4H_9)_4N^+$ cations;
τ_{exp} – experimental relaxation time obtained from the Cole-Cole plot;
β – angle between C_p axis and the radius of the aec of the Cole-Cole (ωR_p^{-1} vs. C_p) plot.

Table 3. Non-linear regression analysis data for Bi($01\bar{1}$) | 0.05 M Na_2SO_4 + x M $(C_4H_9)_4N^+$ + H_2O interface.

x / M	E / V vs Ag|AgCl	$10^{-4}\ \omega_0$ / s^{-1} (Eq. 18)	$10^4\ k_1$ (Eq. 18)	$10^3\ k_2$ (Eq. 18)	k_3 (Eq. 18)	R^2
5×10^{-4}	-1.05	1.89±0.65	7.9±3.0	6.9±3.1	0.78±0.08	0.88
	-1.35	1.17±0.35	12.2±4.0	6.6±2.9	0.84±0.08	0.91
	-1.65	0.28±0.03	114.5±16.9	-28.6±4.6	0.62±0.05	0.94
$5x10^{-2}$	-1.05	2.83±1.07	6.8±2.8	4.7±2.3	0.81±0.09	0.88
	-1.35	2.84±0.99	6.6±2.5	3.3±1.6	0.79±0.08	0.90
	-1.65	0.87±0.10	101.1±13.2	-6.4±1.3	1.38±0.10	0.97

R^2 – the correlation coefficient

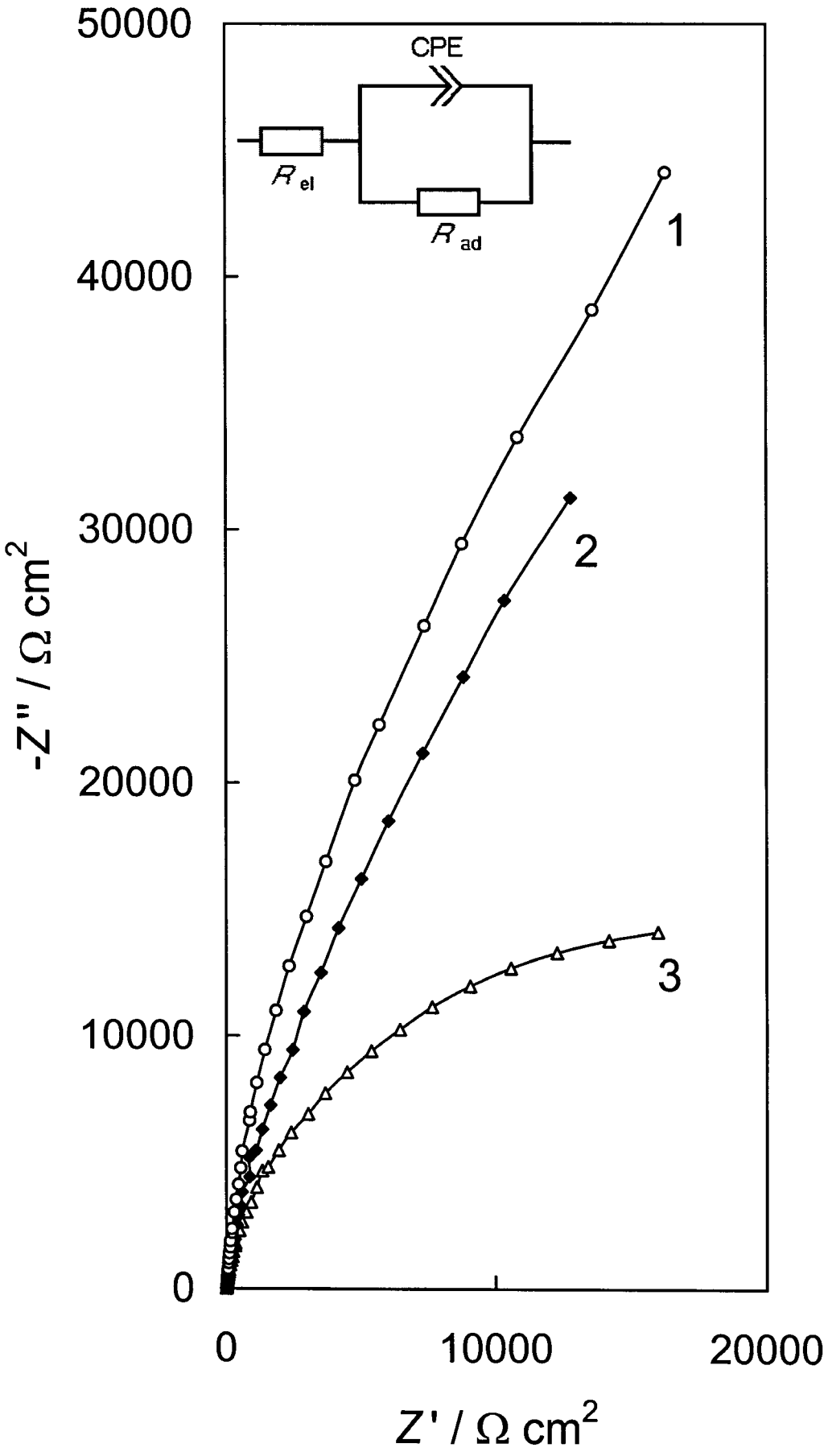
50000
40000
30000
20000
10000
0
-Z'' / Ω cm2
0
10000
20000
Z' / Ω cm2
CPE
Rel
Rad
1
2
3

Fig. 1.

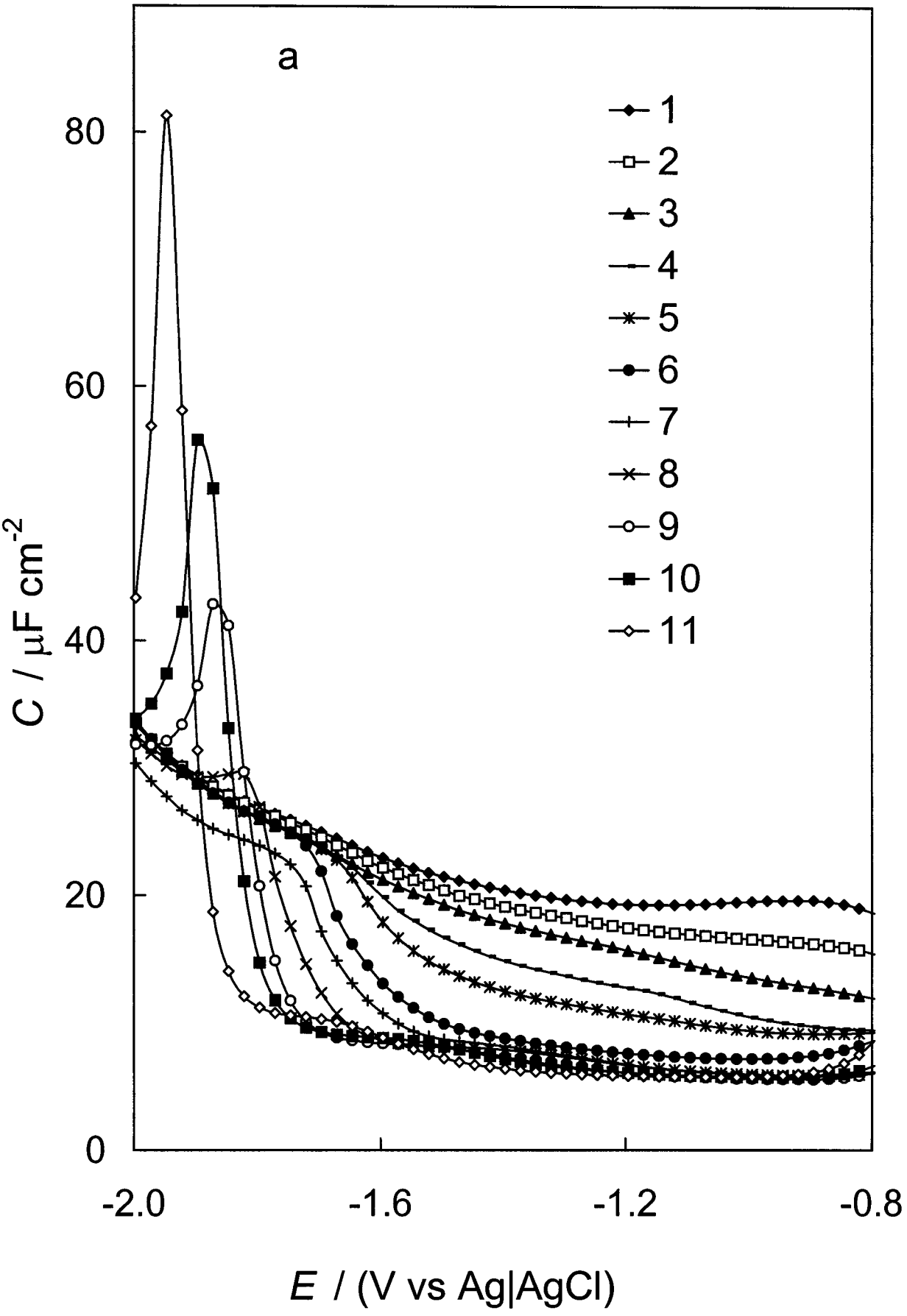

Fig. 2a.

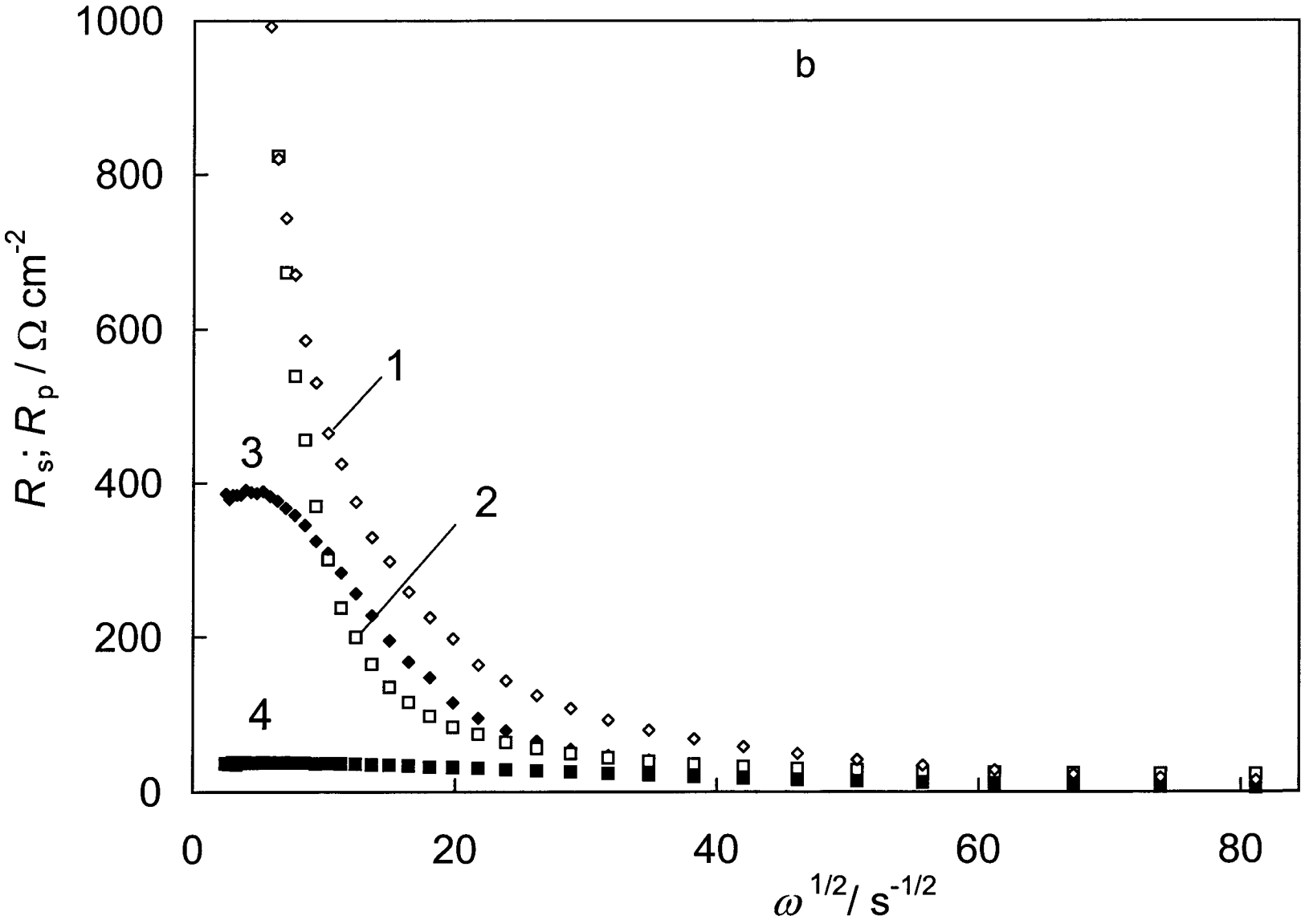

Fig. 2b.

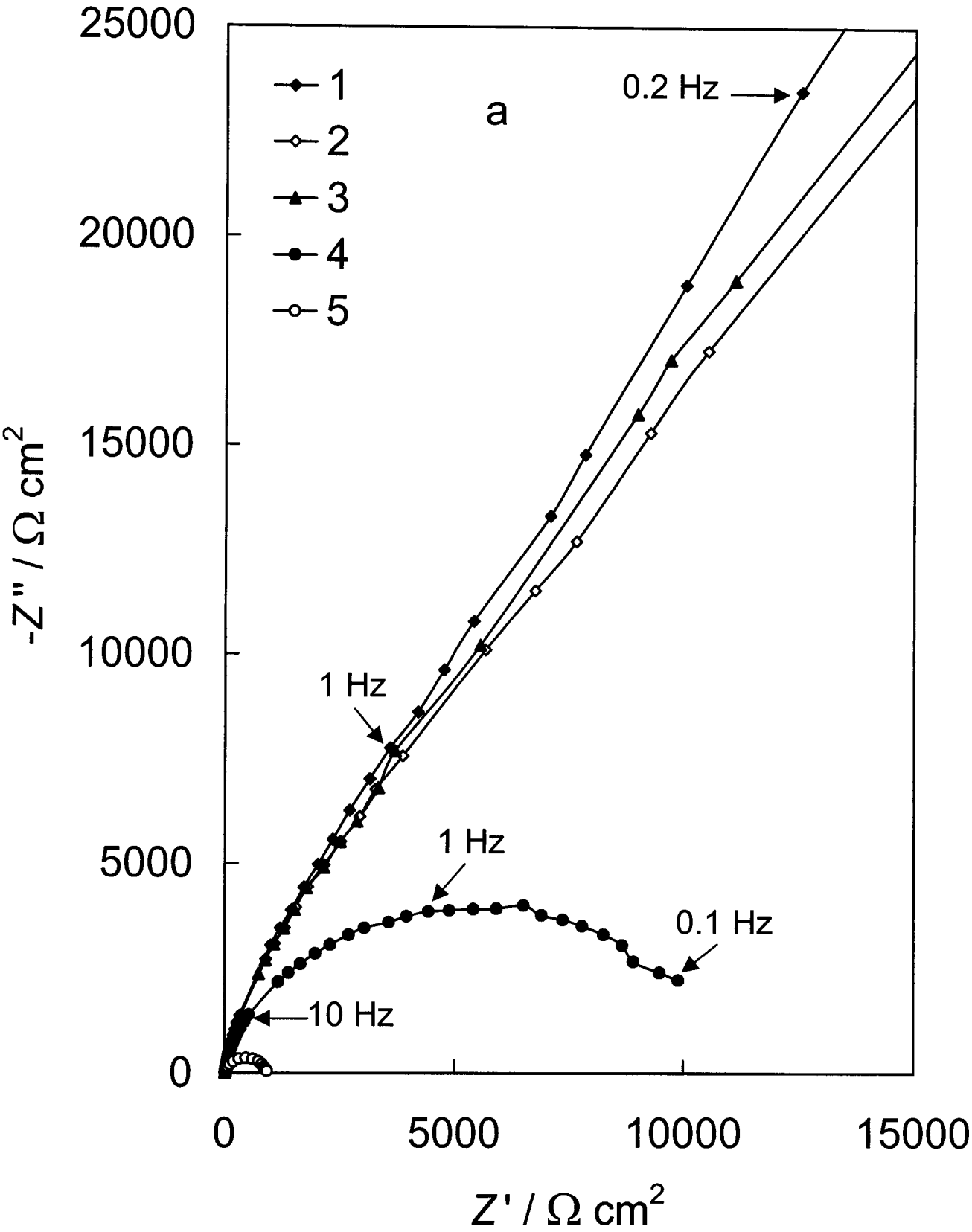
25000
20000
15000
10000
5000
0
-Z'' / Ω cm2
0
5000
10000
15000
Z' / Ω cm2
1
2
3
4
5
a
0.2 Hz
1 Hz
1 Hz
0.1 Hz
10 Hz

Fig. 3a.

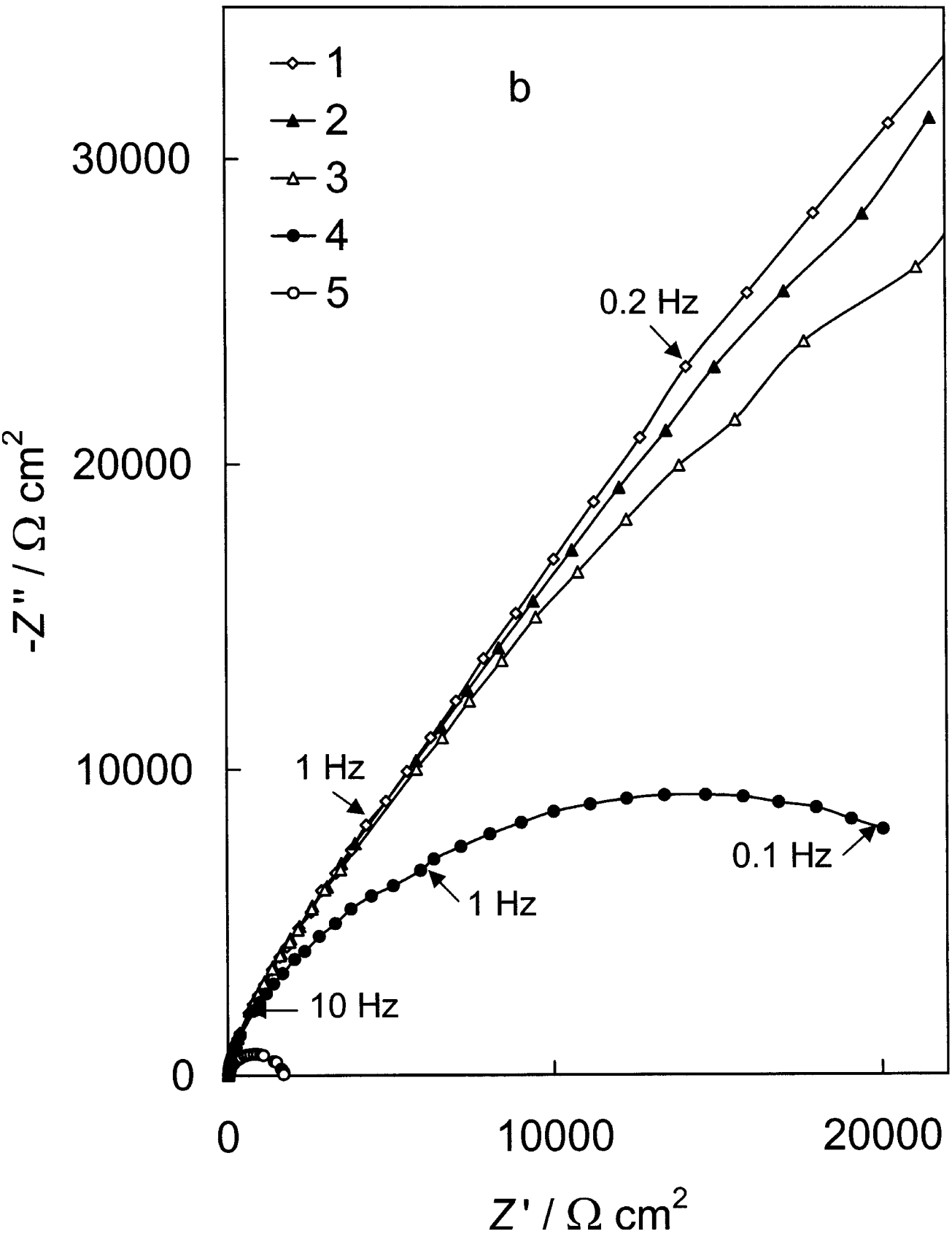
b
1
2
3
4
5
0.2 Hz
1 Hz
0.1 Hz
1 Hz
10 Hz
30000
20000
10000
0
0
10000
20000
-Z'' / Ω cm2
Z' / Ω cm2

Fig. 3b.

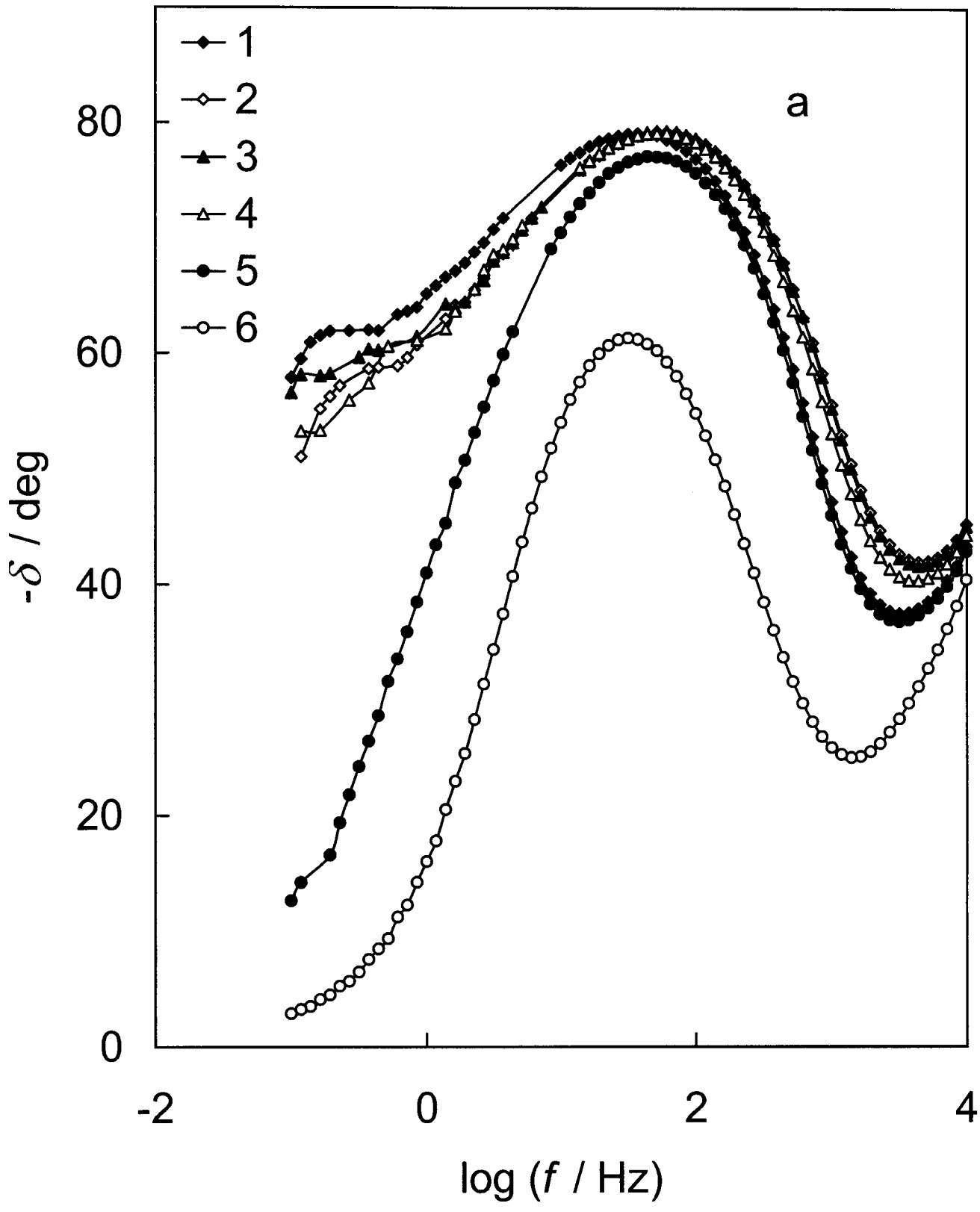

Fig. 4a.

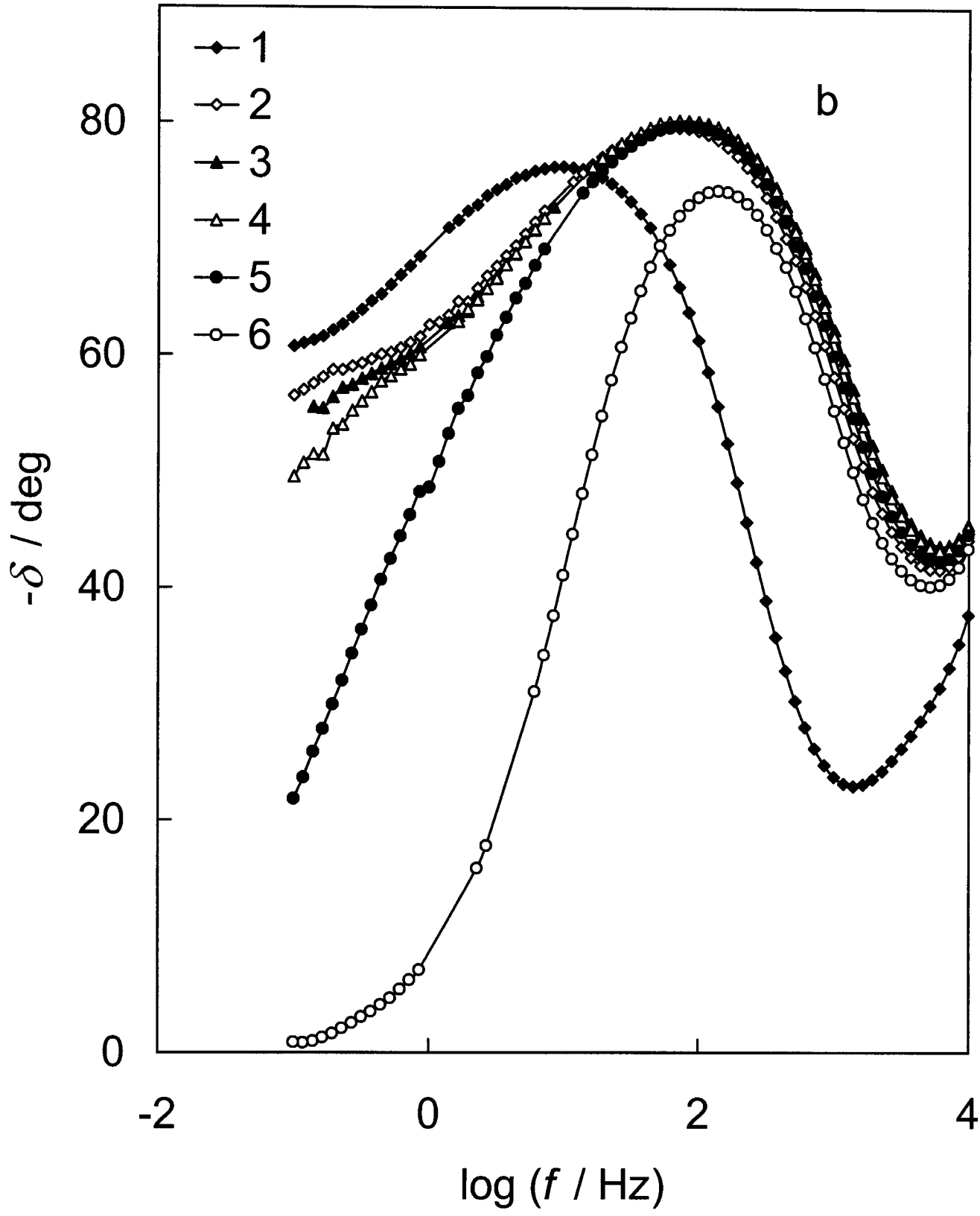

Fig. 4b.

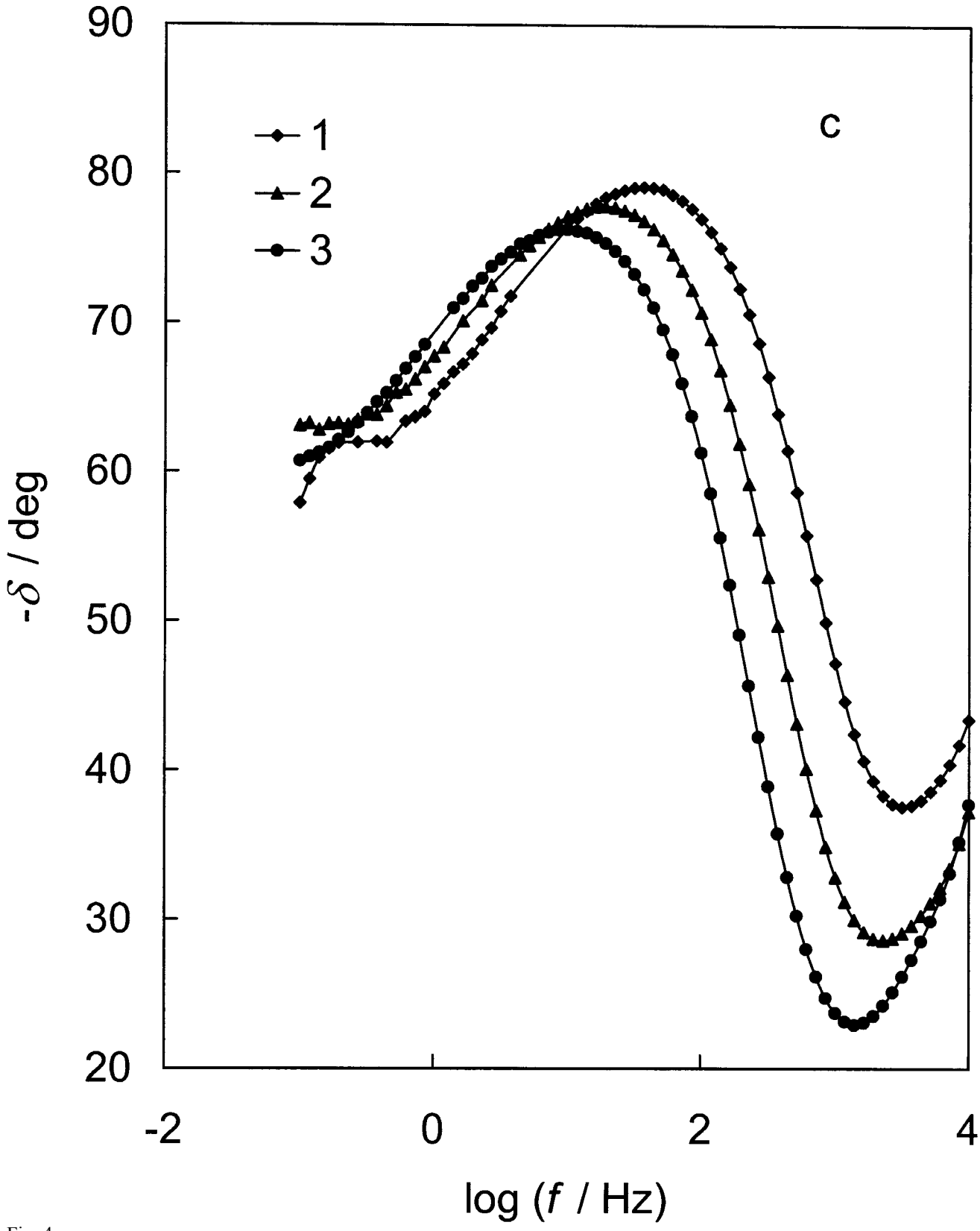

Fig. 4c.

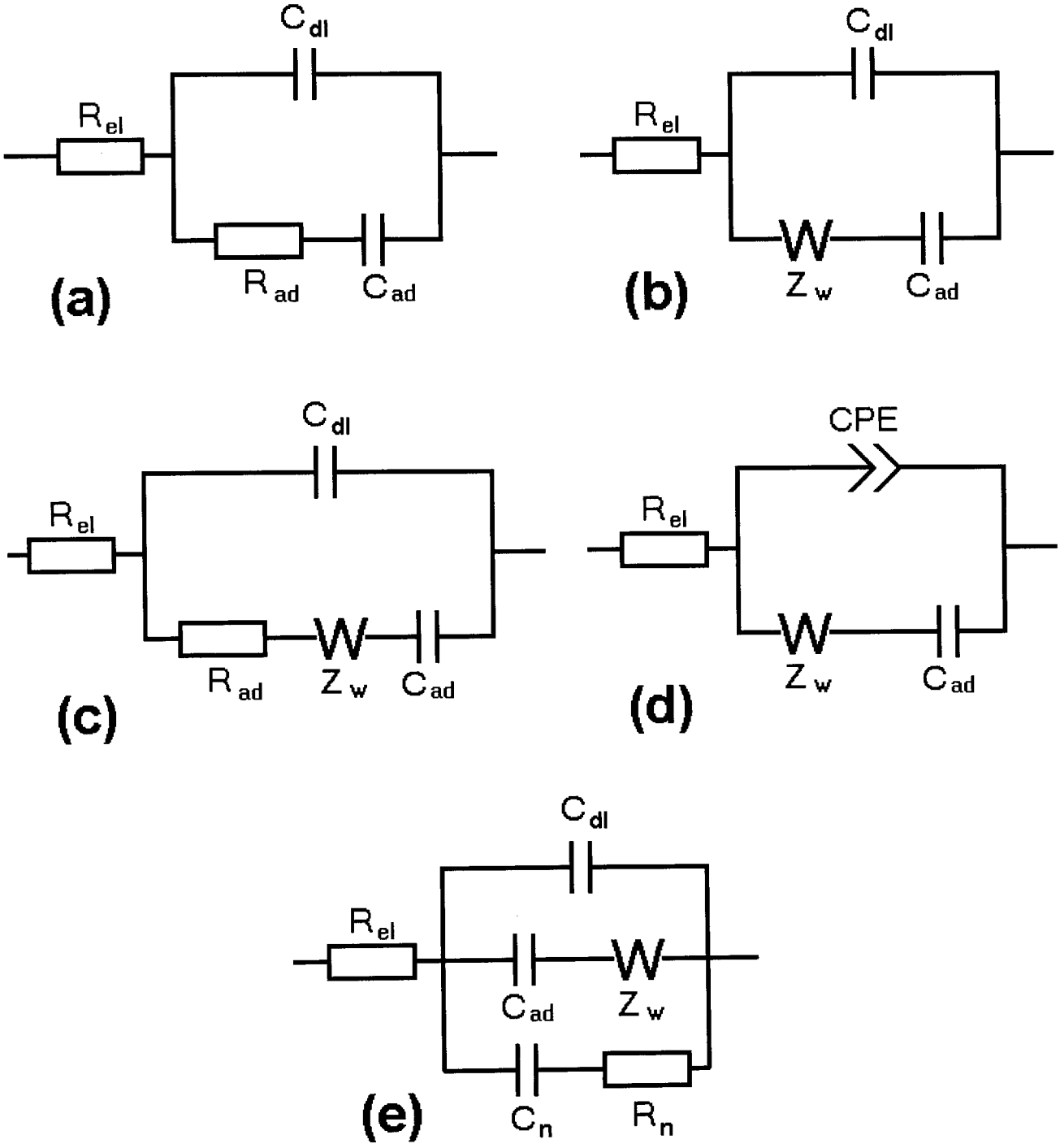
C dl
R el
R ad
C ad
(a)
C dl
R el
W
Z w
C ad
(b)
C dl
R el
R ad
W
Z w
C ad
(c)
CPE
R el
W
Z w
C ad
(d)
C dl
R el
C ad
W
Z w
C n
R n
(e)

Fig. 5.

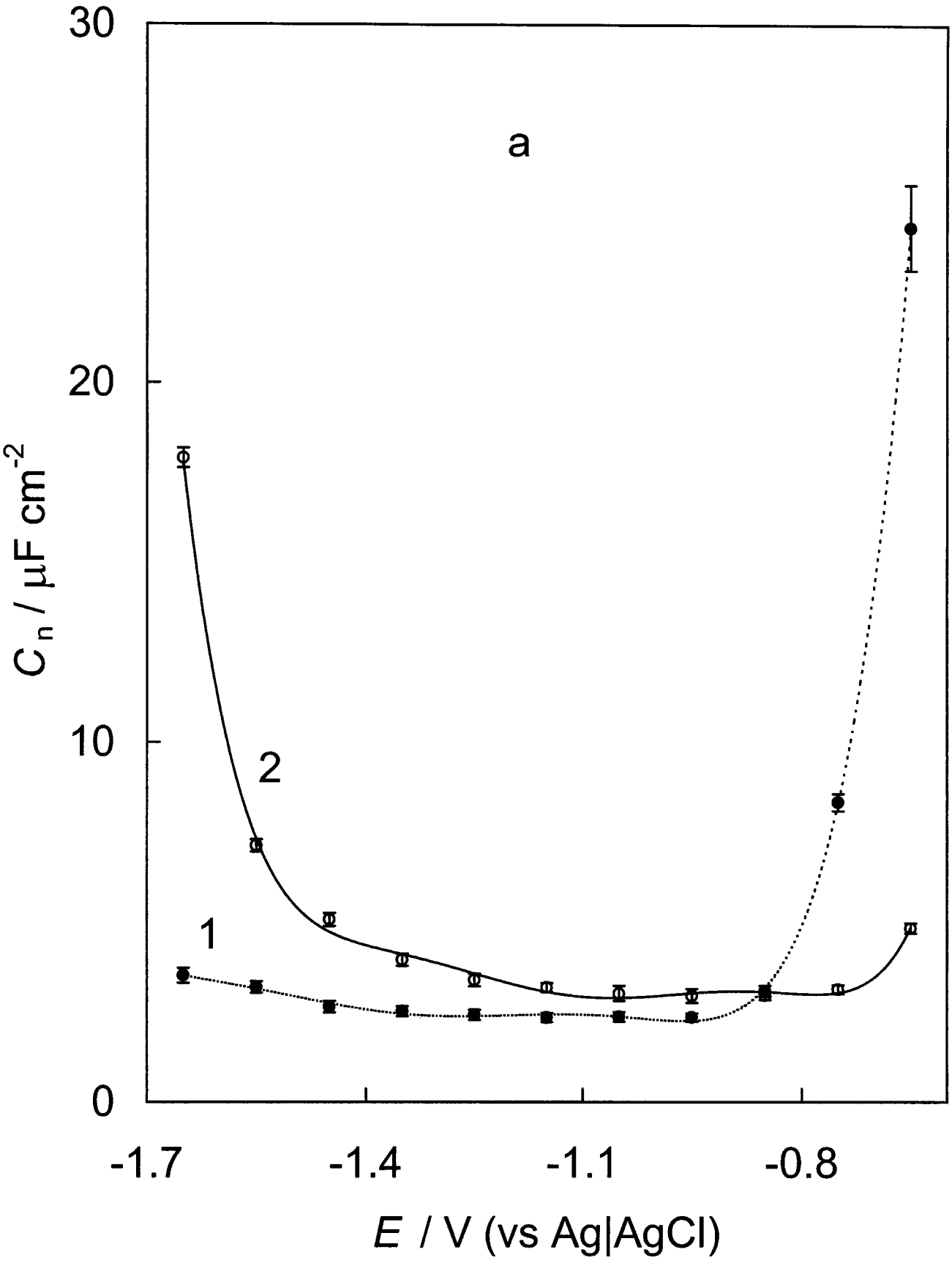

Fig. 6a.

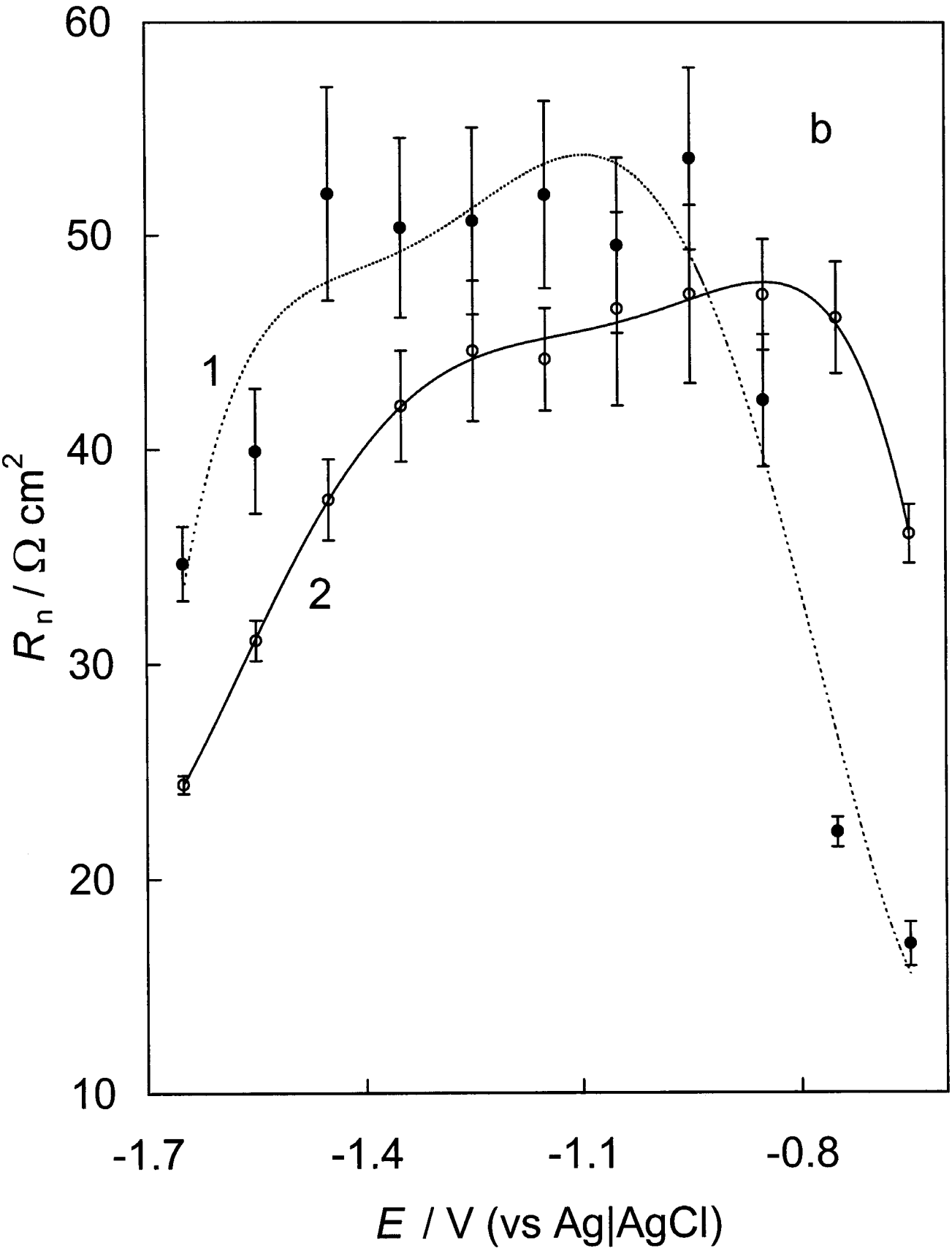

Fig. 6b.

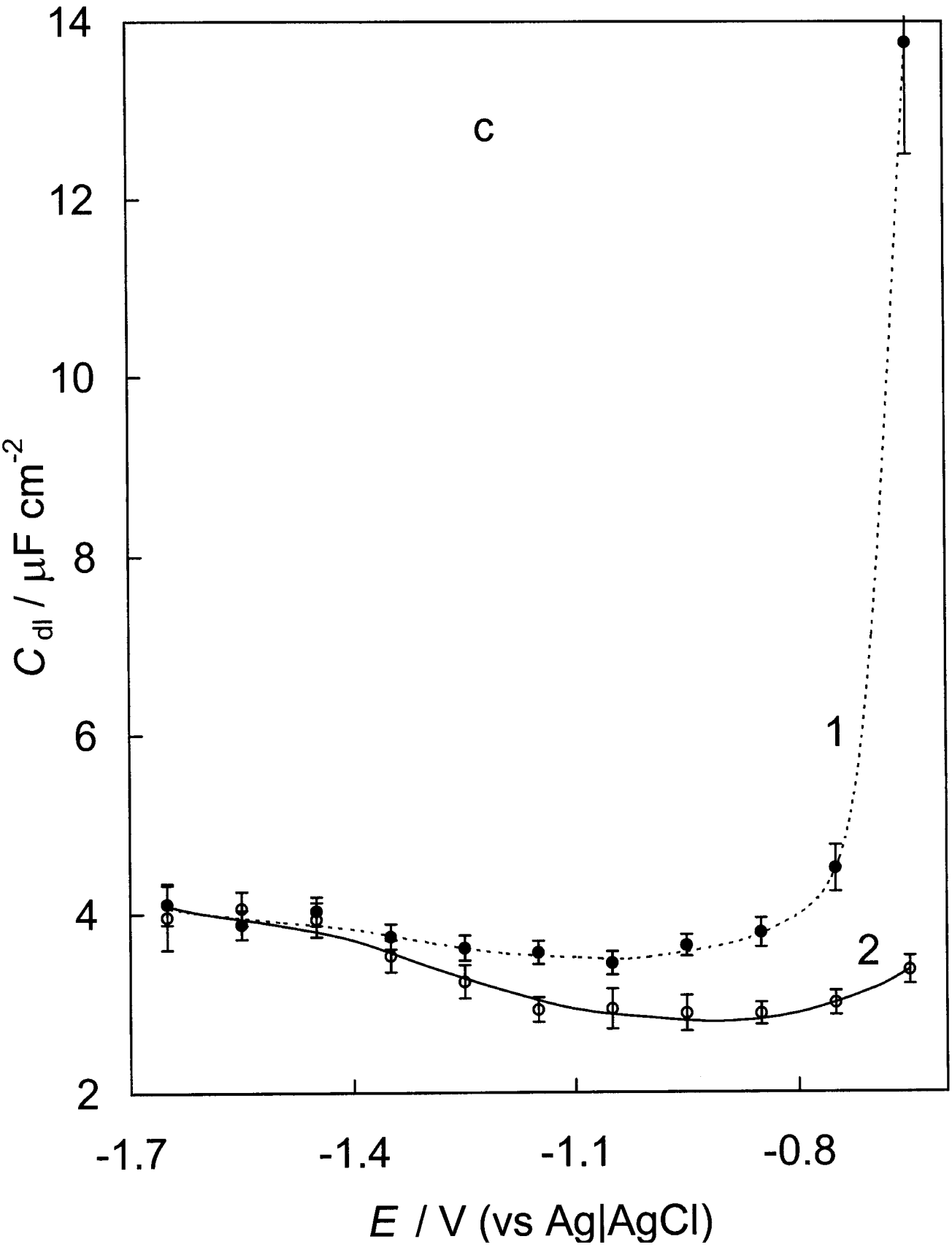

Fig. 6c.

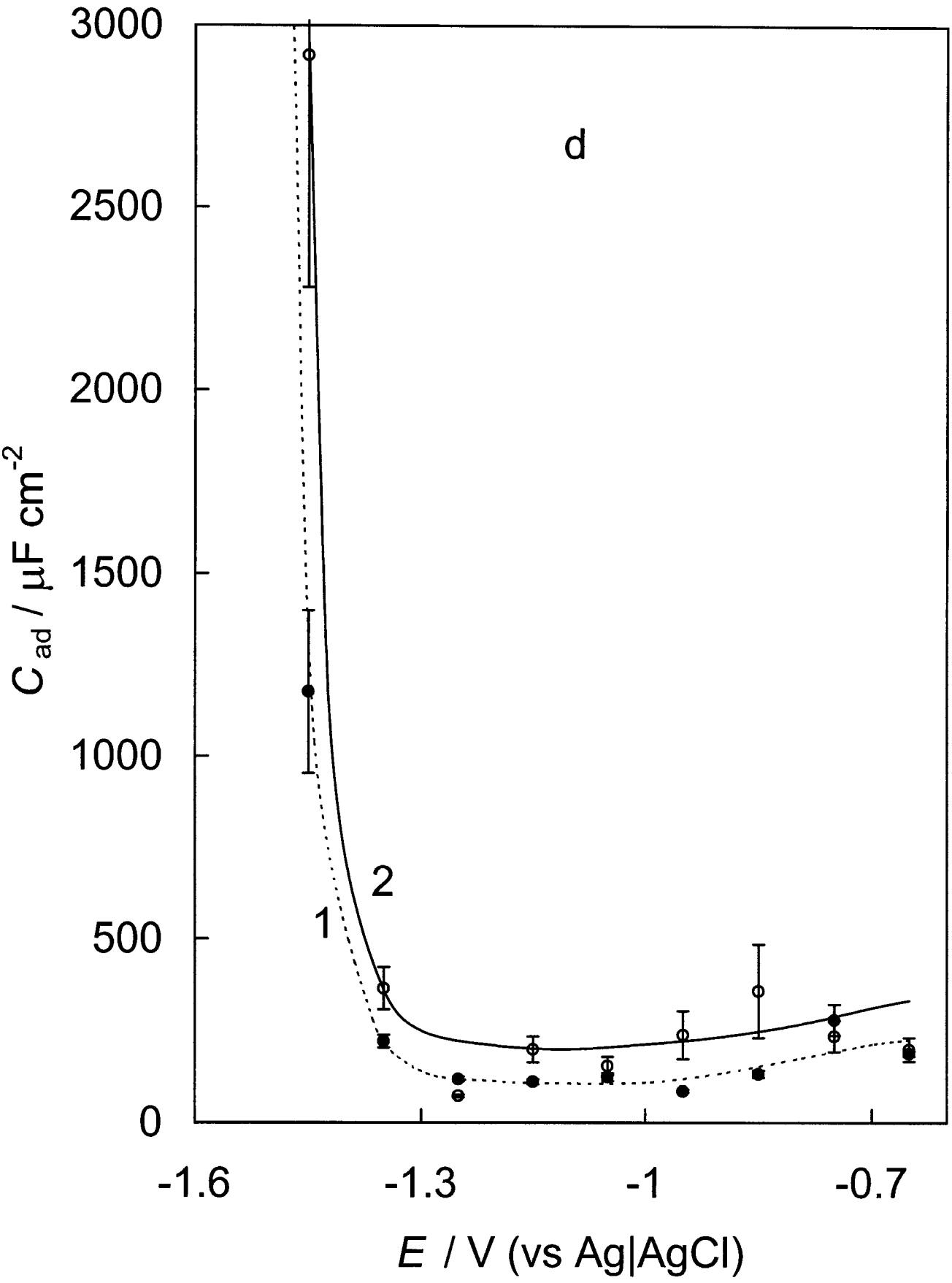
3000
2500
2000
1500
1000
500
0
d
2
1
C_{ad} / μF cm^{-2}
-1.6
-1.3
-1
-0.7
E / V (vs Ag|AgCl)

Fig. 6d.

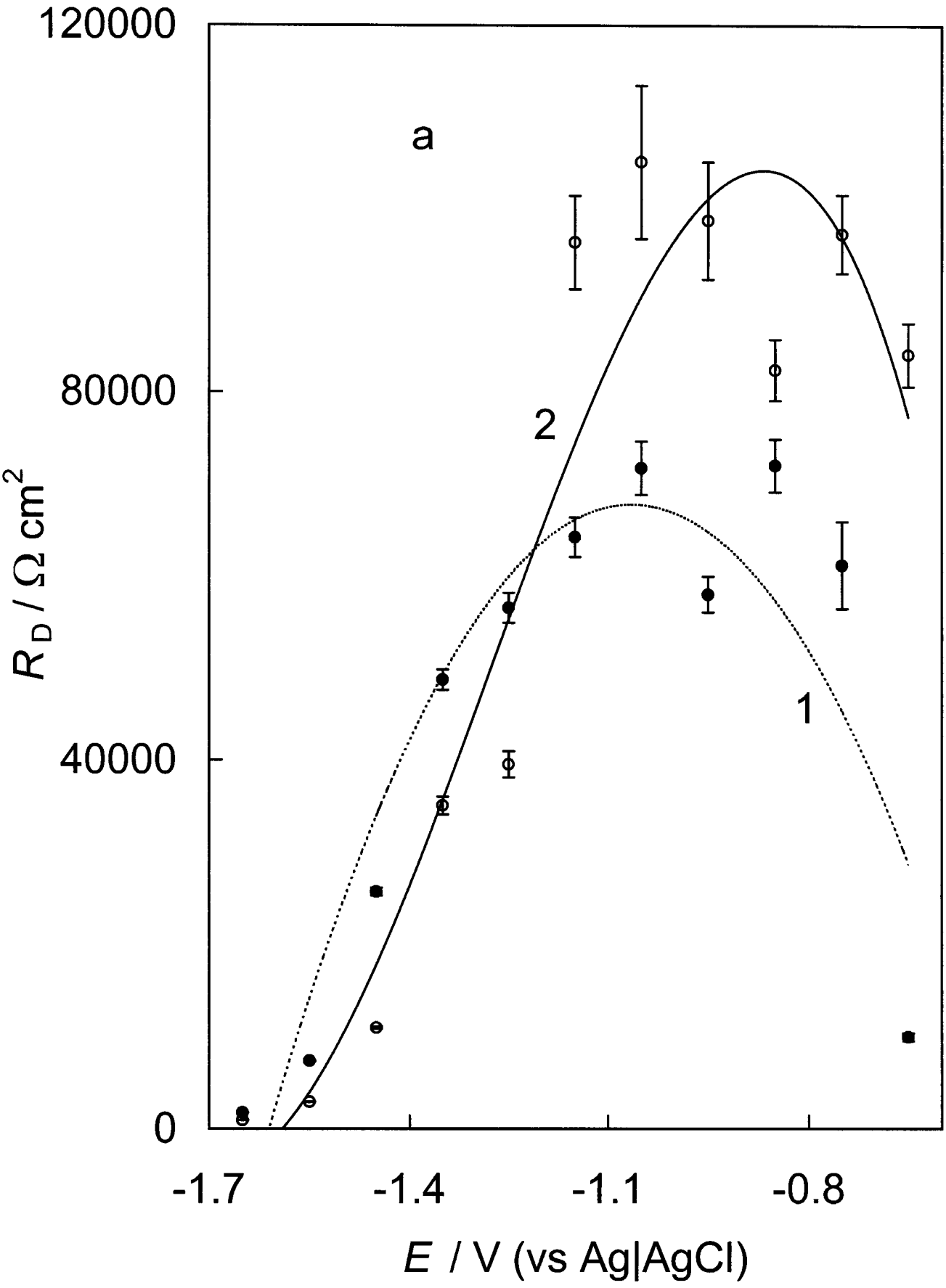

Fig. 7a.

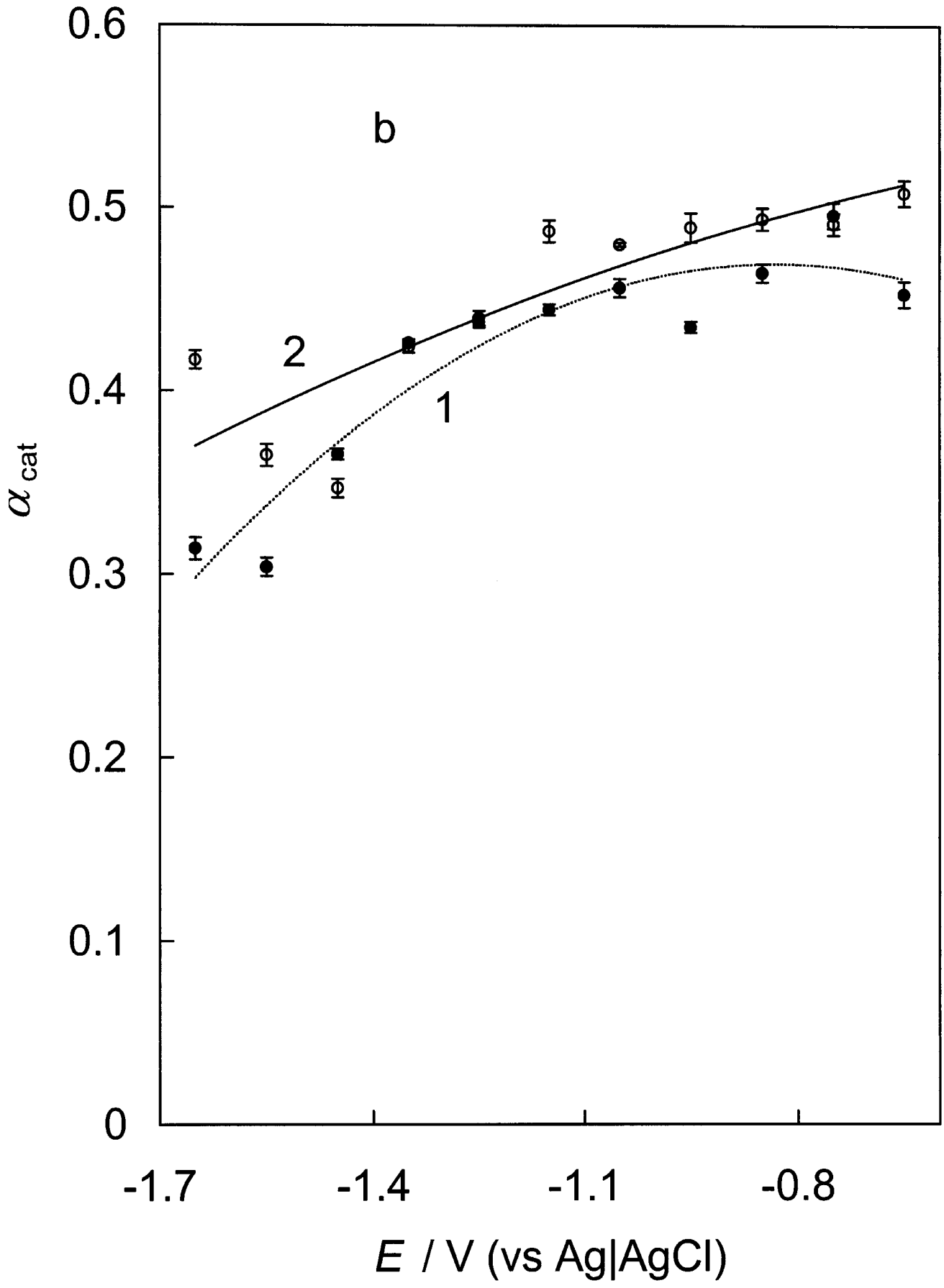

Fig. 7b.

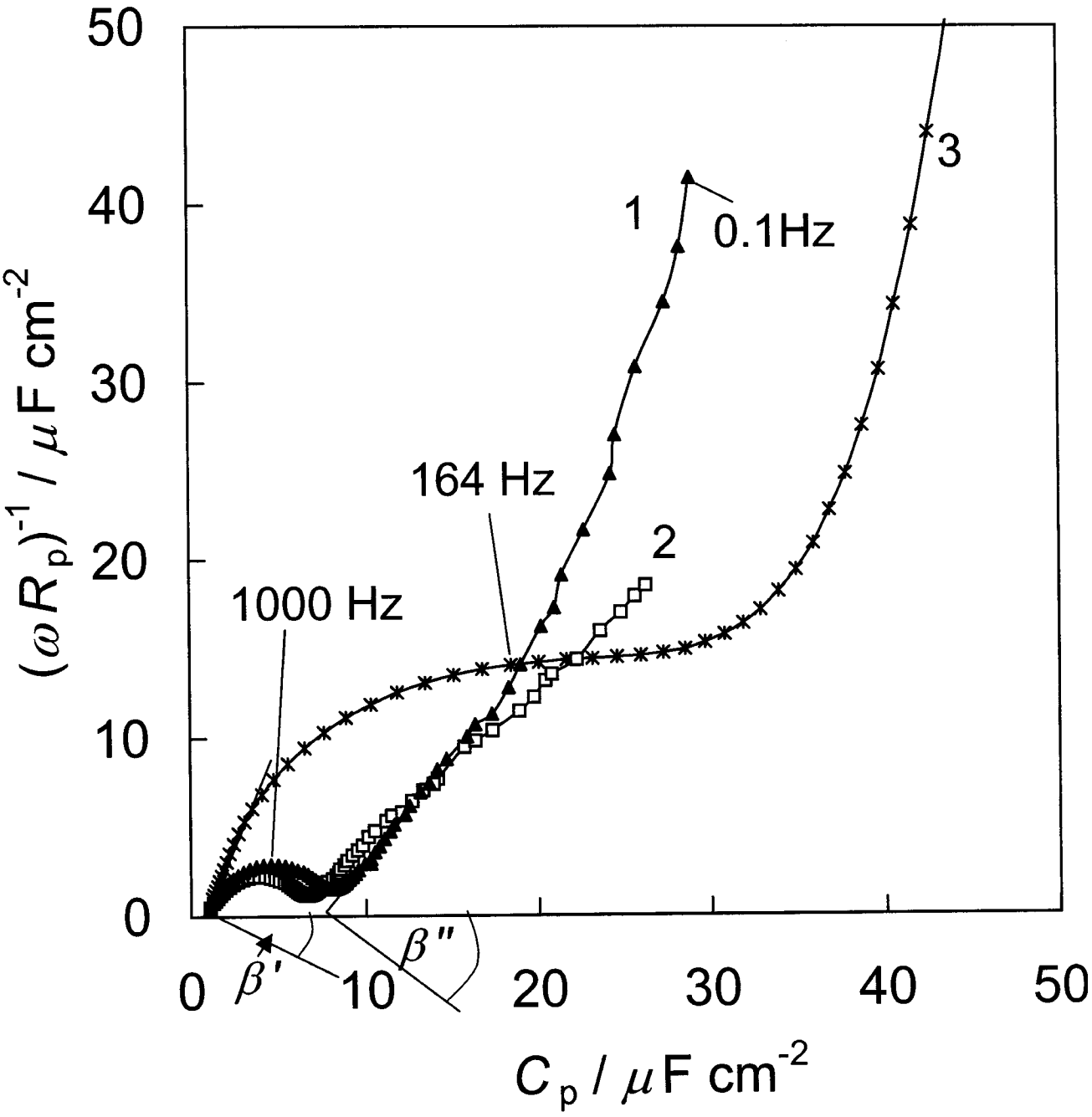
50
40
30
20
10
0
0
10
20
30
40
50
$(\omega R_p)^{-1}$ / μF cm^{-2}
C_p / μF cm^{-2}
1
2
3
0.1Hz
164 Hz
1000 Hz
β'
β''

Fig. 8.

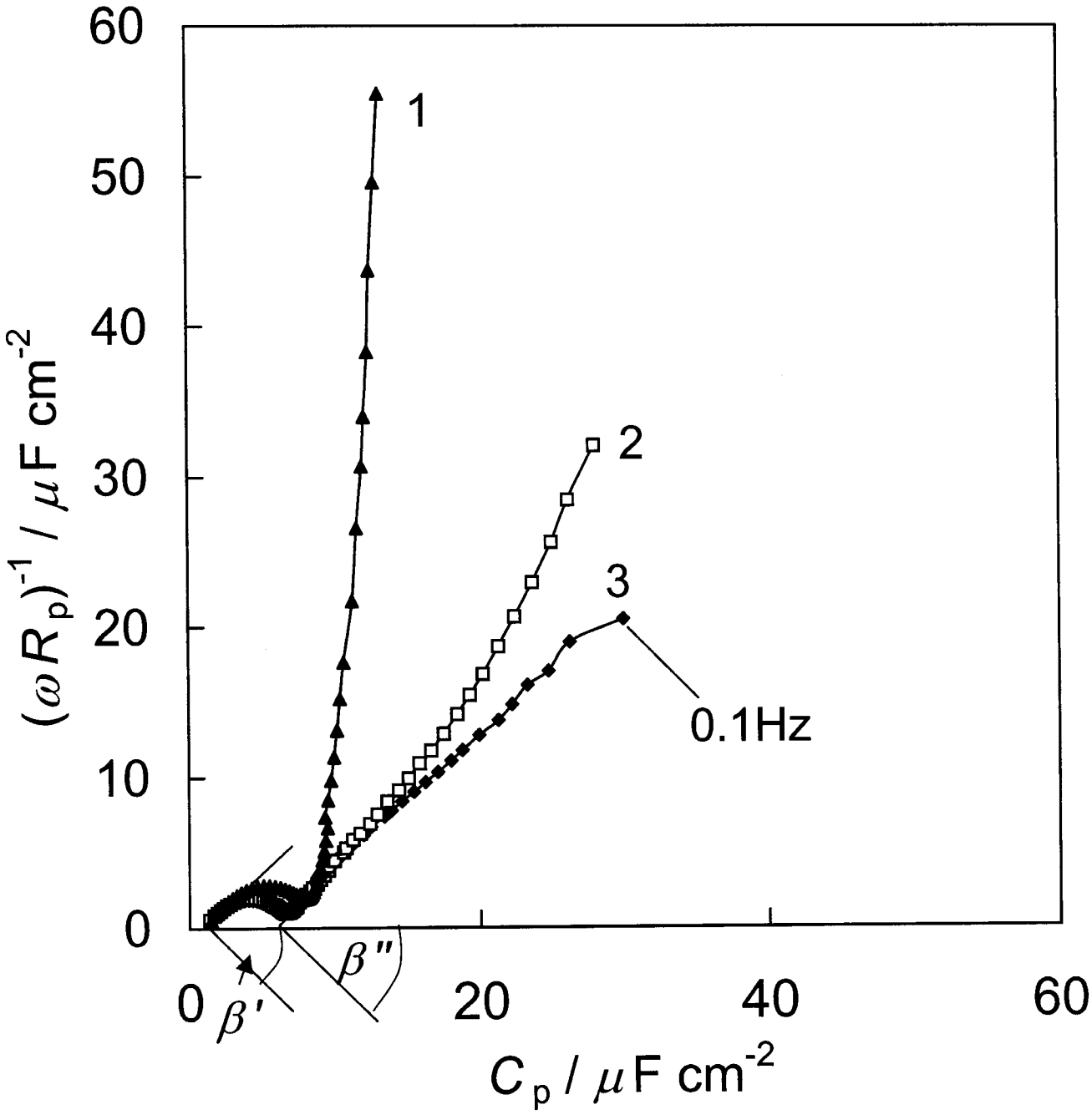

Fig. 9.

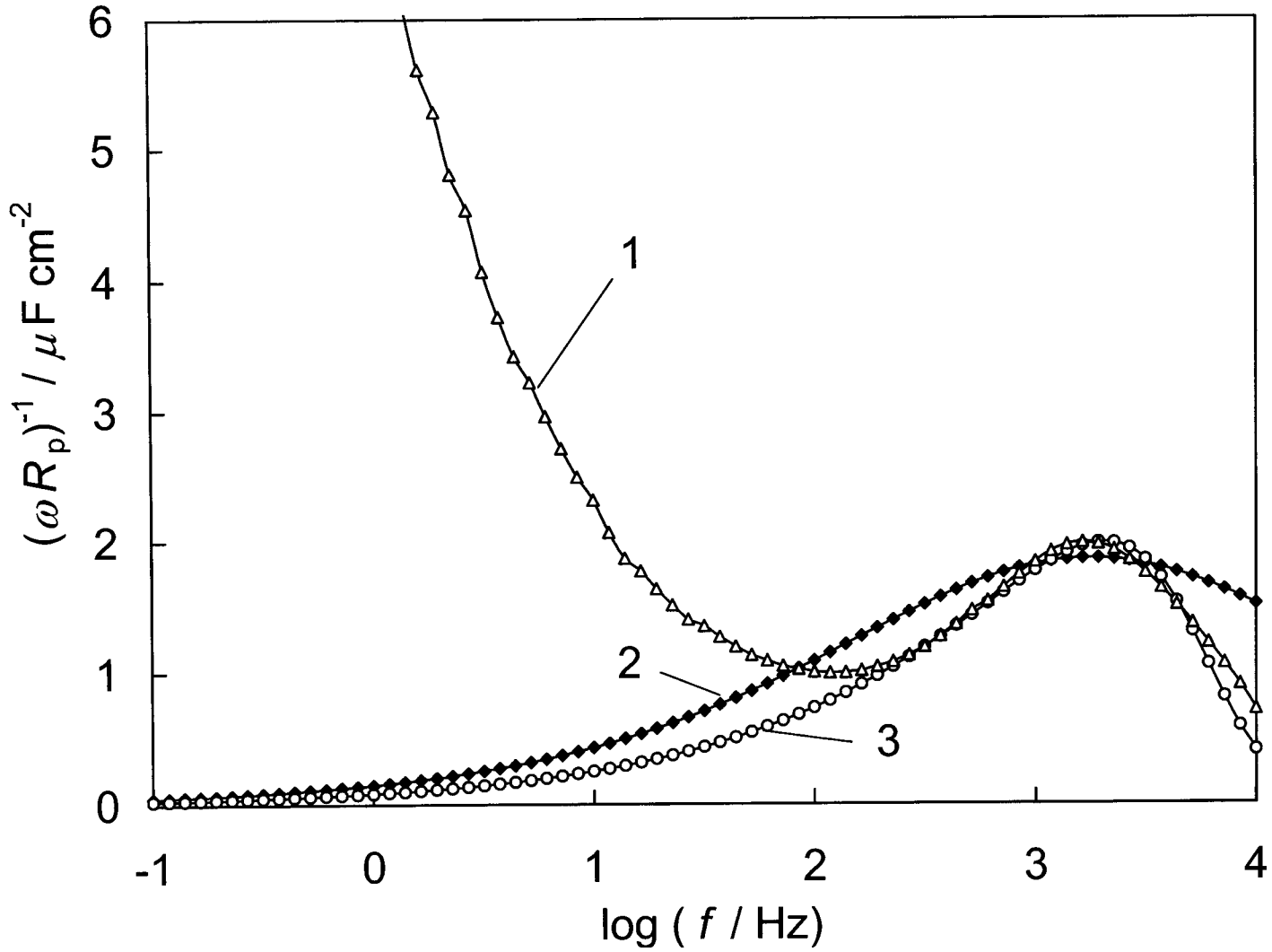

Fig. 10.

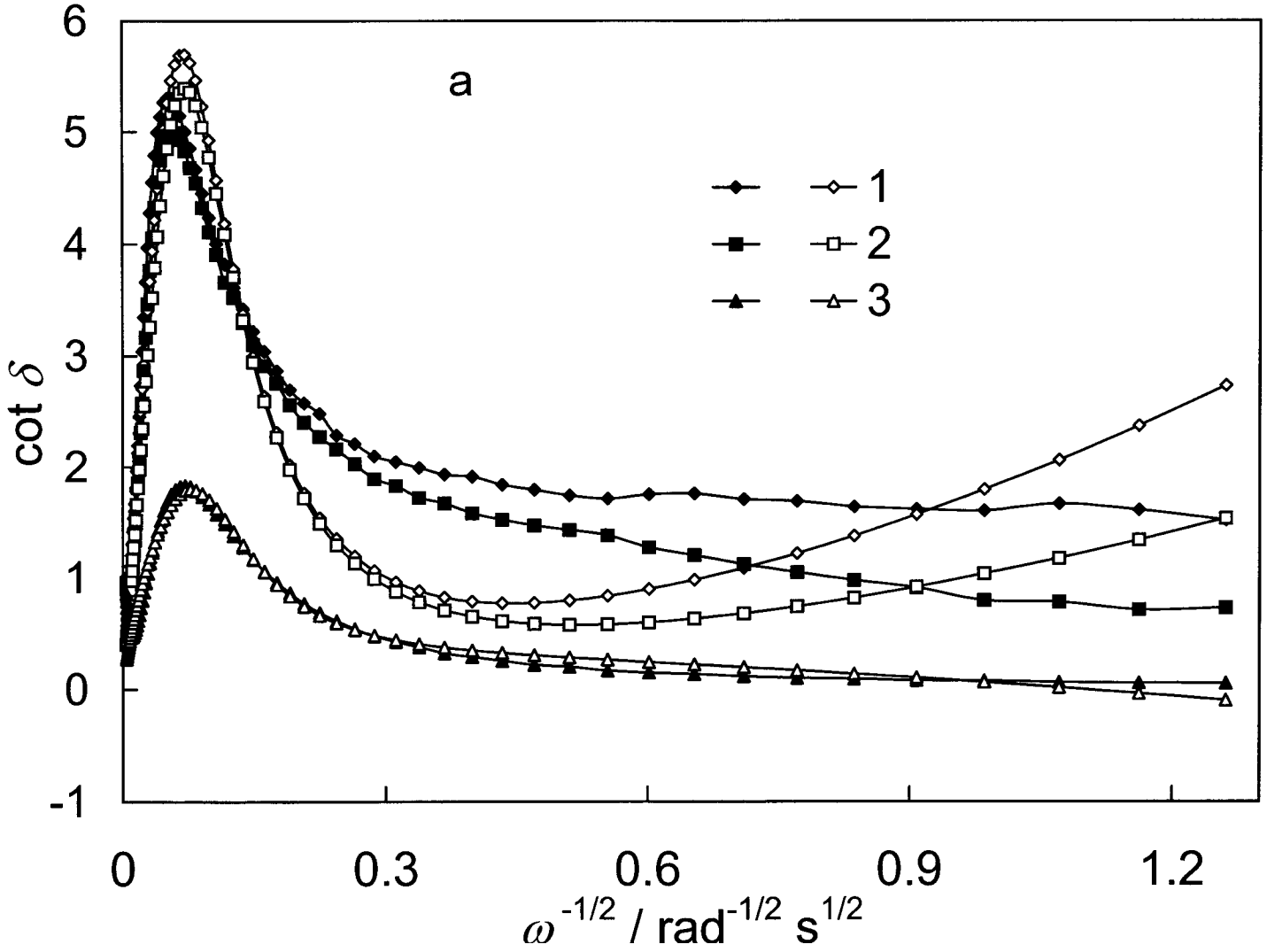

Fig. 11a.

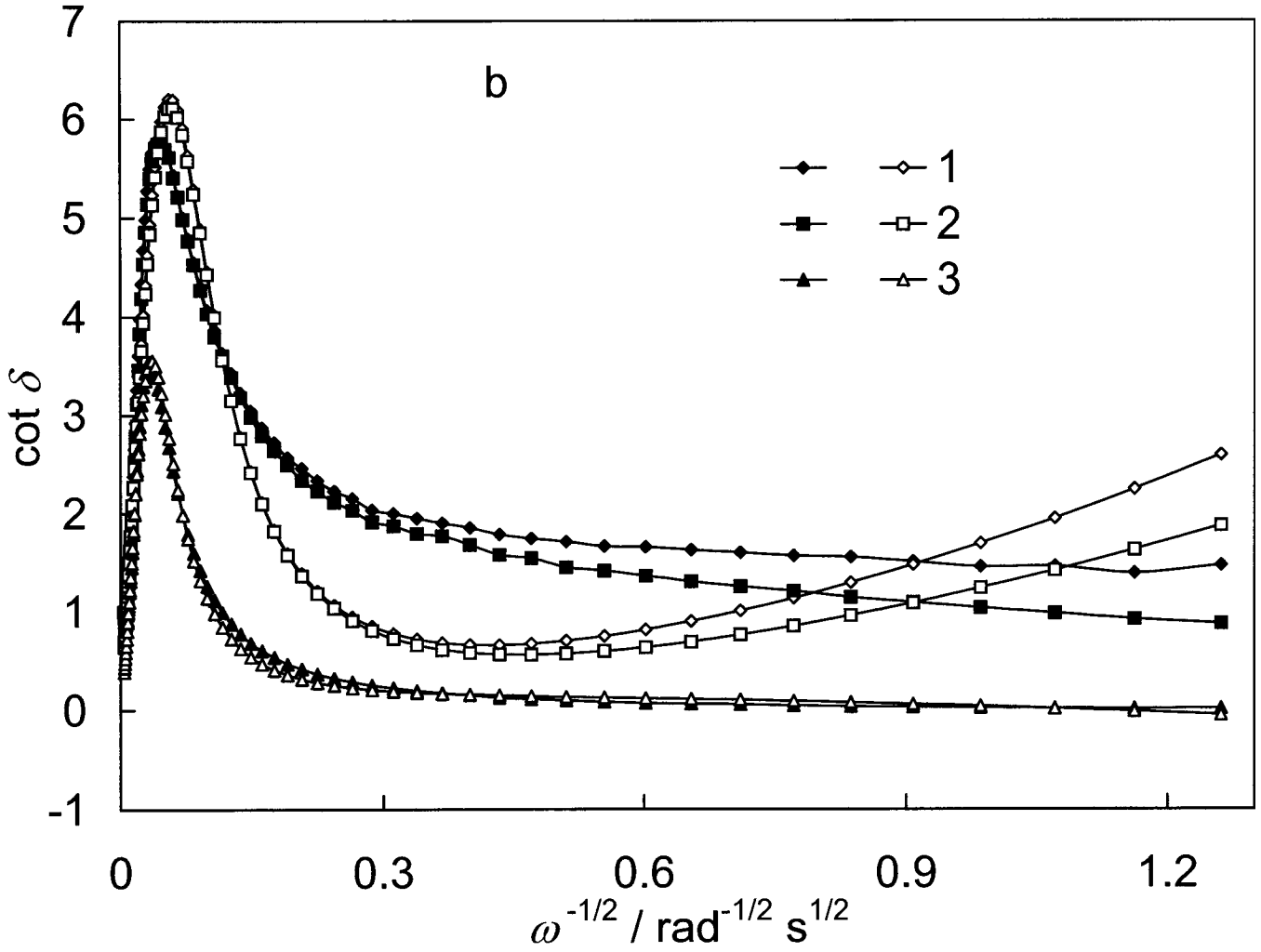

Fig. 11b.